2012-12-20

INTEGRATION OF UWB RANGING AND GPS FOR IMPROVED RELATIVE VEHICLE POSITIONING AND AMBIGUITY RESOLUTION

Jiang, Yuhang

UNIVERSITY OF CALGARY

INTEGRATION OF UWB RANGING AND GPS FOR IMPROVED RELATIVE VEHICLE POSITIONING AND AMBIGUITY RESOLUTION

by

Yuhang Jiang

A THESIS

SUBMITTED TO THE FACULTY OF GRADUATE STUDIES

IN PARTIAL FULFILMENT OF THE REQUIREMENTS FOR THE

DEGREE OF MASTER SCIENCE

DEPARTMENT OF GEOMATICS ENGINEERING

CALGARY, ALBERTA

DECEMBER 2012

ABSTRACT

In this thesis, a system for GPS positioning augmented with Ultra-Wideband (UWB) ranges for vehicle relative positioning applied in Vehicle-to-Infrastructure (V2I) navigation is developed and tested. It is assumed that UWB ranging information and carrier-phase differential GPS (DGPS) corrections are only available via a limited-range communication link between the vehicle and the infrastructure points. The navigation solution is implemented in an extended Kalman filter where differential GPS pseudorange, Doppler and carrier phase measurements are used in conjunction with UWB ranges measured between the vehicle and infrastructure points purposefully chosen on the road. Results indicate that the GPS and UWB integrated positioning system can improve the float solution and ambiguity resolution compared to the GPS-only case. When a single UWB radio is located roughly 300 m north of a fictitious intersection in 25 out of 40 cases the RMS position errors improved before the vehicle approaching the intersection. The inclusion of UWB ranges also improves in the time to fix ambiguities by 4.1% (0.4 seconds), 9.4% (0.9 seconds), 16.8% (2.4 seconds), 16.9% (3.2 seconds) and 15% (4.0 seconds) when the additional UWB measurements are available for 25 m, 50 m, 100 m, 200 m, and 300 m, respectively.

ACKNOWLEDGEMENTS

First and foremost, I wish to express my appreciation to my supervisors, Drs. Mark Petovello and Kyle O'Keefe, and my project sponsor Dr. Chaminda Basnayake, for their academic and financial support, during the period of my graduate studies. I would not have been able to complete my Master's degree without their help. I thank them for their thoughtful questions and valuable suggestions to improve my thesis.

I would like to acknowledge the financial support of the Natural Science and Engineering Research Council of Canada (NSERC), and General Motors of Canada.

I would like to thank friends throughout my graduate studies: Da Wang, Bo Li, Billy Chan, Peng Xie, Zhe He, Aiden Morrison, Jared Bancroft, James Curran, Ali Broumandan, Boxiong Wang, Tao Lin, Tao Li, Anup Dhital, Ali Jafarnia, Saeed Daneshmand, Junbo Shi, Bei Huang. Special thanks are to Dr. Glenn MacGougan for his previous work and code. Da Wang and Zhe He are thanked for their unselfish knowledge sharing, beneficial discussions and suggestive comments, and Bo Li for his fruitful discussions on Ultra-Wideband technology and his unselfish help with data collection.

I would like to thank my girlfriend for her support during my graduate studies. My warmest gratitude goes to my parents and little sister who always encouraged me throughout my life.

TABLE OF CONTENTS

LIST OF TABLES

LIST OF FIGURES AND ILLUSTRATIONS

LIST OF SYMBOLS AND ABBREVIATIONS

List of Symbols

b	UWB range bias
B	Transformation matrix from SD to DD ambiguities
c	light speed
cdT	receiver clock offset error state
dT	receiver clock error
$d\dot{T}$	receiver clock error drift
dt	satellite clock error
$d\dot{t}$	satellite clock error drift
$d\rho$	orbital errors
$d\dot{\rho}$	orbital error drift
d_{ion}	ionospheric delay
$\dot{d}_{ion}$	ionospheric delay drift
d_{trop}	tropospheric delay
$\dot{d}_{trop}$	tropospheric delay drift
dr	relative position vector
dv	relative velocity vector
D	Transformation matrix from SD to DD float states
e_A	frequency standard bias for the transmitter
e_B	frequency standard bias for the receiver
f_C	center frequency
f_H	frequency upper bounded
f_L	frequency lower boundary
f_{L_1}	L1 carrier frequency
f_M	frequency at which the highest radiated emission occurs
$F(t)$	dynamics matrix at time t
$G(t)$	the shaping matrix at time t
$G_{k,k+1}$	shaping matrix from epoch k to k+1
$h(\bullet)$	non-linear function of the state vector
H	design matrix
H_k	design matrix at epoch k
K	Kalman Filter gain matrix
K_k	Kalman Filter gain matrix at epoch k
N	integer cycle ambiguities
N_{SD}, N_{DD}	single difference and double difference ambiguity state vector

N_i	carrier phase ambiguity on the i^{th} frequency
$\hat{N}$	float DD phase ambiguity
$\breve{N}$	integer DD phase ambiguity
P	states covariance matrix
$P_{N_{SD}}, P_{N_{DD}}$	covariance matrix of SD and DD ambiguity state vector
P_{psr}	receiver pseudorange measurement in metres
P_k	state vector variance-covariance matrix at epoch k
$P_{x_{SD}}, P_{x_{DD}}$	covariance matrix of SD and DD state vector
q	spectral density
Q	states noise covariance matrix
$Q(t)$	spectral density matrix
Q_k	process noise matrix at epoch k
R	measurement variance-covariance matrix
R_k	measurement variance-covariance matrix at epoch k
R_U	UWB range measurement
t_{flight}	time-of-flight
$t_{round-trip}$	round-trip time measurements
$t_{turn-around}$	turn-around time accounting for delays from reception to retransmission
v	measurement error
$w(t)$	system driving noise at time t
w_k	discrete-time system driving noise
x	state vector
x_{SD}, x_{DD}	SD and DD state vector
x_a, y_a, z_a	Earth-Centered Earth-Fixed coordinates of UWB radio a
x_b, y_b, z_b	Earth-Centered Earth-Fixed coordinates of UWB radio b
$\hat{x}$	float estimated state vector
$\hat{x}_k$	State vector estimated at epoch k
z	measurement vector
z_k	measurement vector at epoch k
β	reciprocal of the time constant τ
β_f	received signal bandwidth
δz	measurement error vector
δz_k	measurement error vector at epoch k
δx	state error vector
$\delta \hat{x}_k$	state error vector estimated at epoch k
Δ	between receivers single-differencing
ΔN	single difference ambiguity state between base and rover receivers

Δt	time interval
$\Delta\nabla$	double-differencing
ε_P	receiver noise in pseudorange measurement equation
ε_{UWB}	receiver noise in UWB ranging measurement equation
ε_Φ	receiver noise in carrier phase measurement equation
$\varepsilon_{\dot{\Phi}}$	receiver noise in Doppler measurement equation
κ	scale factor error of UWB ranges
λ	carrier wavelength
ρ	geometric range between satellite and receiver
$\dot{\rho}$	geometric range rate between satellite and receiver
σ	standard deviation
$\sigma_{\hat{\tau}}$	variance of the estimate via CRLB
τ	time constant
Φ	receiver carrier measurement scaled to units of range
Φ_k	transition matrix at epoch k
$\Phi_{k,k+1}$	state transition matrix, which converts the state from epoch k to k+1
$\dot{\Phi}$	Doppler measurement scaled to units of range
ω	Gauss-Markov process driving noise

List of Abbreviations

AOA	Angle of Arrival
AR	Ambiguity Resolution
CRLB	Cramer-Rao Lower Bound
DD	Double-difference
DGPS	Differential GPS
DOP	Dilution of Precision
DRMS	Distance Root Mean Square
ECEF	Earth-Centred Earth-Fixed
EKF	Extended Kalman Filter
FASF	Fast Ambiguity Search Filter
FCC	Federal Communications Commission
GDOP	Geometric Dilution of Precision
GPS	Global Positioning System
HDOP	Horizontal Dilution of Precision
IEEE	Institute of Electrical and Electronics Engineers
IMU	Inertial Measurement Unit
INS	Inertial Navigation System
IR	Infrared radiation
ITS	Intelligent Transportation Systems
LAMBDA	least-squares Ambiguity Decorrelation Adjustment
LOS	Line-of-Sight
LSAST	least-squares Ambiguity Search Technique
LSQ	least-squares
MSS	Multispectral Solutions
NLOS	Non-line-of-sight
OTF	On-the-fly
PCF	Probability of Correct Fix
PDOP	Position Dilution of Precision
PIF	Probability of Incorrect Fix
PRN	Pseudo-Random Noise
RF	Radio Frequency
RMS	Root Mean Square
RSS	Received Signal Strength
RTK	Real-Time Kinematic
SA	Selective Availability
SD	Single-difference
SNR	Signal-To-Noise Ratio
TDOA	Time Difference of Arrival
TEC	Total Electron Content
TOA	Time of arrival
TTFF	Time To First Fix
UD	Un-differenced
UWB	Ultra-Wideband

V2I	Vehicle-to-Infrastructure
V2V	Vehicle-to-Vehicle
WGS84	World Geodetic System 1984

CHAPTER 1: INTRODUCTION

1.1 Background

With the rapidly growing demand of safety and reliability applications in land vehicles (e.g. collision warning systems, lane/road departure warning, and in-lane assistance), Intelligent Transportation Systems (ITS) have been given more and more attention in recent years. Among the various technologies (e.g. wireless communications, sensing and navigation), vehicle positioning has played a fundamental and important role in ITS implementation. For vehicle positioning applications in ITS, relative positioning is often applied, where the relative positioning solution is solved among multiple vehicles (Vehicle-to-Vehicle, or V2V), or between a vehicle and fixed infrastructures (Vehicle-to-Infrastructure, or V2I).

Generally, in V2I architectures, vehicles are allowed to transmit their position and velocity data to a central server. The central server will collect and analyze all the data, give instructions (e.g. slow down, change lane) to the vehicles, thus the drivers are informed of important infrastructures (e.g. traffic lights, stop signs) even in poor visibility conditions (Fukushima & Seto, 2006).

The Global Positioning System (GPS) is a standard method for vehicle positioning. It was developed by the U.S. government in 1973 to overcome limitations of previous positioning and navigation systems such as LORAN and Decca Navigator (US National Research Council, 1995). It is capable of providing position, velocity and time information all day, in all weather and open areas on Earth. GPS receivers use the messages from GPS satellites to determine users'

position and velocity. In order to reduce atmospheric errors, satellite based errors, and receiver clock error, differential methods are often used to obtain a better and more reliable solution (Lachapelle, 2010; Misra & Enge, 2006). For carrier-phase GPS positioning, Kalman filtering is generally used to estimate unknown states including both the user position and ambiguities.

However, the quality of the estimated position varies from meters to centimeters depending on the equipment, communication link, measurement type, and estimation algorithm used. Generally, carrier-phase based GPS positioning has a higher accuracy than code based GPS positioning. Carrier-phase based GPS positioning such as real-time kinematic (RTK) positioning is now commonly implemented in industry, for example in surveying and airborne mapping, but has limitations when used in urban environments or under dense foliage due to problems with attenuation, multipath, satellite availability and ambiguity fix reliability. Carrier-phase based GPS positioning can only be achieved in a reasonable amount of time if the initial unknown carrier-phase ambiguities can be reliably resolved as integers. Several algorithms to resolve the integer ambiguities have been developed including Fast Ambiguity Search Filter (FASF) (Chen & Lachapelle, 1994), Least-squares ambiguity Decorrelation (LAMBDA) (Teunissen & Tiberius, 1994) and others. These methods provide the most likely candidate set of integer ambiguity but are not guaranteed to be correct. As a consequence, information from other sensors may be required to augment GPS in order to improve performance to a satisfactory level.

Many positioning and navigation sensors have been investigated in order to augment GPS. Of these, radio frequency (RF) based technologies including WiFi, pseudolites, ultra-wideband

(UWB), and self-contained sensor based technologies such as inertial measurement units (IMUs) are generally used to augment GPS in order to give better and more reliable solutions.

WiFi signals can be exploited for positioning by comparing the received signal strength fingerprints with a database of access point locations or previously mapped signal strengths. However, the accuracy decreases over time and the database will need to be updated, which implies financial cost (Pahlavan et al., 2010; Shafiee et al., 2011).

Pseudolites are ground-based transmitters which provide GPS-like signals, such that a modified receiver can obtain both GPS and pseudolite signals (Cobb, 1997; O'Keefe et al., 1999; Wang & Zhong, 2007). However, their application is difficult to implement due to multipath, tropospheric effects, pseudolite synchronization, and regulatory approval for terrestrial transmission at GPS frequencies (Wang, 2002). In addition, pseudolite carrier phase measurements behave differently due to the fact that the carrier phase is as a function of changing range between transmitter and receiver, while pseudolites are usually not moving, which makes ambiguity resolution difficult for all applications but the fast moving mobile users (Wan et al., 2010).

An Inertial Measurement Unit (IMU) is a dead-reckoning sensor which provides acceleration, angular velocity and attitude data at high update rates. The advantages of the IMU are no possibility of jamming or signal loss and high frequency sampling. However, there are also some issues surrounding IMU use including sensor bias, misalignment, vehicle vibration and the fact that IMU errors are generally unbounded and accumulate with time. For GPS ambiguity

resolution, once the inertial navigation system (INS) degrades to GPS code accuracy, little benefit will be gained (Petovello et al., 2003; Zhang et al., 2010).

UWB signals are defined as signals with large bandwidth equal to or greater than 500MHz. It is a relatively new technology which has been approved by Federal Communications Commission (FCC) in 2002 (FCC, 2002). Due to extra-large transmission bandwidths, UWB offers benefits of accurate ranging, robustness to jamming and interference as well as high obstacle penetration (Win et al., 2009).

1.2 Previous Research

For UWB and GPS integrated system, Fontana (2002) discussed the potential use of UWB technology for augmenting GPS RTK. UWB round-trip measurements are assumed to be unbiased with a constant standard deviation (Opshaug & Enge, 2002) and simulations predicted 15% horizontal accuracy improvement of GPS+UWB over GPS-only and 25% of DGPS+UWB over DGPS strategy. However, later experiments and analysis show that UWB measurements suffer from UWB range systematic errors such as bias and scale factor errors (MacGougan et al., 2008).

Some loosely-coupled – or position-level – approaches were implemented by Fernandez-Madrigal et al., (2007), Gonzalez et al. (2007) and Tanigawa et al., (2004). Tightly-coupled – or measurement-level – integration of GPS and UWB was developed especially for high precision RTK surveying (i.e. centimeter level) applications. In 2008, the UWB radio range accuracy assessment was conducted by Chiu (2008), Chiu & O'Keefe (2008) and MacGougan et al.

(2008), where they found that UWB ranges from two different brands of UWB ranging radio were affected by bias and scale factor errors. UWB improves measurement redundancy when the tightly-coupled GPS + UWB integration is implemented (MacGougan & O'Keefe, 2009). When GPS suffers satellite outages, typically in indoor and hostile environments, multiple UWB ranges can augment GPS allowing for continued position availability. To do this, UWB range systematic errors can be obtained and corrected post mission and ambiguity resolution was performed for a stationary user (MacGougan & Klukas, 2009), however UWB systematic errors cannot be estimated during one single epoch due to the fact that a bias and scale factor cannot be simultaneously observed without changing the UWB range.

The use of UWB integrated with GPS for vehicle-to-vehicle relative positioning simulated by Petovello et al. (2010), it provides improved performance (-0.10 m mean and 0.49 m standard deviation along track error for GPS+UWB solution for the first vehicle) over the GPS-alone solution (-0.82 m mean and 1.27 m standard deviation) in Partial Urban areas. The UWB ranges were found to provide the most advantage in the along-track direction, a carrier phase solution using float ambiguities was tested and results showed that it was considerably better than when using the GPS code-only solution. However, compensation for UWB systematic errors was accomplished using linear fits to the UWB errors with respect to the reference solution to estimate scale factor and bias for each UWB radio pair. Additional methods need to be developed to model and estimate these systematic errors along with the relative navigation solution. Centimetre to decimetre level accuracy positioning is occasionally needed to satisfy the safety and reliability applications for ITS, fixed ambiguity solution has not been implemented for V2V relative navigation solution.

1.3 Research Objectives

In the context of this research, focus is given to the relative position of a vehicle to a fixed infrastructure point (i.e. relative positioning in V2I applications). An infrastructure point could be a traffic signal, a stop sign at an intersection or an infrared radiation (IR) beacon by the side of the road. For example, when a vehicle is approaching an intersection with traffic lights, the ITS could determine and transmit the relative position information of the vehicle to the traffic signal lights, as well as the color of traffic signal lights to the vehicle, thus implementing a red light violation avoidance system (Fukushima & Seto, 2006). In turn, this will help avoid danger, and increase the safety, efficiency and convenience of the transportation system.

The primary objective of this research is to investigate the benefit of integrating UWB ranges with GPS for V2I application, where it is assumed that UWB ranging information and DGPS corrections are only available via a limited-range communication link between the vehicle and the infrastructure points. Specifically, the case considered is that the vehicle and the infrastructure points are all equipped with GPS receivers (to broadcast differential data/corrections) and UWB radios (to obtain UWB ranging measurements).

With this in mind, the research seeks to answer two questions. First, can a fixed ambiguity solution be obtained, to meet the where-in-lane requirement with better than 1 metre level relative positioning accuracy with 95% confidence level (95% probability) (Basnayake et al., 2011), during the time an approaching vehicle enters the infrastructure points' coverage area, and does direct UWB ranging improve the performance? Second, can the UWB systematic errors be

estimated quickly enough at typical relative land vehicle speeds to permit the successful use of high precision UWB range augmentation in the carrier-phase GPS solution?

Furthermore, these questions are investigated using a Geodetic-Grade, and a Consumer-Grade GPS receiver, and as a function of the operational range to the infrastructure points. The latter is important because it may impact the practical deployment of such a system. Performance is assessed by comparing the GPS-only and GPS+UWB solutions in three ways. First, the position accuracy using float ambiguities. Second, the theoretical probability of correctly resolving the integer ambiguities is assessed. Third, the actual ambiguity resolution performance is assessed. Finally, in order to gain insight into the practical limitations of using UWB for V2I positioning, different initial distances (and thus time) to the UWB radios are considered.

The contribution of this thesis is analyzing the UWB range accuracy in detail and introducing a new time synchronization method for UWB ranges. The systematic errors of UWB ranges are characterized with respect to distance for the relative vehicle positioning. The system model of the GPS and UWB integrated system is derived and implemented in an extended Kalman filter. To accomplish the above, pre-existing software from the PLAN group at the University of Calgary was modified and further developed, and field tests were conducted. Four different test scenarios are described, the results are evaluated by comparing the performance of GPS+UWB to that of GPS-alone solution with different initial UWB ranging distances, as well as comparing a Geodetic-Grade GPS receiver with a Consumer-Grade GPS receiver. The work presented in this thesis has been presented in a conference paper in the proceedings of the Institute of Navigation GNSS 2012 Meeting (Jiang et al., 2012).

1.4 Thesis Outline

The remainder of this thesis is organized as follows:

Chapter 2 gives an overview of GPS and UWB fundamentals and discusses the two systems and their characteristics as relevant to this thesis. GPS, GPS observables and relevant differencing techniques are introduced. The pros and cons of using different kinds of observables are compared. GPS error sources and limitations related to this research are discussed. For UWB, the UWB technology is discussed in detail concentrating on ranging methods, accuracy, systematic errors and time synchronization with GPS.

Chapter 3 mainly discusses the theoretical aspect of the integration of GPS and UWB ranges. In the first part of this chapter estimation theory and the Extended Kalman Filter (EKF) are presented. Then it follows with a discussion of the integrated filter, the system model including the dynamics model and the measurement model. The proposed algorithm for ambiguity resolution is also described.

Chapter 4 presents the conditions and setup for V2I applications in order to assess the performance of the proposed GPS/UWB integrated system. A brief overview of V2I positioning concepts and fundamentals is introduced. A description of the different strategies for data processing is then given.

Chapter 5 presents the results of the four test scenarios described in chapter 4. Performance metrics are described and the results are presented in this chapter. A performance comparison between the two types of receivers (i.e. Geodetic-Grade receiver and Consumer-Grade receiver) is also presented in terms of availability, positioning accuracy, probability of correct fix and ambiguity resolution.

Chapter 6 provides the conclusions from the preceding chapters and summarizes the conclusion of the research. Ideas for future investigation are also recommended.

CHAPTER 2: SYSTEMS OVERVIEW

This chapter is an overview of the GPS and UWB fundamentals. The two systems are reviewed in terms of their characteristics related to this thesis. With respect of GPS, observables and different differencing techniques are introduced. The pros and cons of implementing different kinds of observables are compared. GPS error sources and limitations related to this research are discussed. UWB technology including ranging methods, accuracy, errors and time synchronization with GPS are then discussed in detail.

2.1 Global Positioning System Overview

GPS is a satellite based navigation system based on time measurements. The receivers use the particular signals from GPS satellites to determine users' position, velocity and time. Generally, the carrier phase observable is the most precise measurement with lower measurement noise and limited multipath effects (0.25 cycle or less than 5 cm) (Misra & Enge, 2006).

Differential methods are often used to minimize atmospheric errors and orbital errors and eliminate satellite and receiver clock errors in order to obtain a better and more reliable solution. However, high-precision relative positioning can only be achieved in a reasonable amount of time if the initial unknown carrier-phase ambiguities can be reliably resolved as integers. Several algorithms to resolve the integer ambiguities have been developed such as FASF, and LAMBDA. The LAMBDA method provides the most likely candidate for resolving integer ambiguities but is not guaranteed to be correct (Verhagen, 2005). Further details on GPS are well introduced in Kaplan & Hegarty (2006); Misra & Enge (2006).

2.1.1 GPS Observables

In this thesis, three types of measurements are considered: pseudorange, Doppler and carrier phase. All three measurements are used in this work, thus they will be described in detail in this section.

Pseudorange is the measurement of the distance between the receiver and the satellite. It is generated by measuring the difference between the transmission time and reception time and is obtained by tracking the GPS Pseudo-Random Noise (PRN) codes modulated on the satellite signals. By considering error sources, the pseudorange measurement equation can be written as:

$$P_{psr} = \rho + d\rho + c(dt - dT) + d_{ion} + d_{trop} + \varepsilon_P \qquad (2.1)$$

where P_{psr} is receiver pseudorange measurement in metres, ρ is geometric range between satellite and receiver, $d\rho$ is orbital error, c is the light speed, dt is satellite clock error, dT is receiver clock error, d_{ion} is ionospheric delay, d_{trop} is tropospheric delay, ε_P is receiver noise and multipath. More details about the GPS error sources can be found in section 2.1.2.

Carrier phase is another way of obtaining the ranges between the satellites and receivers. It is generated by the satellite signal processor by accumulating the change in phase (and therefore range) required to maintain phase lock. Thus, it is also appropriate to be called the "accumulated delta range" (Axelrad & Brown, 1996). Since carrier phase measurements are ambiguous (with an unknown constant or integer number of cycles between satellites and receivers), the phase

observable can only keep track of the total change of range between the satellite and the receiver unless this ambiguity is resolved.

The accuracy of the carrier phase measurements are better than those of pseudoranges. The carrier phase measurement equation can be written as:

$$\Phi = \rho + d\rho + c(dt - dT) + \lambda N - d_{ion} + d_{trop} + \varepsilon_{\Phi} \tag{2.2}$$

where Φ is receiver carrier measurement scaled to units of range, N is integer cycle ambiguities, λ is carrier wavelength, ε_{Φ} is receiver noise and multipath.

Doppler is a frequency shift of a signal generated by the relative motion of the GPS satellites and receivers. It is the rate of change of the carrier phase measurement. The Doppler measurement equation (in m/s) can be written as:

$$\dot{\Phi} = \dot{\rho} + d\dot{\rho} + c(d\dot{t} - d\dot{T}) - \dot{d}_{ion} + \dot{d}_{trop} + \dot{\varepsilon}_{\dot{\Phi}} \tag{2.3}$$

where $\dot{\Phi}$ is Doppler measurement scaled to units of range, $\dot{\rho}$ is geometric range rate between satellite and receiver, $d\dot{\rho}$ is orbital error drift $d\dot{t}$ is satellite clock error drift, $d\dot{T}$ is receiver clock error drift, $\dot{d}_{ion}$ is ionospheric delay drift, $\dot{d}_{trop}$ is tropospheric delay drift, $\varepsilon_{\dot{\Phi}}$ is receiver noise and multipath.

2.1.2 Error sources

GPS observables are usually contaminated by errors which include satellite orbit error, satellite clock error, ionospheric and tropospheric delay, multipath and receiver noise.

The orbit error results from a discrepancy in broadcast ephemerides in the navigation message. This discrepancy will lead to inaccuracies of the computed satellite positions compared with their actual values (Cai, 2009).

Both satellites and receivers suffer from clock errors. Atomic clocks are used in both GPS satellites and the control segments on earth. They are extremely accurate with frequency stability of better than 2×10^{-13} second over one day (Spilker, 1996). Due to the poorer quality of the oscillator, the receiver clock drift is usually worse than that of satellite clock drift.

Ionospheric error is caused by electrons affecting GPS signal at the band of atmosphere extending from 50 to 1500 kilometres above the surface of the Earth. The ionospheric error is frequency dependent and is proportional to the Total Electron Content (TEC) along the signal path, which varies with solar and magnetic activity, geographic location and observing direction (Skone, 2011).

Tropospheric error is caused by the neutral atmosphere slowing and bending the GPS signal transmitting path. It consists of two components; the wet and dry delay. The wet delay contains 10% of the total tropospheric delay (Misra & Enge, 2006), while the dry component represents 90% of the total tropospheric delay. The wet tropospheric delay is usually modeled as a function of atmospheric pressure, temperature, humidity and satellite elevation (Tao, 2008; Zhang & Gao, 2007), while the dry tropospheric delay is only weakly dependent on temperature, and mainly

dependant on pressure and is easy to predict as an exponentially decaying function with respect to height.

Multipath is the reception of the signal arriving from multiple paths because of reflections and diffraction. Since the error from multipath is dependent on the signal strength, the environment, and the measuring technique (Misra & Enge, 2006), the magnitude of the error differs from 0.5 cm to 1 m (see Table 2.1). Thus it is challenging to estimate and compensate the multipath effect. Typically, the effect of multipath on code pseudorange measurements can reach several metres or more in hostile environments, and is at the decimetre level (20 cm at 1σ level) under benign conditions. The L1 carrier phase measurements are not free from multipath either, the effect of the multipath on carrier phase measurements is at the centimetre level (2 cm at 1σ level) (Kaplan et al., 2006; Ward et al., 2006).

Receiver noise is generated by the receiver itself in the process of code or phase tracking. It is considered to be white noise and non-correlated between measurements due to independent tracking loops for each separate measurement. The pseudorange code measurement noise can be reduced to the 10 cm level or lower by using modern GPS receivers with narrow correlators or high-quality receiver oscillator. The noise level of the carrier phase measurement is 0.8 mm for the L1 carrier and 1 mm for the L2 carrier (Conley et al., 2006).

Table 2.1 summarizes the GPS error sources and their magnitude.

Table 2.1 GPS Error Sources and Magnitude (Hofmann-Wellenhof et al., 2001; Misra & Enge, 2006; Olynik, 2002)

Error Source	Magnitude
Orbit error	Real time Broadcast: ~160 cm
Satellite clock error	~2 m
Ionospheric delay	zenith delay: 2 m ~ 10 m
Tropospheric delay	zenith delay: 2.3 m ~ 2.5 m
Multipath	Code: 0.5 m ~ 1 m Phase: 0.5 cm ~ 5 cm
Receiver Noise	Code: 0.1 m ~ 3 m Phase: 0.2 mm ~ 5 mm

Several GPS error sources including satellite antenna phase center offset, phase wind up, earth tide, ocean tide loading, and atmosphere loading have not been mentioned due to the relatively small errors.

2.1.3 Differential Techniques

In order to achieve a solution with 1 metre level relative positioning accuracy with 95% confidence level, DGPS is often implemented where the relative positioning between the base (GPS receiver on the ground in a known location to act as a static reference point) and the rover (GPS receiver in an unknown location to be determined) receivers is desired, which is often applied to reduce or eliminate atmospheric error and other sources of errors from the

measurement equations. In this section, single-difference and double-difference methods are introduced.

The single-difference takes a difference of measurements between the rover and base receivers at the same epoch. The model for single-difference measurements for a short baseline is as follows:

$$\begin{aligned}
\Delta P_{ab}^{i} &= \Delta\rho_{ab}^{i} + \Delta d\,\rho_{ab}^{i} - c\Delta dT_{ab} + \Delta d_{ion} + \Delta d_{trop} + \varepsilon_{\Delta P} \\
\Delta \Phi_{ab}^{i} &= \Delta\rho_{ab}^{i} + \Delta d\,\rho_{ab}^{i} - c\Delta dT_{ab} + \lambda\Delta N_{ab}^{i} - \Delta d_{ion} + \Delta d_{trop} + \varepsilon_{\Delta\Phi} \\
\Delta \dot{\Phi}_{ab}^{i} &= \Delta\dot{\rho}_{ab}^{i} + \Delta d\,\dot{\rho}_{ab}^{i} - c\Delta d\dot{T}_{ab} - \Delta\dot{d}_{ion} + \Delta\dot{d}_{trop} + \dot{\varepsilon}_{\Delta\dot{\Phi}}
\end{aligned} \tag{2.4}$$

where Δ means between receivers single-differencing.

To achieve centimetre-level accuracies in a reasonable amount of time, double differenced carrier phase measurements are generally used with ambiguities being resolved to their correct integer values (Cosentino et al., 2006; Hofmann-Wellenhof et al., 2001). Double differencing GPS measurements are computed between the base and the rover as well as between two satellites to eliminate the atmospheric error and other sources of errors such as receiver and satellite clock errors. In the process, the orbital, ionospheric and tropospheric errors are reduced, and their reductions are correlated with spatial separation of the two receivers. The noise level in the double differenced measurements, however, is amplified depending on the satellite elevation, and the noises become correlated due to the linear combinations in the double differenced operation.

$$\begin{aligned}
\Delta\nabla P_{ab}^{ij} &= \Delta\nabla\rho_{ab}^{ij} + \Delta\nabla d\,\rho_{ab}^{ij} + \Delta\nabla d_{ion} + \Delta\nabla d_{trop} + \varepsilon_{\Delta\nabla P} \\
\Delta\nabla \Phi_{ab}^{ij} &= \Delta\nabla\rho_{ab}^{ij} + \Delta\nabla d\,\rho_{ab}^{ij} + \lambda\Delta\nabla N_{ab}^{ij} - \Delta\nabla d_{ion} + \Delta\nabla d_{trop} + \varepsilon_{\Delta\nabla\Phi} \\
\Delta\nabla \dot{\Phi}_{ab}^{ij} &= \Delta\nabla\dot{\rho}_{ab}^{ij} + \Delta\nabla d\,\dot{\rho}_{ab}^{ij} - \Delta\nabla\dot{d}_{ion} + \Delta\nabla\dot{d}_{trop} + \dot{\varepsilon}_{\Delta\nabla\dot{\Phi}}
\end{aligned} \tag{2.5}$$

where $\Delta\nabla$ means double-differencing. The advantage of double differencing is that it eliminates the satellite and receiver clock errors as well as hard-to-estimate error terms, as mentioned in section 2.1.2, by taking one equation and differencing the ambiguities.

Double differencing is used when carrier phase ambiguity resolution is required, since the removal of the receiver clock error means that only one bias (the ambiguity) needs to be estimated for each range.

2.1.4 Limitations of GPS

Unfortunately, GPS is limited by obstructions to the line-of-sight path to the satellite when operating in urban canyon environments or under dense foliage. These environments may block, reflect or weaken much of the signals by causing signal attenuation and multipath, reducing satellite availability and observation geometry. Solar activity, jamming or interference may also cause the loss of the GPS signal, and thus results in discontinuous measurements which will limit positioning accuracy, reliability and radio communication. In addition, it is assumed that differential GPS is only available via a short-range communication link between the vehicle and the infrastructure, where differential corrections are only available for a very limited range on a low power radio, it only allows limited time to resolve ambiguities when the vehicle is approaching the intersection. As a consequence, information from other sensors may be required to augment GPS and improve performance to a satisfactory level (i.e., 1 metre or better with confidence level of 95%).

2.2 Ultra Wideband System Overview

Due to its extremely large bandwidth, and correspondingly high time resolution, UWB technology is emerging as a method for communications and high precision ranging. It offers techniques for applications that require high speed communications and accurate position estimation (Arslan et al., 2006; Gezici et al., 2005; Sahinoglu et al., 2008). For positioning and navigation applications, UWB signals provide high accuracy ranging with the benefits of robustness to multipath, jamming and interference, and better obstacle penetration (Win et al., 2009). In theory and practice, centimetre-accurate ranging estimation has been achieved by using UWB ranging measurements after compensating for the UWB systematic errors (MacGougan & O'Keefe, 2009).

2.2.1 UWB Definition

In 2002, FCC released the First Report and Order on UWB technology allowing unlicensed UWB transmissions in the frequency range from 3.1 to 10.6 GHz. The FCC provides the following definition for UWB (FCC, 2002):

"Section 15.503 definitions. (a) UWB Bandwidth. For the purpose of this subpart, the UWB bandwidth is the frequency band bounded by the points that are 10 dB below the highest radiated emission, as based on the complete transmission system including the antenna. The upper boundary is designated f_H *and the lower boundary is designated* f_L*. The frequency at which the highest radiated emission occurs is designated* f_M*. (b) Center frequency. The center frequency,* f_C*, equals* $(f_H + f_L)/2$*. (c) Fractional bandwidth. The fractional bandwidth equals* $2(f_H - f_L)/(f_H + f_L)$*. (d) Ultra-wideband (UWB) transmitter. An intentional radiator that, at*

any point in time, has a fractional bandwidth equal to or greater than 0.20 or has a UWB bandwidth equal to or greater than 500 MHz, regardless of the fractional bandwidth."

In order to protect other RF signals, the FCC provides a -41.3 dBm/MHz power spectral density emission limit for UWB transmitters. However, the emission limit for UWB transmitters may be even lower (as low as -75 dBm/MHz) in other segments of the spectrum. For GPS signal bands including GPS L1, L2, and L5, an emission limit with -85.3 dBm/MHz is applied to avoid serious detrimental impact on public safety.

2.2.2 Ranging Methods

There are various ways to use UWB signals for navigation, such as received signal strength (RSS), time-of-arrival (TOA), angle of arrival (AOA) and time-difference-of-arrival (TDOA) (Gezici & Poor, 2009). However, without having the synchronous time between UWB transmitter and receiver, these techniques (i.e. TOA and AOA) cannot provide usable ranging measurements. In addition, all of them (TOA, AOA and TDOA) require expensive and precise oscillators to mitigate the clock offset and clock drift for synchronization. In this thesis, a UWB ranging system that estimates the range using a two-way time-of-flight (TOF) is employed instead of global synchronization. This system was selected because it does not require tight time synchronization between transmitters and it can be commercially used at low cost.

The basic concept of the two-way TOF ranging is to estimate the distance between transmitter and receiver. It measures a round trip time to obtain the propagation time and consequently the physical distance between transmitter and receiver as shown in Figure 2.1. The range can be

computed according to Equation (2.6) where c is the speed of light, $t_{round-trip}$ is the round-trip-time measurements, and $t_{turn-around}$ is a turn-around time accounting for delays from reception to retransmission.

$$range = c \cdot \frac{t_{round-trip} - t_{turn-around}}{2} \tag{2.6}$$

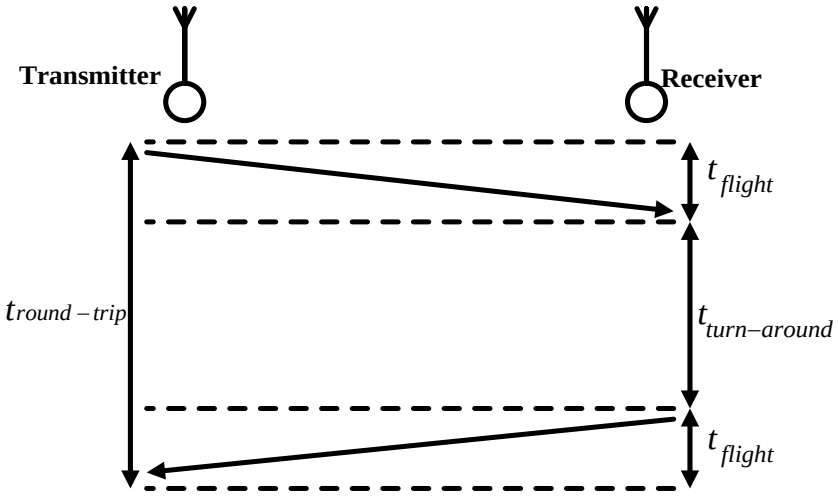

Figure 2.1 Evaluation of Signal Round-trip Time using Two-way Time-Of-Flight Ranging Technique

2.2.3 Ranging Accuracy

For RF time-of-flight ranging systems, the achievable accuracy will be limited and degraded by the random errors. Random errors are measurement errors that are caused by unknown and unpredictable changes. These errors include noise and interference. Noise can affect the receiver such that it detects signals at the wrong time, which will lead to faulty measurements. To

quantify the effect of noise in RF-ranging methods, the Signal-To-Noise Ratio (SNR) on the receiver's side and the occupied bandwidth are generally used. These measures are linked via the Cramer-Rao Lower Bound (CRLB). The CRLB is a statistical measure described by Kay (1993) which is a fundamental lower bound on the variance of any unbiased estimator.

It can be implemented for an estimate of how well the two-way TOF ranging systems can determine a range. The CRLB of variance $\sigma_{\hat{\tau}}$ is given by the following relationship:

$$\sigma_{\hat{\tau}}^2 = \frac{1}{8\pi^2 \beta_f^2 SNR} \tag{2.7}$$

where $\sigma_{\hat{\tau}}^2$ is the variance of the estimate, β_f is the received signal bandwidth, SNR is the signal-to-noise. From Equation (2.7), the SNR and bandwidth of the signal have an inverse linear and an inverse quadratic effect on the ranging accuracy. Since UWB signals use an extra-large bandwidth, ranging accuracy can be relatively precise. For example, a system with 3.75 GHz of bandwidth leads to a CRLB of 6.5 mm at one standard deviation for 14 dB SNR (MacGougan & O'Keefe, 2009).

2.2.4 Systematic Errors

For RF TOF ranging systems, the time measurements are usually based on frequency standards which often have a bias or frequency offset. As a consequence, the frequency biases in the transmitter and receiver result in a small scale factor error and a relatively larger bias in the range measurement. More details are discussed in the IEEE 802.15.4a standard (IEEE802-15.4a, 2007). Due to frequency bias error in the oscillators (frequency standards) used by the UWB

transmitter and receiver, the total ranging error can be separated into two components (MacGougan, 2009):

$$error = t_{flight}(e_A) + \frac{t_{turn-around}}{2}(e_A + e_B + e_A e_B) \tag{2.8}$$

where t_{flight} is time-of-flight, $t_{turn-around}$ is the fixed turn-around time, e_A is the frequency standard bias for the transmitter, and e_B is the frequency standard bias for the receiver. The first term in Equation (2.8) is a scale factor error. The second term is independent of the distance measured and is thus a bias term which can reach the metre level.

In MacGougan (2009), the UWB systematic measurement errors are proved to be stable and can be modeled as a bias and a scale factor affecting each ranging radio pair. The corresponding non-linear UWB range measurement R_U model is:

$$R_U = \kappa\sqrt{(x_a - x_b)^2 + (y_a - y_b)^2 + (z_a - z_b)^2} + b + \varepsilon_{UWB} \tag{2.9}$$

The standard deviation of UWB error σ_U is expressed as:

$$\sigma_U = \sqrt{\sigma_b^2 + R_U{}^2 \cdot \sigma_\kappa^2 + \sigma_{noise}^2} \tag{2.10}$$

where x_a, y_a, z_a are the Earth-Centered Earth-Fixed (ECEF) coordinates of UWB radio a and x_b, y_b, z_b are the unknown ECEF coordinates of UWB radio b, which is assumed to be located at the user. κ and b are the scale factor and bias, respectively. ε_{UWB} includes multipath, noise, and unmodelled error effects. $\sigma_U, \sigma_b, \sigma_\kappa, \sigma_{noise}$ is the standard deviation of UWB bias, scale factor and noise, respectively. The range error as a function of distance for one UWB pair is shown as Figure 2.2.

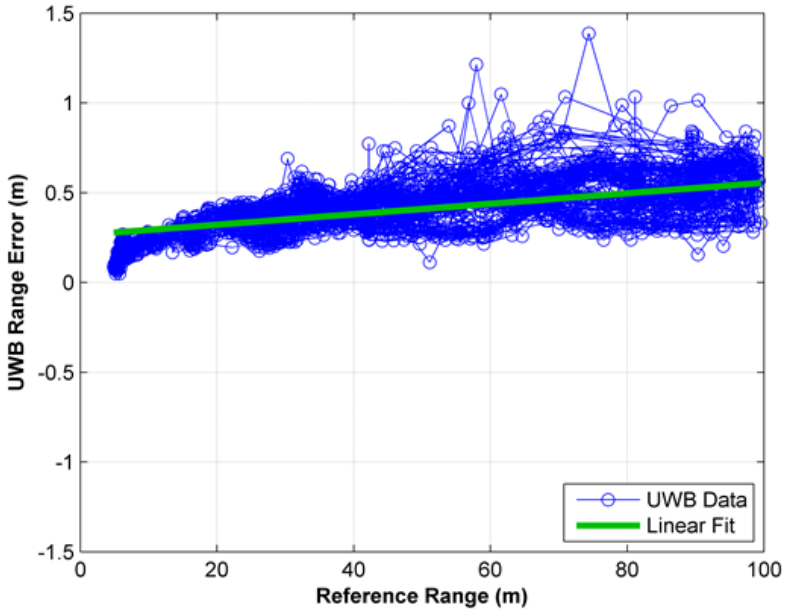

Figure 2.2 Range errors as a function of reference range for one UWB pair (between radio a and b)

2.2.5 Time Synchronization

In order to integrate GPS measurements and UWB ranging measurements with high accuracy, both systems' measurements need to be time tagged using the same time frame. The goal of synchronizing GPS and UWB measurements is to ensure that measured UWB ranges correspond to observed GPS baselines at the same time. As such, it is not required that the two measuring systems be synchronized to the nanosecond level (which is the theoretical precision of both systems) but instead the timing requirements are determined by the dynamics of the user. For example, a10 millisecond synchronization error when travelling at a speed of 60-80 km/h (17-22 m/s relative motion between the two radios) will result in a UWB ranging error on the order of 17-22 centimetres which will affect the ability to use this measurements for cm-level positioning.

To accomplish millisecond level synchronization in this thesis, a laptop computer was used to log both GPS data and UWB ranges. Although details are provided in later chapters, the idea is to use the GPS receiver to calibrate the laptop clock, which is then used to time tag the UWB ranges. By updating the laptop's estimate of GPS time every second, UWB ranges were time tagged with an accuracy of less than 5 ms.

To illustrate the effect of a time synchronization error, the plot in Figure 2.3 shows an example of a UWB range error as a function of the reference range when a time synchronization error of 25 ms is present for a vehicle that is travelling at 15m/s. The corresponding error histogram (after removing the linear fit to the data) is shown in Figure 2.4. An obvious slope and bias to the errors (see linear fit line) can be seen in the figures which are consistent with the UWB radios used. For the results contained in this thesis, the bias and scale factor are obtained post mission to provide the reference of UWB errors. The range errors show very systematic behaviours as a function of the reference range. This is because, as the vehicle moves towards the infrastructure point, the timing error makes the UWB range error look larger or smaller depending on the "sign" of the synchronization error. As the vehicle passes the infrastructure point, the sign of the error reverses.

After one second update time synchronization is implemented, the time synchronization error is minimized, the results shown in Figure 2.5 and Figure 2.6 are obtained. The error histogram is more peaked, indicating less spread in the errors. For the data plotted, the standard deviation of the error is 9.6 cm, which is consistent with Figure 2.3 and Figure 2.4.

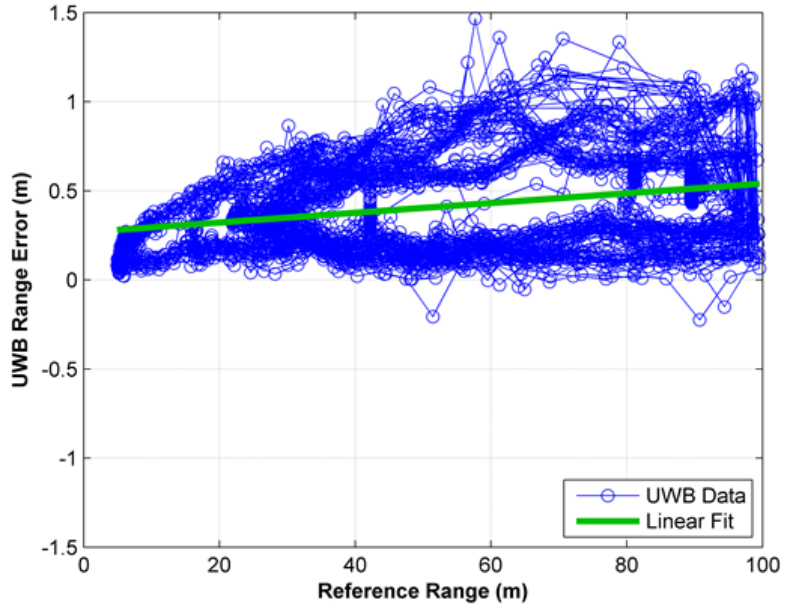

Figure 2.3 Example of UWB range error as a function of reference range with a time synchronization error of 25 ms

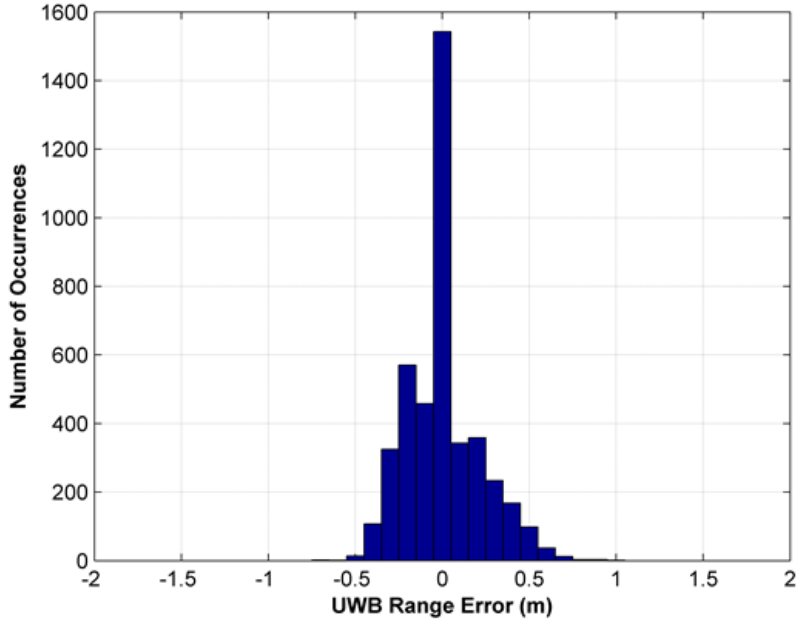

Figure 2.4 Example of UWB range error histogram after removing the linear best fit with a time synchronization error of 25 ms

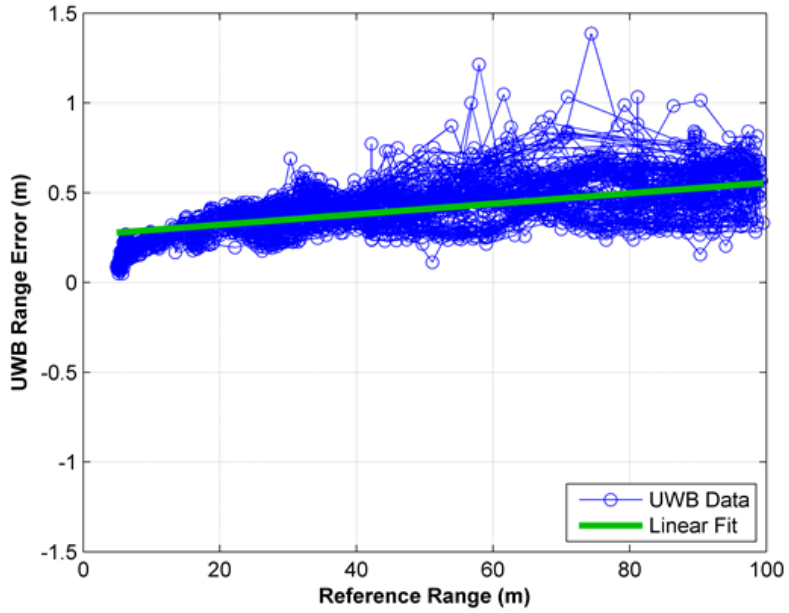

Figure 2.5 Example of UWB range error as a function of reference range with a time synchronization error of 0 ms

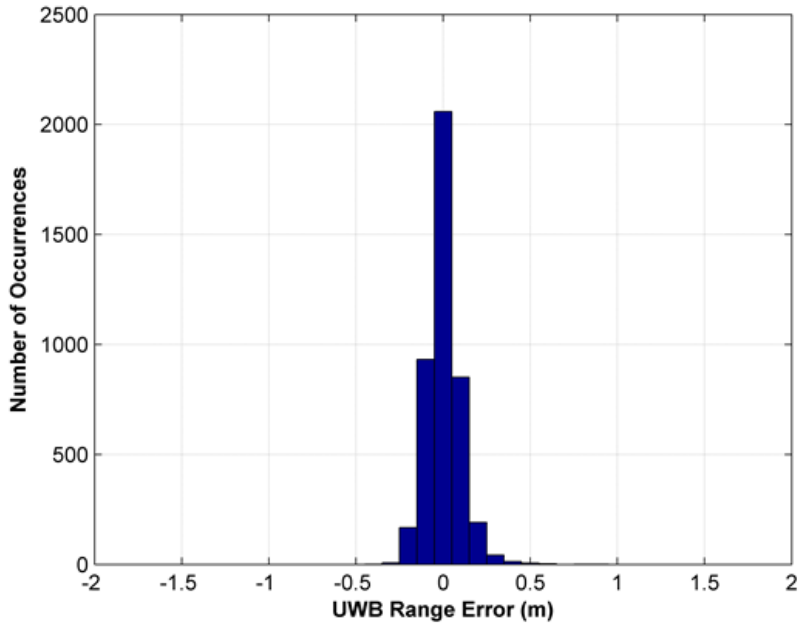

Figure 2.6 Example of UWB range error histogram with a time synchronization error of 0 ms

CHAPTER 3: RELATIVE POSITIONING FOR INTEGRATED SYSTEM

This chapter discusses the theoretical aspects of the tight integration of GPS measurements and the UWB ranges. In the first part of this chapter estimation theory and EKF are presented. The proposed algorithm of integrated filter and ambiguity resolution are then described.

3.1 Estimation

Estimation, generally, is a process of acquiring a set of unknowns of interest (i.e. unknown parameters) from a set of uncertain measurements (e.g., code phase and carrier phase in GPS usage) using an optimal estimator (e.g., least-squares or Kalman Filtering to estimate the position and velocity states). Under normal conditions, the unknown parameters are represented as a system state vector while the uncertain measurements are related to parameters through a measurement model. The optimal estimator is the method that will process the uncertain measurements to determine the minimum error estimate of the unknown parameters (Gelb, 1974).

In a system where the number of independent measurement equations is greater than the number of unknown parameters, the unknown parameters can be solved from the measurement model. In this case, the selection of the optimal estimator is generally based on the minimum sum of the square error. Minimum variances, implementation efficiency, knowledge of the system, and prior information are also important considerations when implementing an optimal estimator. In addition, the optimal estimator should ideally also use all other information, including system dynamics, and initial constraints. Since random noise affects the uncertainty of measurements, in

order to obtain information of interest from the measurements, the random behavior of the noise should be considered (Tiberius et al., 1999). Therefore a process describing measurement noises as random processes should be considered to perform the estimation process.

3.2 Extended Kalman Filtering

This section will begin with a brief look at the basic concepts of the least-squares method, followed by an overview of Kalman filter method. Finally, the discrete-time extended Kalman filter is introduced and a description of its implementation is given in this section.

For many geomatics applications, the least-squares method is the most common estimation procedure. It is a method where the unknown parameters are only computed using measurements, that is, without a priori knowledge or a system model. Since the least-squares method has important optimality characteristics based on the minimum sum of the square errors, it is simple to apply (Verhagen, 2005). In addition, least-squares estimation is equal to maximum-likelihood estimation and best linear unbiased estimation if the model is linear and is Gaussian distributed (Teunissen, 2000; Verhagen, 2005).

The least-squares optimality criteria is the minimization of the sum of the square errors, the value of the result can be then calculated by taking the derivative of the sum of the square errors with respect to the unknown parameters. For the measurement model written as equation (3.3) the estimator will be defined as:

$$\hat{x} = \arg\min \| z - H \cdot x \|_R^2 \qquad (3.1)$$

and its solution using the least-squares algorithm is given by:

$$\hat{x} = (H^T R^{-1} H)^{-1} H^T R^{-1} z$$
$$P = (H^T R^{-1} H)^{-1} \tag{3.2}$$

where H is the design matrix, $\hat{x}$ is the float estimated state vector, $\arg\min(f, x)$ gives a position $x_{\min}$ at which f is minimized, R is variance-covariance matrix of the measurement, and P is covariance matrix of the states.

The Kalman filter is a recursive estimator which deals with information from the system model and measurements. It extends the least-squares method to incorporate the knowledge of how the state vector behaves over time. This is assuming the entity's behaviour (motion and clock errors) can be modeled well enough during the estimation procedure. For many navigation systems with non-linear models relating the measurements to the estimated parameters, an extended Kalman filter is often applied by expanding the most recent estimate of state vector using a first order Taylor series expansion (Petovello, 2010).

First, by considering the effect of measurement error, the non-linear measurement model can be given by

$$\begin{aligned} z &= h(x) + v \\ &\approx h(\hat{x}) + \frac{dh(x)}{dx}\Big|_{x=\hat{x}} + v \\ z &= h(\hat{x}) + H\delta x + v \\ z - h(\hat{x}) &= H\delta x + v \\ \delta z &= H\delta x + v \end{aligned} \tag{3.3}$$

where z is the measurement vector, x is the state vector and v is the measurement error, $\delta z = z - h(\hat{x})$ is the "error" in measurement vector, $\delta x = x - \hat{x}$ is the "error" in the state vector, $h(\bullet)$ is the non-linear function of the state vector, H is the design matrix meaning the measurement geometry with respect to the state vector.

The linear system model, which generally describes the state vector over time, can be given as:

$$\dot{x}(t) = F(t) \cdot x(t) + G(t) \cdot w(t) \tag{3.4}$$

where the 'dot' notation indicates the time derivative of a parameter, $F(t)$ is the dynamics matrix, describing the dynamics of the system at time t, $F(t) \cdot x(t)$ is the dynamics model which defines the states change over time based on the known relationship, $G(t)$ is the shaping matrix at time t, shaping the input white noise and matching the true characteristics of the system, $G(t) \cdot w(t)$ is defined as stochastic model, which defines the uncertainty in the dynamics model, $w(t)$ is the system driving noise at time t, a vector of zero-mean, unit variance white noise with spectral density matrix $Q(t)$.

In this thesis, the continuous-time system equations need to be transformed to their corresponding discrete-time system model, which is written as:

$$x_{k+1} = \Phi_{k,k+1} x_k + G_{k,k+1} w_k \tag{3.5}$$

where subscript k represents the time epoch, $\Phi_{k,k+1}$ is the state transition matrix, which converts the state from epoch k to $k+1$, and is the discrete-time equivalent of the dynamics matrix $F(t)$ in

Equation (3.4). $G_{k,k+1}$ is the discrete-time equivalent of the shaping matrix $G(t)$ in Equation (3.4), w_k is the discrete-time equivalent of system driving noise.

The transition matrix can be described by (Gelb, 1974; Petovello, 2010):

$$\Phi_{k,k+1} = e^{F(t_k)\Delta t_{k+1}} \approx I + F(t_k)\Delta t_{k+1} \tag{3.6}$$

where $\Delta t_{k+1} = t_{k+1} - t_k$ is the time interval, $e^A = I + A + \frac{A^2}{2!} + \cdots$. In this thesis, only the first order effects are considered.

The covariance matrix of the system driving noise w_k, which also indicates the process noise matrix Q_k, can be computed by:

$$\begin{aligned} Q_k &= E\{w_k w_l^T\} = \begin{cases} Q_k, l = k \\ 0, l \neq k \end{cases} \\ Q_k &= \int_{t_k}^{t_{k+1}} \Phi(t_{k+1}, \tau) G(\tau) Q(\tau) G^T(\tau) \Phi^T(t_{k+1}, \tau) d\tau \end{aligned} \tag{3.7}$$

where $Q(\tau)$ is the spectral density matrix of $w(\tau)$.

The Extended Kalman filter computation procedure is illustrated in Figure 3.1, where $\delta\hat{x}_k$ is state error vector estimated at epoch k, δz_k is measurement error vector at epoch k, H_k is design matrix at epoch k, R_k is measurement variance-covariance matrix at epoch k, P_k is state vector variance-covariance matrix at epoch k, Q_k is process noise matrix at epoch k, Φ_k is

transition matrix at epoch k, K_k is Kalman Filter gain matrix at epoch k, $+$ indicates the state and corresponding covariance estimate after the "Update" step, $-$ indicates the state and corresponding covariance estimate before the "Update" step

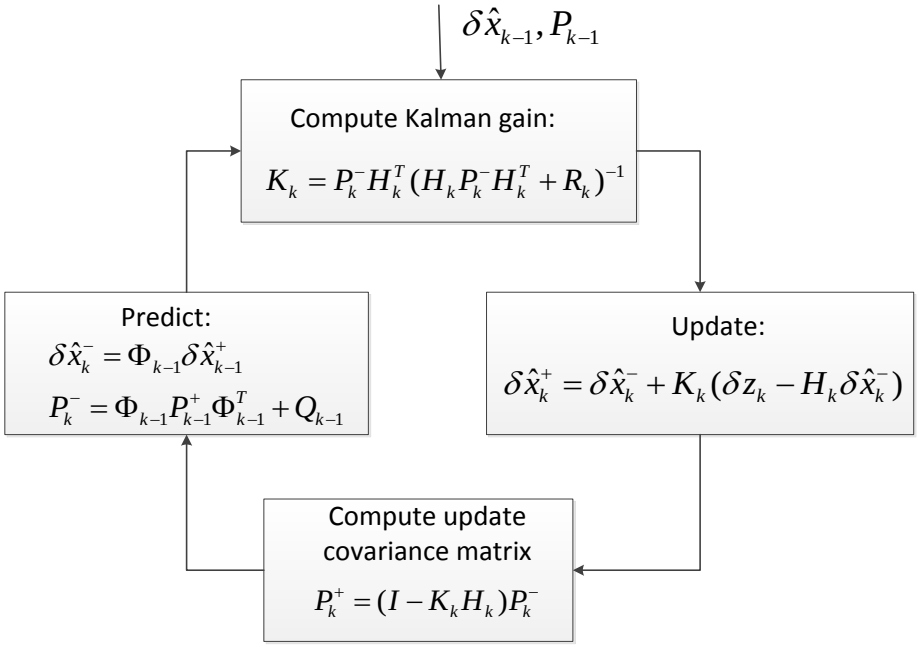

Figure 3.1 Extended Kalman filter computation procedure

In this work, the EKF is chosen because it is developed for non-linear discrete-time processes. In practise, it can lead to very reliable state estimation when the process being estimated can be accurately linearized at each point along the trajectory of the states. The EKF can also assimilate measurements from sources with varying data rates. More details are given in many sources (e.g. Brown & Hwang (1997); Gelb (1974); Grewal et al., (2001); Maybeck (1979)).

3.3 GPS/UWB Integrated System

A basic carrier phase GPS system error state vector consists of position error states, velocity error states, and corresponding ambiguity error states. However, due to sensor errors of UWB radios discussed in the previous chapter, carrier phase GPS augmentation with UWB will require the system state vector to be augmented with UWB systematic error states. For the UWB radios, each UWB range pair has separate bias and scale factor states (MacGougan et al., 2008). The bias term is induced by radio oscillator frequency offsets, and the scale factor term is due to pulse detection and fine timing methods used by UWB radios to estimate the TOF of UWB signal. The bias and scale factor errors vary little over time when temperature is stable and there is a sufficient power supply. Since it is not practical to calibrate these errors each time when different radio pairs are used, one solution is to estimate the errors as additional states in the extended Kalman filter. This section will describe how the relative navigation solution is implemented using an extended Kalman filter.

3.3.1 System States

The estimated variables herein are 3 position error states, 3 velocity error states, receiver clock offset and drift, UWB systematic errors including bias and scale factor for each UWB radio pair, and the single difference (SD) carrier phase ambiguities. In this thesis, the single difference carrier phase ambiguities are then differenced between satellites, LAMBDA method is implemented to obtain double difference (DD) ambiguities, which will be discussed in section 3.4. The error state is shown in the following:

$$x = \begin{bmatrix} \mathbf{dr} & \mathbf{dv} & cdT & c\dot{d}T & b_1 & \kappa_1 & \cdots & b_m & \kappa_m & \lambda\Delta N_1 & \cdots & \lambda\Delta N_n \end{bmatrix}^T \qquad (3.8)$$

where **dr** and **dv** are the relative position and velocity vectors, cdT and $c\dot{d}T$ are the receiver clock offset and drift error states, b_i is the UWB bias error states and κ_i is the UWB scale factor error states for the UWB radio pair i. ΔN_i is the single difference ambiguity state between base and rover receivers.

3.3.2 System Model

The design of the system model for the GPS position, velocity, clock offset and drift filter, and UWB systematic error filter is based on GPS/UWB integrated error dynamics and stochastic models. The dynamics model defines how the state vector changes with time based on some known relationships (Petovello, 2010). The stochastic model is used primarily as a means of defining the uncertainty in the dynamics model. The system model for the combined GPS and UWB radios is developed and presented in this section.

The system models are usually expressed by Equation(3.3). The first derivative of the position errors is related to velocity errors, which is described in Equation (3.9):

$$\dot{\mathbf{dr}} = F_{\mathbf{\delta r}} \cdot \mathbf{dv} \tag{3.9}$$

where $F_{\mathbf{dr}} = \begin{bmatrix} 1 & 0 & 0 \\ 0 & 1 & 0 \\ 0 & 0 & 1 \end{bmatrix}$

The velocity errors in this thesis are modeled as a first order Gauss-Markov process, which is described as:

$$\dot{\mathbf{dv}} = -\beta_{\mathbf{dv}} \cdot \mathbf{dv} + \omega_{\mathbf{dv}} \tag{3.10}$$

where $\beta_{\mathbf{dv}}$ is the reciprocal of the time constant $\tau_{\mathbf{dv}}$, $\omega_{\mathbf{dv}} = \sqrt{2\sigma_{\mathbf{dv}}{}^2 \beta_{\mathbf{dv}}}$ is the Gauss-Markov process driving noise with spectral density $q_{\mathbf{dv}} = 2\beta_{\mathbf{dv}}\sigma_{\mathbf{dv}}{}^2$.

The clock offset and drift errors can be modeled and described as Equation (3.11) in Brown & Hwang (1997):

$$\begin{aligned} c\dot{dT} &= F_{cdT} \cdot c\dot{dT} \\ c\ddot{dT} &= -\beta_{c\dot{dT}} \cdot c\dot{dT} + \omega_{c\dot{dT}} \end{aligned} \tag{3.11}$$

where $F_{cdT} = I$, $\beta_{c\dot{dT}}$ is the reciprocal of the time constant $\tau_{c\dot{dT}}$, $\omega_{c\dot{dT}} = \sqrt{2\sigma_{c\dot{dT}}{}^2 \beta_{c\dot{dT}}}$ is the Gauss-Markov process driving noise with spectral density $q_{c\dot{dT}} = 2\beta_{c\dot{dT}}\sigma_{c\dot{dT}}{}^2$.

The ambiguity and UWB systematic errors terms are modeled as random constant processes. The error state of the stochastic model is summarized in Table 3.1.

Table 3.1 Stochastic model of the error states

States	Stochastic model
Position, velocity, clock offset and drift	Integrated Gauss-Markov model (Brown & Hwang, 1997)
Ambiguity	Random constant
Bias and scale factor	Random constant

Figure 3.3 shows the structure of the transition matrix used in the GPS/UWB integrated filter. The size of the position and velocity transition matrix $\Phi_{\mathbf{dr\&dv}}$ is 6x6, Φ_{clock} is 2x2, Φ_{UWB} is 2(m-1) x 2(m-1) and Φ_{N} is n x n, where m is the number of observed UWB radios, and n is the number of observed satellites.

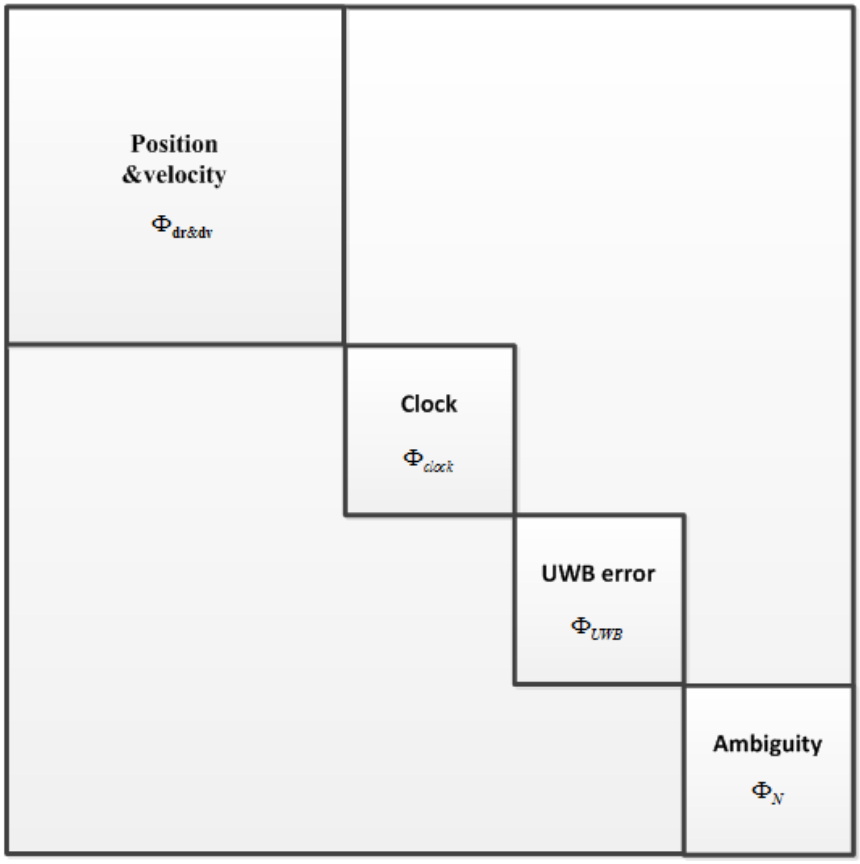

Figure 3.2 Process noise matrix structure

The position and velocity block in the transition matrix is given by Equation (3.12):

$$\Phi_{\mathbf{dr\&dv}} = \begin{bmatrix} 1 & 0 & 0 & \frac{1-e^{-\beta_{vn}\cdot\tau}}{\beta_{vn}} & 0 & 0 \\ 0 & 1 & 0 & 0 & \frac{1-e^{-\beta_{ve}\cdot\tau}}{\beta_{ve}} & 0 \\ 0 & 0 & 1 & 0 & 0 & \frac{1-e^{-\beta_{vu}\cdot\tau}}{\beta_{vu}} \\ 0 & 0 & 0 & e^{-\beta_{vn}\cdot\tau} & 0 & 0 \\ 0 & 0 & 0 & 0 & e^{-\beta_{ve}\cdot\tau} & 0 \\ 0 & 0 & 0 & 0 & 0 & e^{-\beta_{vu}\cdot\tau} \end{bmatrix} \tag{3.12}$$

The clock offset and drift block in the transition matrix is given by Equation (3.13):

$$\Phi_{clock} = \begin{bmatrix} 1 & \dfrac{1-e^{-\beta_{drift}\cdot\tau}}{\beta_{drift}} \\ 0 & e^{-\beta_{drift}\cdot\tau} \end{bmatrix} \tag{3.13}$$

Since the stochastic model of the UWB systematic errors and ambiguities states are defined as random constant, their transition matrix is an identity matrix.

Based on a random process model for the system states, the noise matrix Q is given herein. For the purpose of illustration, the structure of the noise matrix is divided into sub-blocks, in which each block represents a set of related parameters, such as position and velocity error block, receiver clock error block, ambiguities block and UWB systematic error block. Figure 3.3 shows the structure of the noise matrix used in the GPS/UWB integrated filter. The size of position and velocity process noise matrix $Q_{\mathbf{dr\&dv}}$ is 6x6, Q_{clock} is 2x2, Q_{UWB} is 2(m-1) x 2(m-1) and Q_N is n x n.

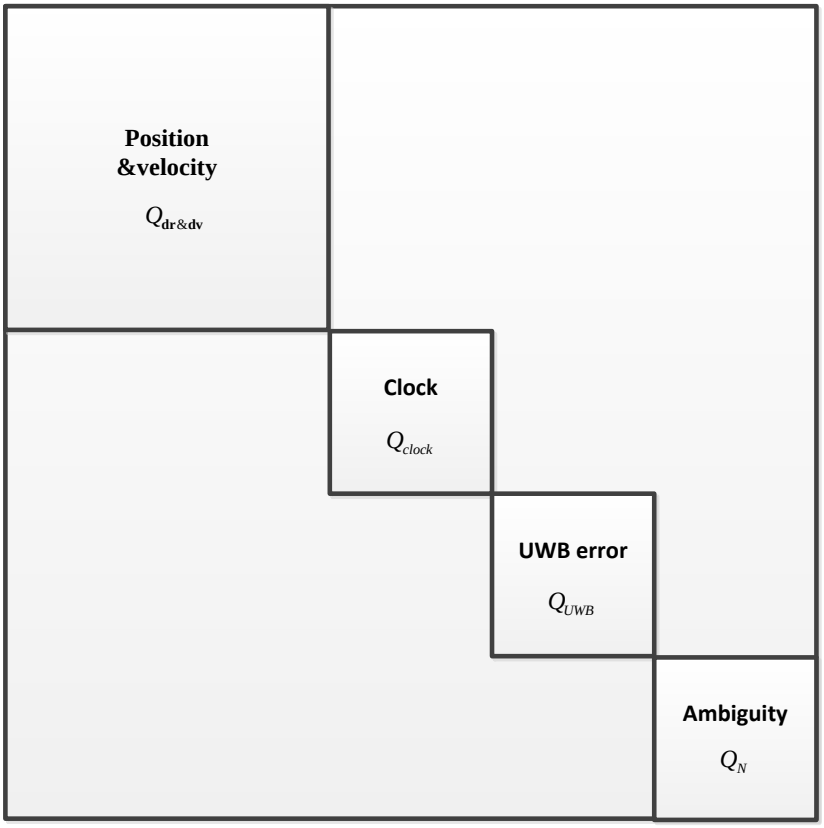

Figure 3.3 Process noise matrix structure

The noise matrix of position and velocity errors are described by Equations (3.14) and (3.15). The elements of matrix which are not listed are zero.

$$
\begin{aligned}
Q_{0,0} &= \frac{q_{vn}}{\beta_{vn}^2}\cdot\left(\tau-\frac{2(1-e^{-\beta_{vn}\cdot\tau})}{\beta_{vn}}+\frac{1-e^{-2\beta_{vn}\cdot\tau}}{2\beta_{vn}}\right)\\
Q_{1,1} &= \frac{q_{ve}}{\beta_{ve}^2}\cdot\left(\tau-\frac{2(1-e^{-\beta_{ve}\cdot\tau})}{\beta_{ve}}+\frac{1-e^{-2\beta_{ve}\cdot\tau}}{2\beta_{ve}}\right)\\
Q_{2,2} &= \frac{q_{vu}}{\beta_{vu}^2}\cdot\left(\tau-\frac{2(1-e^{-\beta_{vu}\cdot\tau})}{\beta_{vu}}+\frac{1-e^{-2\beta_{vu}\cdot\tau}}{2\beta_{vu}}\right)\\
Q_{0,3} &= \frac{q_{vn}}{\beta_{vn}}\cdot\left(\frac{1-e^{-\beta_{vn}\cdot\tau}}{\beta_{vn}}-\frac{1-e^{-2\beta_{vn}\cdot\tau}}{2\beta_{vn}}\right)\\
Q_{1,4} &= \frac{q_{ve}}{\beta_{ve}}\cdot\left(\frac{1-e^{-\beta_{ve}\cdot\tau}}{\beta_{ve}}-\frac{1-e^{-2\beta_{ve}\cdot\tau}}{2\beta_{ve}}\right)\\
Q_{2,5} &= \frac{q_{vu}}{\beta_{vu}}\cdot\left(\frac{1-e^{-\beta_{vu}\cdot\tau}}{\beta_{vu}}-\frac{1-e^{-2\beta_{vu}\cdot\tau}}{2\beta_{vu}}\right)\\
Q_{0,3} &= Q_{3,0}\\
Q_{1,4} &= Q_{4,1}\\
Q_{2,5} &= Q_{5,2}
\end{aligned}
\tag{3.14}
$$

$$
\begin{aligned}
Q_{3,3} &= \frac{q_{vn}(1-e^{-2\beta_{vn}\cdot\tau})}{2\beta_{vn}}\\
Q_{4,4} &= \frac{q_{ve}(1-e^{-2\beta_{ve}\cdot\tau})}{2\beta_{ve}}\\
Q_{5,5} &= \frac{q_{vu}(1-e^{-2\beta_{vu}\cdot\tau})}{2\beta_{vu}}
\end{aligned}
\tag{3.15}
$$

Where q_{ve}, q_{vn}, q_{vu} are the spectral density of velocity in each direction, $\beta_{ve}, \beta_{vn}, \beta_{vu}$ are the correlation time in each direction, τ is the time interval (Brown & Hwang, 1997).

The process noise matrix for clock offset and drift errors are described by Equation (3.16). The elements of matrix which are not listed are zero.

$$
\begin{aligned}
Q_{6,6} &= \frac{q_{drift}}{\beta_{drift}^2} \cdot \left(\tau - \frac{2(1-e^{-\beta_{drift} \cdot \tau})}{\beta_{drift}} + \frac{1-e^{-2\beta_{drift} \cdot \tau}}{2\beta_{drift}} \right) \\
Q_{6,7} &= \frac{q_{drift}}{\beta_{drift}} \cdot \left(\frac{1-e^{-\beta_{drift} \cdot \tau}}{\beta_{drift}} - \frac{1-e^{-2\beta_{drift} \cdot \tau}}{2\beta_{drift}} \right) \\
Q_{7,6} &= Q_{3,0} \\
Q_{7,7} &= \frac{q_{drift}(1-e^{-2\beta_{drift} \cdot \tau})}{2\beta_{drift}}
\end{aligned}
\tag{3.16}
$$

Where q_{drift} is the spectral density of clock drift, β_{drift} is the clock drift correlation time, τ is the time interval. These values are obtained by analyzing the reference solution from the field data collection as discussed in the following chapter.

Since the UWB systematic errors and ambiguities states are modeled as random constants, their process noise matrices are null.

3.3.3 Measurement Model

Pseudorange, Doppler and carrier phase measurements on L1 between receiver and satellite are described by Equations (2.1) to (2.3). The UWB ranging measurement equation is written by Equation (2.9). Since these measurement equations are non-linear, they need to be linearized when they are used in the Extended Kalman filter. More details about the linearization can be found in (Kaplan et al., 2006). After the linearization procedure, the design matrix for the pseudorange, carrier phase, Doppler and UWB ranging measurements can be described by Equation (3.17) to (3.20), respectively.

$$H_{psr}=\begin{bmatrix} \frac{\partial P^1}{\partial x} & \frac{\partial P^1_{psr}}{\partial y} & \frac{\partial P^1_{psr}}{\partial z} & \frac{\partial P^1_{psr}}{\partial v_x} & \frac{\partial P^1_{psr}}{\partial v_y} & \frac{\partial P^1_{psr}}{\partial v_z} & 1 & 0 & \frac{\partial P^1_{psr}}{\partial b_m} & \frac{\partial P^1_{psr}}{\partial \kappa_m} & 0\cdots 0 \\ & \vdots & & & \vdots & & \vdots & \vdots & \vdots & \vdots & \vdots \\ \frac{\partial P^n}{\partial x} & \frac{\partial P^n_{psr}}{\partial y} & \frac{\partial P^n_{psr}}{\partial z} & \frac{\partial P^n_{psr}}{\partial v_x} & \frac{\partial P^n_{psr}}{\partial v_y} & \frac{\partial P^n_{psr}}{\partial v_z} & 1 & 0 & \frac{\partial P^n_{psr}}{\partial b_m} & \frac{\partial P^n_{psr}}{\partial \kappa_m} & 0\cdots 0 \end{bmatrix} \tag{3.17}$$

$$H_{dpr}=\begin{bmatrix} \frac{\partial \dot{\Phi}^1}{\partial x} & \frac{\partial \dot{\Phi}^1}{\partial y} & \frac{\partial \dot{\Phi}^1}{\partial z} & \frac{\partial \dot{\Phi}^1}{\partial v_x} & \frac{\partial \dot{\Phi}^1}{\partial v_y} & \frac{\partial \dot{\Phi}^1}{\partial v_z} & 0 & 1 & \frac{\partial \dot{\Phi}^1}{\partial b_m} & \frac{\partial \dot{\Phi}^1}{\partial \kappa_m} & 0\cdots 0 \\ & \vdots & & & \vdots & & \vdots & \vdots & \vdots & \vdots & \vdots \\ \frac{\partial \dot{\Phi}^n}{\partial x} & \frac{\partial \dot{\Phi}^n}{\partial y} & \frac{\partial \dot{\Phi}^n}{\partial z} & \frac{\partial \dot{\Phi}^n}{\partial v_x} & \frac{\partial \dot{\Phi}^n}{\partial v_y} & \frac{\partial \dot{\Phi}^n}{\partial v_z} & 0 & 1 & \frac{\partial \dot{\Phi}^n}{\partial b_m} & \frac{\partial \dot{\Phi}^n}{\partial \kappa_m} & 0\cdots 0 \end{bmatrix} \tag{3.18}$$

$$H_{adr}=\begin{bmatrix} \frac{\partial \Phi^1}{\partial x} & \frac{\partial \Phi^1}{\partial y} & \frac{\partial \Phi^1}{\partial z} & \frac{\partial \Phi^1}{\partial v_x} & \frac{\partial \Phi^1}{\partial v_y} & \frac{\partial \Phi^1}{\partial v_z} & 1 & 0 & \frac{\partial \Phi^1}{\partial b_m} & \frac{\partial \Phi^1}{\partial \kappa_m} & \lambda\cdots 0 \\ & \vdots & & & \vdots & & \vdots & \vdots & \vdots & \vdots & \vdots \\ \frac{\partial \Phi^n}{\partial x} & \frac{\partial \Phi^n}{\partial y} & \frac{\partial \Phi^n}{\partial z} & \frac{\partial \Phi^n}{\partial v_x} & \frac{\partial \Phi^n}{\partial v_y} & \frac{\partial \Phi^n}{\partial v_z} & 1 & 0 & \frac{\partial \Phi^n}{\partial b_m} & \frac{\partial \Phi^n}{\partial \kappa_m} & 0\cdots \lambda \end{bmatrix} \tag{3.19}$$

$$H_{uwb}=\begin{bmatrix} \frac{\partial R^1_U}{\partial x} & \frac{\partial R^1_U}{\partial y} & \frac{\partial R^1_U}{\partial z} & \frac{\partial R^1_U}{\partial v_x} & \frac{\partial R^1_U}{\partial v_y} & \frac{\partial R^1_U}{\partial v_z} & 0 & 0 & \frac{\partial R^1_U}{\partial b_m}=1 & \frac{\partial R^1_U}{\partial \kappa_m}=R^1_U & 0\cdots 0 \\ & \vdots & & & \vdots & & \vdots & \vdots & \vdots & \vdots & \vdots \\ \frac{\partial R^n_U}{\partial x} & \frac{\partial R^n_U}{\partial y} & \frac{\partial R^n_U}{\partial z} & \frac{\partial R^n_U}{\partial v_x} & \frac{\partial R^n_U}{\partial v_y} & \frac{\partial R^n_U}{\partial v_z} & 0 & 0 & \frac{\partial R^n_U}{\partial b_m}=1 & \frac{\partial R^n_U}{\partial \kappa_m}=R^n_U & 0\cdots 0 \end{bmatrix} \tag{3.20}$$

where n is the number of satellites observed, $\frac{\partial \bullet}{\partial x},\frac{\partial \bullet}{\partial y},\frac{\partial \bullet}{\partial z}$ are the partial derivatives with respect to the position error vector, $\frac{\partial \bullet}{\partial v_x},\frac{\partial \bullet}{\partial v_y},\frac{\partial \bullet}{\partial v_z}$ are the partial derivatives with respect to the velocity error vector.

3.4 Ambiguity Resolution

In order to exploit the best accuracy from carrier phase measurements, the ambiguities need to be resolved to their correct integer values. Numerous methods are available for ambiguity resolution and validation such as the least-squares ambiguity search technique (LSAST) (Hatch, 1990), the least-squares ambiguity decorrelation adjustment method (LAMBDA), the fast ambiguity search filter (FASF), and sequential integer rounding (i.e. Bootstrapping Method) (Han, 1997). Even though these methods are different in some aspects, most of them follow similar procedures that include estimation of real-valued ambiguity values and their corresponding covariance matrices by least-squares or Kalman filtering, the definition of a search space, the determination of correct integers and the validation of the selected set. The LAMBDA method is used in this thesis as it has been shown to be both computationally efficient and reliable.

In this research, the SD float solution ignoring the integer characteristic of ambiguities is first determined. However, it has been proven that using both SD measurements, and DD measurements are equivalent (Shen & Xu, 2008). But SD ambiguities cannot be estimated separately from the common receiver clock offset, which is not an integer value, and thus the SD ambiguities must be differenced before being fixed, and it is easy to fix DD ambiguities since they are integers (Cao, 2009). The SD float ambiguity solution is then differenced using transformation matrix B to obtain DD ambiguities. The transformation matrix B can be applied to get the DD float ambiguities and their corresponding covariance matrix. The transformation matrix D for DD float states and corresponding ambiguities, transformation matrix B for DD

float ambiguities and their transformation processes are shown in Equations (3.21) to (3.23), which can retain position states, remove clock states and perform ambiguity state differencing.

$$D = \begin{bmatrix} 1 & 0 & 0 & 0 & 0 & 0 & 0 & 0 & 0 & 0 & 0 & 0 & 0 & 0 \\ 0 & 1 & 0 & 0 & 0 & 0 & 0 & 0 & 0 & 0 & 0 & 0 & 0 & 0 \\ 0 & 0 & 1 & 0 & 0 & 0 & 0 & 0 & 0 & 0 & 0 & 0 & 0 & 0 \\ 0 & 0 & 0 & 1 & 0 & 0 & 0 & 0 & 0 & 0 & 0 & 0 & 0 & 0 \\ 0 & 0 & 0 & 0 & 1 & 0 & 0 & 0 & 0 & 0 & 0 & 0 & 0 & 0 \\ 0 & 0 & 0 & 0 & 0 & 1 & 0 & 0 & 0 & 0 & 0 & 0 & 0 & 0 \\ 0 & 0 & 0 & 0 & 0 & 0 & 0 & 0 & 1 & 0 & 0 & 0 & 0 & 0 \\ 0 & 0 & 0 & 0 & 0 & 0 & 0 & 0 & 0 & 1 & 0 & 0 & 0 & 0 \\ 0 & 0 & 0 & 0 & 0 & 0 & 0 & 0 & 0 & 0 & 1 & 0 & 0 & 0 \\ 0 & 0 & 0 & 0 & 0 & 0 & 0 & 0 & 0 & 0 & 0 & 1 & 0 & 0 \\ 0 & 0 & 0 & 0 & 0 & 0 & 0 & 0 & 0 & 0 & 0 & 0 & 1 & 0 \\ 0 & 0 & 0 & 0 & 0 & 0 & 0 & 0 & 0 & 0 & 0 & 0 & 0 & B \end{bmatrix} \tag{3.21}$$

$$B = \begin{bmatrix} -1 & 1 & 0 & 0 & 0 & \cdots & 0 \\ -1 & 0 & 1 & 0 & 0 & \cdots & 0 \\ -1 & 0 & 0 & 1 & 0 & \cdots & 0 \\ -1 & \vdots & \vdots & \vdots & \vdots & \vdots & 0 \\ -1 & 0 & 0 & 0 & 0 & \cdots & 1 \end{bmatrix} \tag{3.22}$$

$$\begin{aligned} x_{DD} &= D \cdot x_{SD} \\ P_{x_{DD}} &= D \cdot P_{x_{SD}} \cdot D^T \\ N_{DD} &= B \cdot N_{SD} \\ P_{N_{DD}} &= B \cdot P_{N_{SD}} \cdot B^T \end{aligned} \tag{3.23}$$

where x_{SD}, x_{DD} are single difference and double difference state vectors, $P_{x_{SD}}, P_{x_{DD}}$ are the covariance matrices of the single difference and double difference state vectors, N_{SD}, N_{DD} are

single difference and double difference ambiguity state vectors, $P_{N_{SD}}, P_{N_{DD}}$ are the covariance matrices of single difference and double difference ambiguity state vectors, respectively.

After the DD float solution is obtained, the next step is to find the most likely set of integer ambiguity values. The best set of ambiguities is generally defined as the minimum norm of the difference between the float and integer ambiguities scaled by the covariance matrix of the float ambiguities (Teunissen & Tiberius, 1994), which is can be determined using an integer least squares search approach described by:

$$\chi^2 = \min((\mathbf{a}-\hat{\mathbf{a}})^T Q_{\hat{\mathbf{a}}}^{-1}(\mathbf{a}-\hat{\mathbf{a}})) \tag{3.24}$$

where $\hat{\mathbf{a}}$ is the vector of float ambiguities, $\mathbf{a}$ is the vector of integer ambiguities, and $Q_{\hat{\mathbf{a}}}$ is the covariance matrix of the float ambiguities.

Then the ambiguity vector and its corresponding covariance matrix are transformed with the decorrelating Z matrix using the following equations:

$$\begin{aligned} \hat{\mathbf{z}} &= Z^T \hat{\mathbf{a}} \\ Q_{\hat{\mathbf{z}}} &= Z^T Q_{\hat{\mathbf{a}}} Z \end{aligned} \tag{3.25}$$

where $\hat{\mathbf{z}}$ is the vector of transformed ambiguities and $Q_{\hat{\mathbf{z}}}$ is the corresponding variance covariance matrix.

The solution is not changed by LAMBDA method, but it reduces the size of the search space with the minimum norm in z-space given by:

$$\chi^2 = \min((\mathbf{z} - \hat{\mathbf{z}})^T Q_{\hat{\mathbf{z}}}^{-1}(\mathbf{z} - \hat{\mathbf{z}})) \tag{3.26}$$

Integer ambiguity validation is the process of determining whether the candidate integer ambiguity values are actually correct or not. A validation test should be performed which is usually based on a ratio test called the F-Ratio test. In this test, the ratio of the smallest sum of squared ambiguity residual and the second smallest is tested against a specific threshold (Teunissen & Tiberius, 1994).

A method of ambiguity *bootstrapping* is widely used and adopted to determine a lower bound of the probability of correctly resolving the ambiguities, or the probability of correct fix (PCF) (O'Keefe et al., 2006; Verhagen, 2005). The evaluation is based on the following expressions:

$$P(\mathbf{a}_B = \mathbf{a}) = \prod_{i=1}^{n} \left(2\Phi\left(\frac{1}{2\sigma_{\hat{\mathbf{a}}_{i|I}}} \right) - 1 \right) \tag{3.27}$$

$$\Phi(x) = \frac{1}{\sqrt{2\pi}} \int_{-\infty}^{x} e^{-\frac{1}{2}n^2} dn \tag{3.28}$$

In Equation (3.27), $\mathbf{a}_B$ is the bootstrapped integer ambiguity vector, n is the number of ambiguities to be resolved, $\sigma_{\hat{\mathbf{a}}_{i|I}}$ is the conditional standard deviation of ambiguity i conditioned on the previous $I = (1,2,\dots,i-1)$ambiguities, and $\Phi(x)$ describes the area under the normal distribution up to point x. Fortunately, the bootstrapped-based bound on PCF is effectively a by-product of the LAMBDA algorithm and thus is the approach used in this thesis.

Once the computed integer ambiguities are accepted, the fixed position, fixed velocity, and fixed UWB errors are calculated as the last step in carrier phase positioning based on the above fixed integer ambiguities. The fixed estimates and their variance can be formulated as

$$\begin{aligned} \mathbf{b} &= \hat{\mathbf{b}} - Q_{\hat{\mathbf{b}}\hat{\mathbf{a}}} Q_{\hat{\mathbf{a}}}^{-1} \left(\hat{\mathbf{a}} - \mathbf{a} \right) \\ Q_{\mathbf{b}} &= Q_{\hat{\mathbf{b}}} - Q_{\hat{\mathbf{b}}\hat{\mathbf{a}}} Q_{\hat{\mathbf{a}}}^{-1} Q_{\hat{\mathbf{a}}\hat{\mathbf{b}}} \end{aligned} \tag{3.29}$$

where $\hat{\mathbf{b}}$ and $Q_{\hat{\mathbf{b}}}$ are the float position solution vector and covariance matrix, $\mathbf{b}$ and $Q_{\mathbf{b}}$ are fixed position solution vector and covariance matrix.

Figure 3.4 shows the flowchart of solution using carrier phase DGPS and UWB ranging measurement in this research.

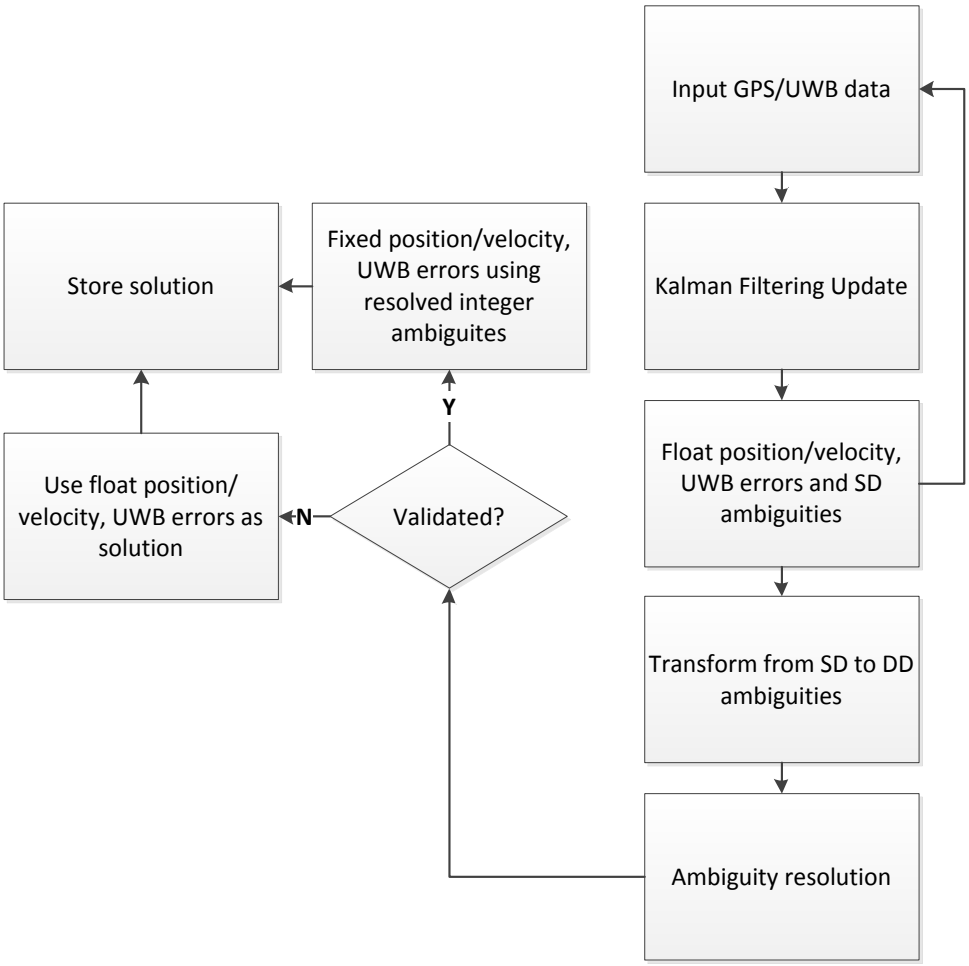

Figure 3.4 Flowchart of solution using carrier phase DGPS and UWB ranging measurement

CHAPTER 4: VEHICLE-TO-INFRASTRUCTURE RELATIVE POSITIONING TESTS

To assess the performance of the proposed GPS/UWB integrated system, this chapter will present the conditions and setup of V2I applications. A brief overview of V2I positioning concepts and fundamentals are introduced. In the following, it gives a description of the different test scenarios and data processing strategies.

4.1 V2I Positioning Concept

The V2I concept has been introduced in Section 1.1 . In this research, infrastructure points in V2I architecture are assumed to transmit UWB ranges, DGPS corrections as well as their coordinates to the land vehicle. Therefore, position and velocity relative to these infrastructure points can be directly determined. For example, as shown in Figure 4.1, when a vehicle enters the coverage areas of infrastructure points (i.e. UWB radios in this case), it will measure the UWB ranges, and receive DGPS corrections and the coordinates of the infrastructure points. Additional information such as the distance between the UWB radios and the next intersection in the along track direction may also be provided. After processing the UWB ranges and GPS data, the vehicle will obtain the relative position and velocity to the intersection or other points of interest. The vehicle or driver can then use this information for various purposes, as discussed in Section 1.1 .

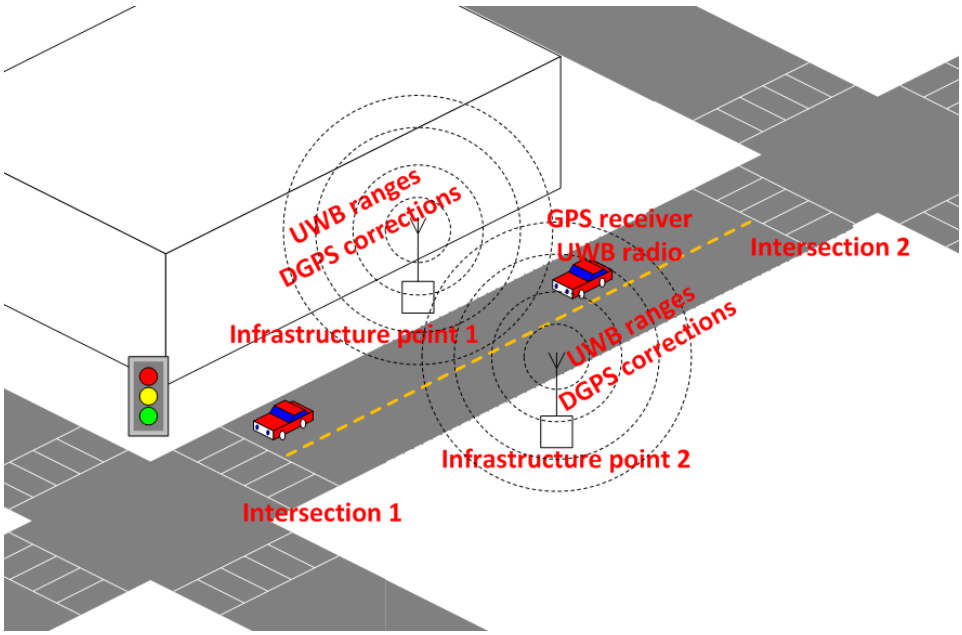

Figure 4.1 Example of V2I relative positioning using DGPS and UWB ranges from side-by-side infrastructure points

In a setup similar to that shown in Figure 4.1, several questions arise. For example, *what is the impact of the UWB radio geometry on performance? Where should the radios be located relative to the intersection? How many radios should be deployed in order to reduce cost? What is the effect of the operating range of the UWB radios? Does the operating range of the UWB radios (both before and after the radios) affect results?* In this thesis, different setups/configurations are considered, namely A) both radios are located at the intersection, B) both radios are located across the road from each other in the midway between the two intersections, C) one radio is located in the midway of the two intersections, and D) one radio is located across the road in the midway of the two intersections, and another at the intersection. By changing the *initial* distance at which DGPS corrections and UWB ranges are available, the impact of operating range of the radios is also assessed. These configurations are discussed in detail in the following section.

4.2 Test Scenarios

4.2.1 Scenario A

Scenario A consists of a T-shaped trajectory centered on an intersection west of the University of Calgary main campus (see Figure 4.5). Two stationary UWB radios were deployed at the northwest (NW) and northeast (NE) corners of the intersection.

The test was conducted on October 14, 2010 on the campus of University of Calgary for approximately one hour. It was performed in an open sky environment. The vehicle was equipped with two geodetic-grade GPS receivers, a consumer-grade GPS receiver, two UWB radios and a reference system (inertial system) including data logging computers as shown in Figure 4.2. The two stations in the intersection were each equipped with a UWB radio and a geodetic-grade GPS receiver. The GPS antennas that were co-located with UWB radios were mounted directly above the UWB radios such that the GPS baseline and inter-radio distance were parallel (and equal in length) when the vehicle was level as shown in Figure 4.3. Table 4.1 summarizes the data collected and the purpose of each data source. Figure 4.4 describes the schematic diagram of the V2I setup implemented for all test scenarios.

Figure 4.2 GPS antenna, UWB, and IMU equipment setup on the test vehicle

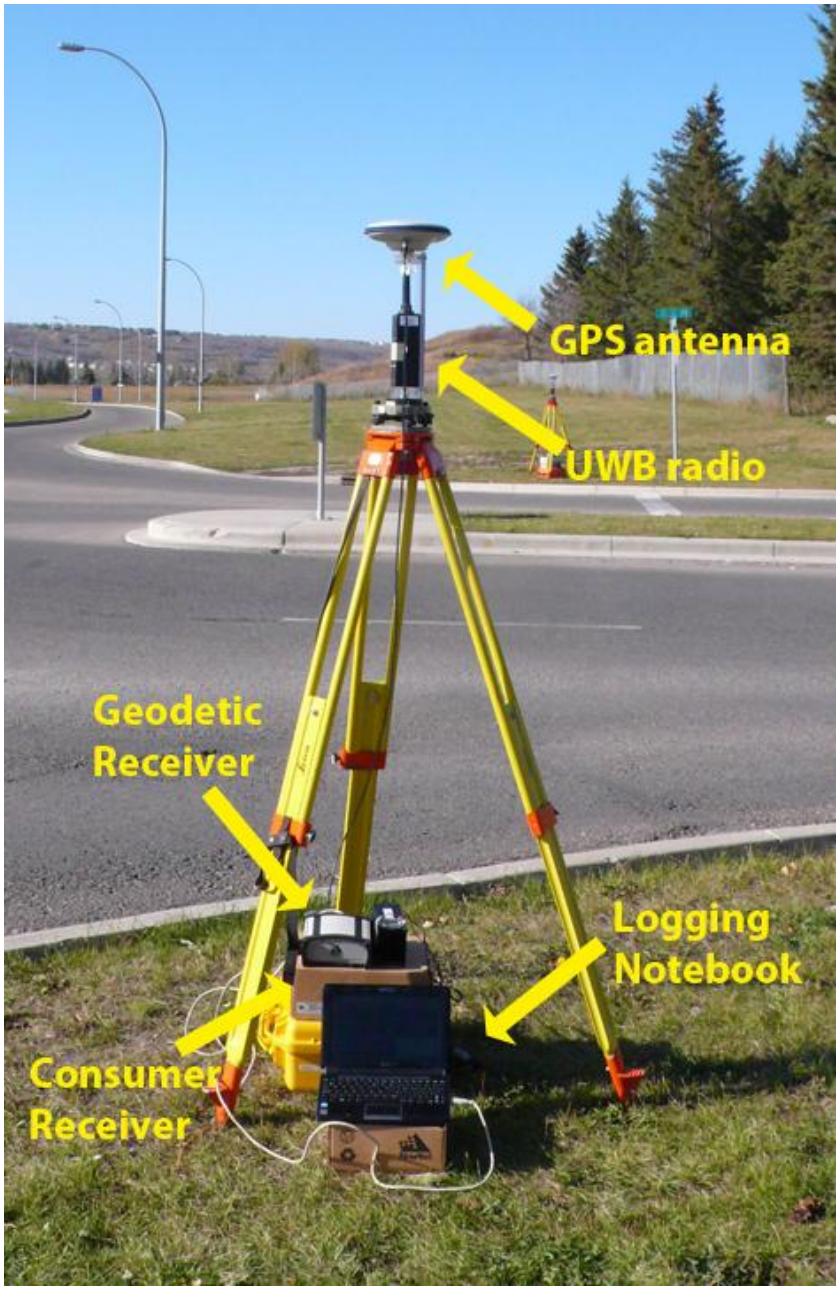

Figure 4.3 GPS receiver and UWB radio setup at one of the infrastructure points

Table 4.1 Summary of systems, data rate and purpose for V2I test

System	Data Rate	Purpose
3 Geodetic-Grade GPS Receivers	10 Hz	One in the vehicle for time tagging UWB data, others at stationary UWB points to observe UWB point locations.
3 Consumer-Grade GPS Receivers	1 Hz	Comparison with geodetic-grade GPS receivers. One in the vehicle, others at stationary UWB points to observe UWB point locations.
1 Geodetic-grade GNSS/INS System	100 Hz	Located in the vehicle for generating vehicle reference solution.
3 UWB Radios	5Hz (approximately)	One in the vehicle, others at stationary UWB points to observe UWB measurements for processing.

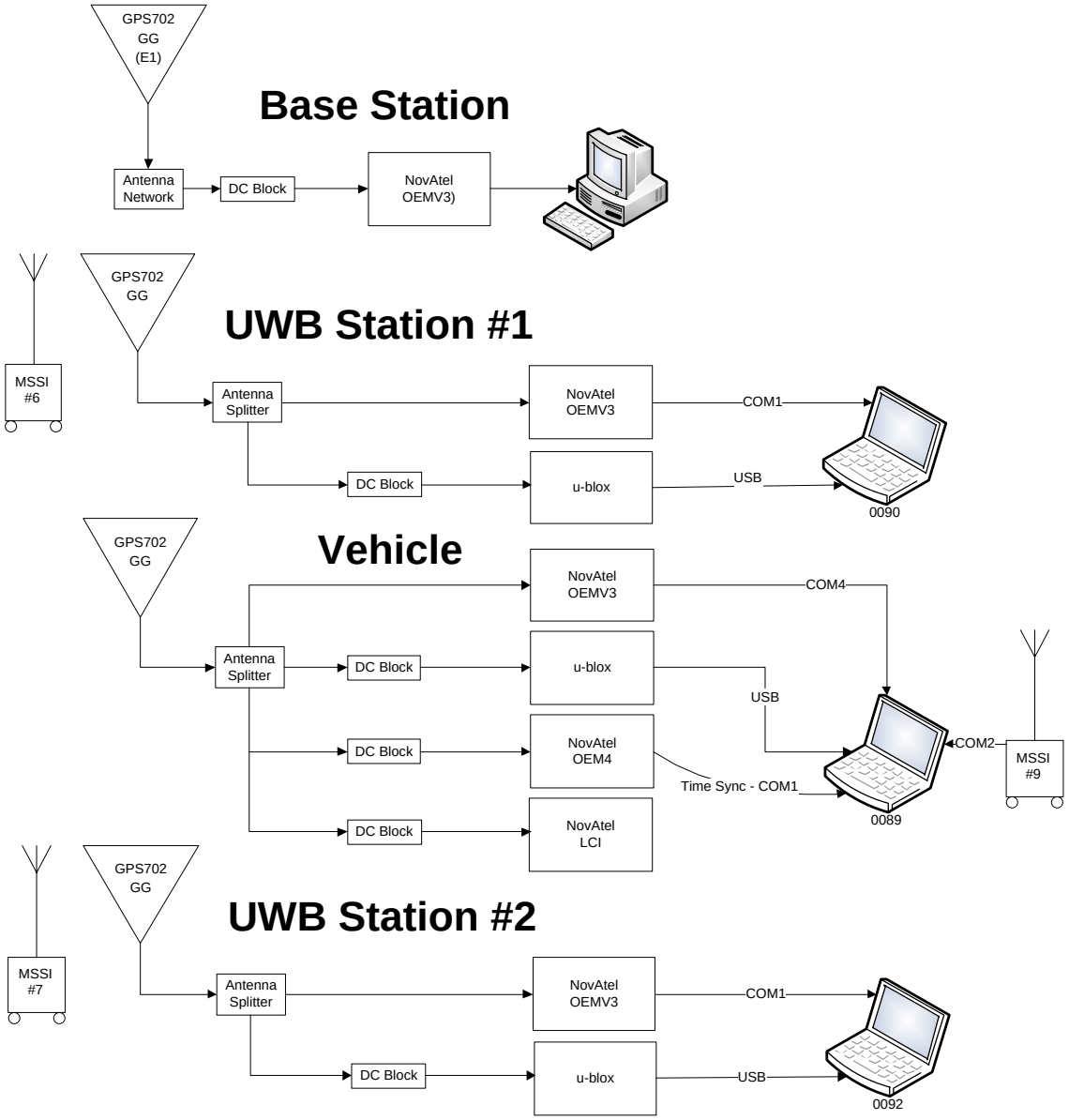

Figure 4.4 Schematic diagram of the V2I setup applied for all the scenarios

The test trajectory of scenario A is shown in Figure 4.5. With reference to the figure, the analysis of the results is presented according to the "approach geometry" of the vehicle as it travels through the intersection, namely: North to West (10 runs), East to West (10 runs), East to North (10 runs), and West to East (20 runs). These approaches were used for the main reason that the

geometry of the UWB stations as seen from the vehicle is different depending on the approach geometry. As such, considering each approach geometry separately will help to isolate the effect of UWB measurement geometry on the overall solution.

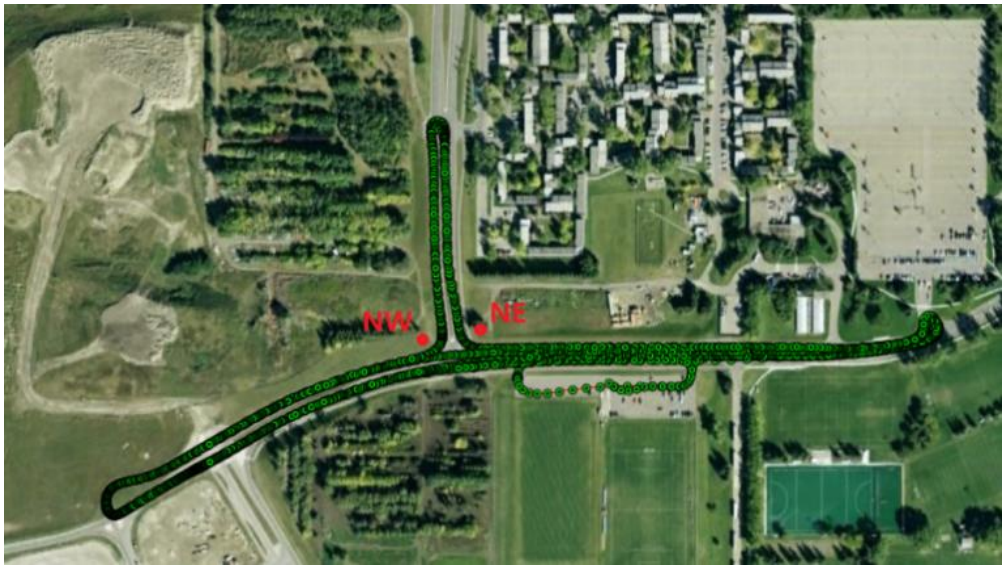

Figure 4.5 Open sky field test route with infrastructure points marked for Scenario A (October 14, 2010) – Google Earth

4.2.2 Scenario B

Scenario B was implemented in order to improve the deployment of UWB radios from Scenario A, as we will discuss in Section 5.1. It consisted of a north-south rural road on the outskirts of Calgary with two UWB radios located on either side of the road roughly 300 m north of a fictitious intersection. This configuration was chosen to test where the radios should be deployed relative to an existing intersection based on the results of this scenario. This setup allows for characterizing performance as the vehicle approaches and departs from the radios, which, as will

be shown later, provides useful information for how such a system should be deployed in an operational setting.

Additionally, unlike Scenario A, this scenario will test the usefulness of longer range (i.e. 300 m) UWB measurements. In principle, having UWB range measurements available for a longer period (i.e., over a larger range of distances between the vehicle and the infrastructure point) will allow for better observability of the two UWB systematic errors, namely bias and scale factor. However, long range UWB measurements have previously been found to be subject to increased multipath, and in some case non-line-of-sight propagation (in the case where a crest in the road blocked the line of sight).

In order to test the usefulness of longer UWB ranges, UWB range data was collected whenever available, but in processing, both UWB and differential carrier phase GPS processing was only carried out when the vehicle was within a specified distance of the UWB radio (considered to be the infrastructure point and also the source of range-limited DGPS corrections). Initial baseline lengths of 25, 50, 100, 200, and 300 metres were considered, corresponding approximately to ¼, ½, 1, 2, and 3 short blocks in a typical North American city. It was assumed that after UWB measurements and DGPS corrections were acquired at these ranges, that these two types of measurement would remain available until the vehicle reached the intersection, approximately 300 m beyond the (first) UWB radio. In addition, this allows for an assessment of performance for extended periods beyond the radios, thus providing insight into possible deployment scenarios.

The data was collected in an open sky environment on a rural road in Springbank, suburb to the northwest of Calgary on June 1, 2012. The configuration is shown in Figure 4.6. Two infrastructure points (i.e., UWB radios) were deployed on opposite sides of the road separated by about 10 m. The UWB radios were located approximately halfway along the length of the test trajectory. The test vehicle, equipped with the third UWB radio, in addition to GPS receivers and a GPS/INS reference system then drove in loops between the north and the south end of the test area with 10 times.

For the purpose of comparing the performance between different GPS receivers, the test vehicle and the two infrastructure points were equipped with a Geodetic-Grade GPS receiver and a low-cost Consumer-Grade GPS receiver. Another Geodetic-Grade GPS receiver was set as the reference station on the roof of the CCIT building at the University of Calgary campus. A Geodetic-Grade GNSS/INS integrated system was used for generating the reference trajectory. In addition, the test vehicle and the two infrastructure points were equipped with UWB ranging radios to obtain UWB ranges. Using dedicated data logging software that interfaces with the UWB radio and the GPS receiver as discussed in Section 2.2.5 , the UWB range measurements were able to be accurately time tagged with GPS time. The V2I data collection campaign lasted about half an hour. The data collected is the same as that collected for Scenario A (see Table 4.1).

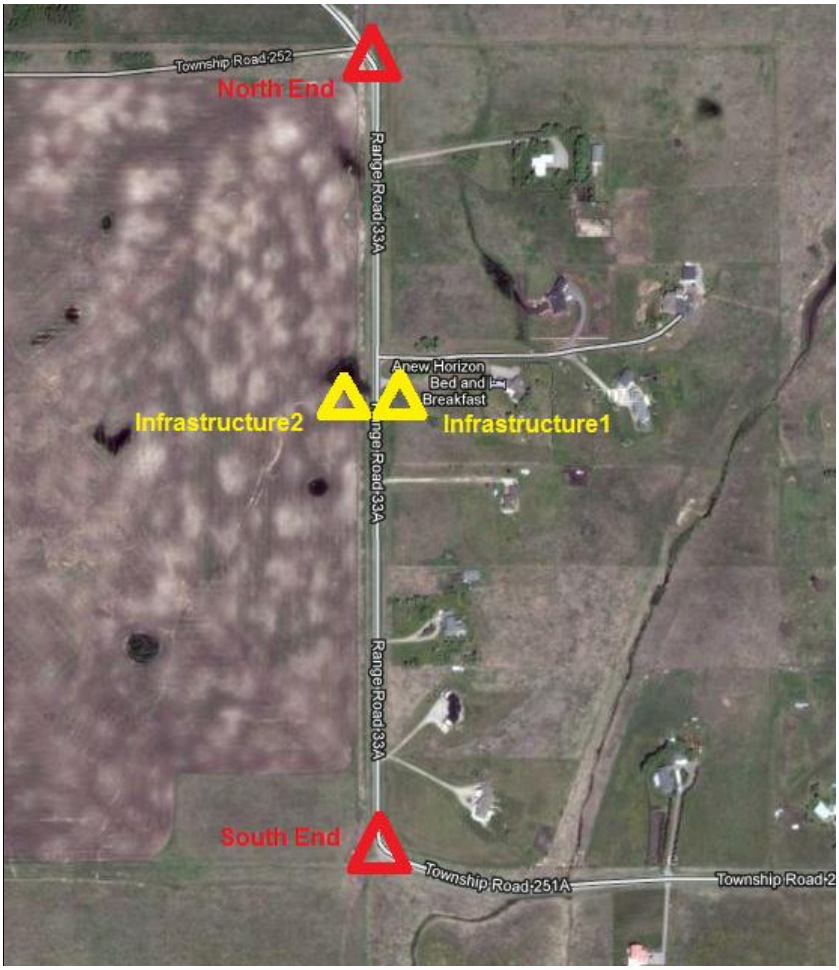

Figure 4.6 Open sky field test location with infrastructure points marked for Scenario B (June 1, 2012) – Google Earth

4.2.3 Scenario C

Scenario C consisted of a north-south rural road on the outskirts of Calgary with only one UWB radio located roughly 300 m north of the intersection, similar to Scenario B. This setup was chosen to investigate the performance of Scenario B with only one UWB radio deployed, and then determine if only one radio would benefit the solution. Data processing for Scenario C is the same as that of Scenario B, but only measurements from one UWB radio was presented. Both UWB and differential carrier phase GPS measurements were carried out when the vehicle was

within a specified distance of the UWB radio (i.e. initial baseline lengths of 25, 50, 100, 200, and 300 metres)

The test location with one infrastructure point marked for Scenario C is as shown in Figure 4.7. One infrastructure point (i.e., UWB radio) was deployed approximately halfway along the length of the test trajectory. The test vehicle, equipped with another UWB radio, in addition to GPS receivers and a GPS/INS reference system then drove in loops between the north and the south end of the test area with 10 times.

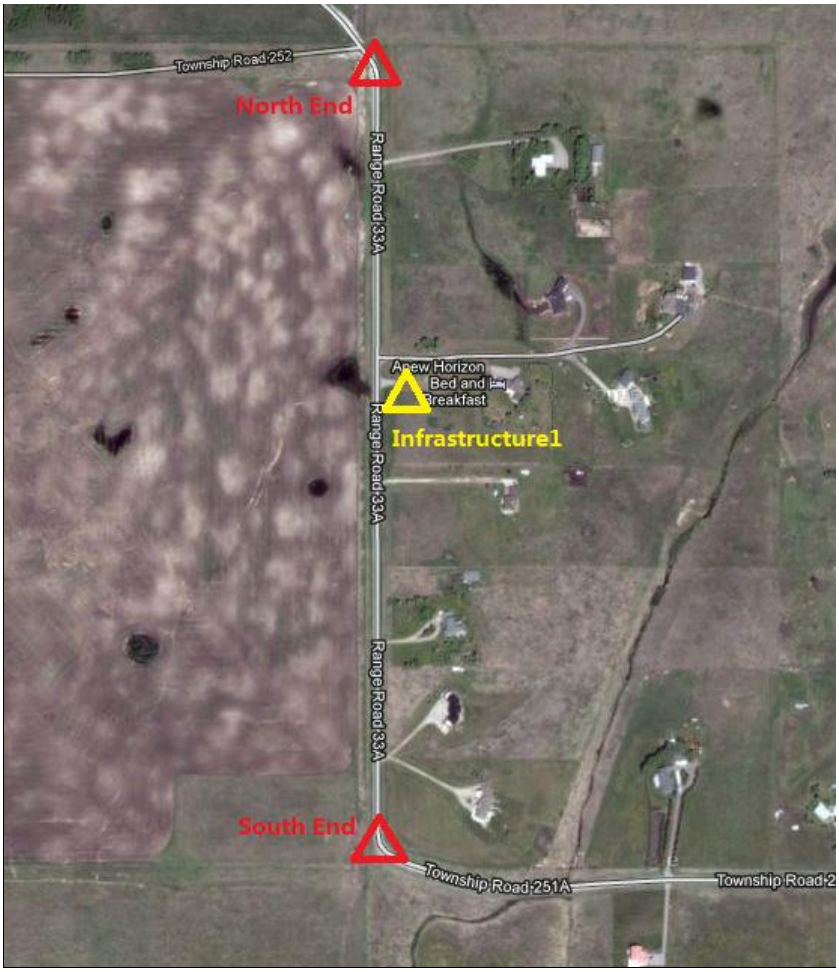

Figure 4.7 Open sky field test location with one infrastructure point marked for Scenario C (June 1, 2012) – Google Earth

4.2.4 Scenario D

Scenario D consisted of a north-south running rural road on the suburb of Calgary with two UWB radios, one located on the side of the road roughly 300 m south of a fictitious intersection, another located near the north intersection.

Scenario D was chosen to test in order to investigate the performance of using the one UWB radio at first, and then switching to another one before approaching the fictitious intersection. This setup will be used to analyse the performance of some cases, where initially only one UWB radio available. This setup will characterize the performance as the vehicle approaches and departs from one UWB radio, applies the overlapping data and then switches to another radio, which could provide useful information on the ideal deployment distance between two UWB radios. UWB range data was collected with its full range, and both UWB and differential carrier phase GPS was implemented when the vehicle was within a specified distance from either of the two UWB radios. Initial baseline lengths of 25, 50, 100, 200, and 300 metres were considered similar to the Scenario B.

The test trajectory is shown in Figure 4.8. The V2I data collection campaign lasted about half an hour and a summary of the data collected is the same with Scenario A and B as shown in Table 4.1.

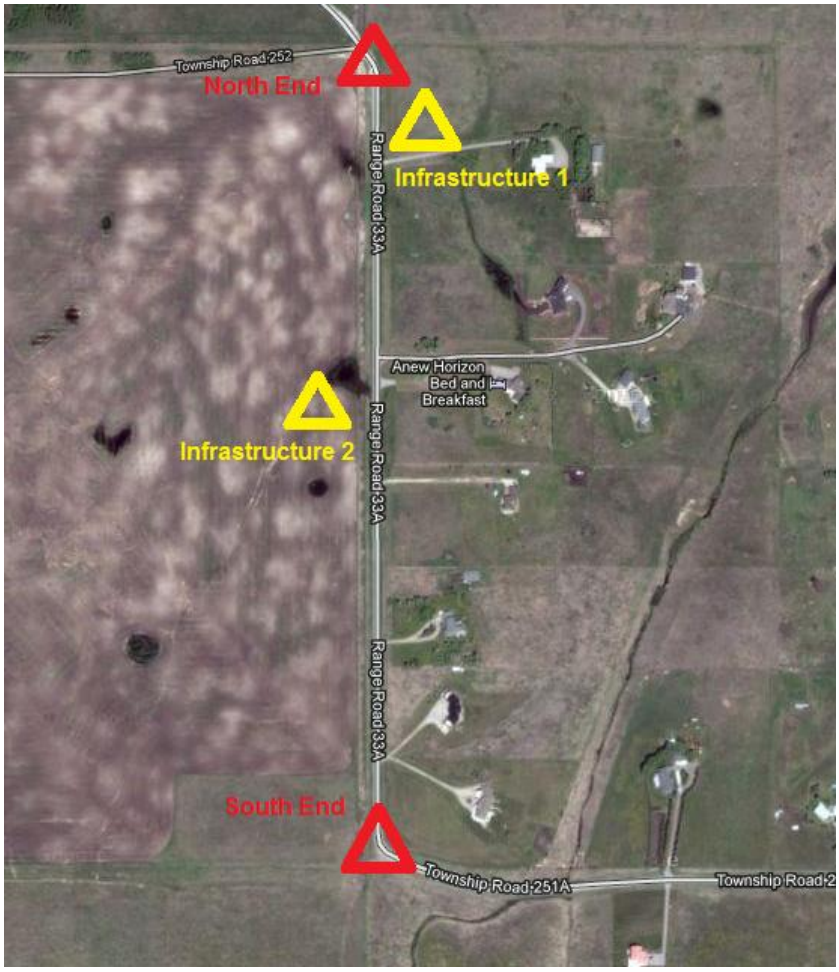

Figure 4.8 Open sky field test location with infrastructure points marked for Scenario D (June 1, 2012) – Google Earth

4.3 Data Processing

The reference solution for all tests was computed from GPS/INS data using commercial GNSS/INS post-processing software. A GPS/GLONASS base station was located on the roof of the Calgary Centre of Innovative Technology (CCIT) building at University of Calgary and was equipped with a high quality dual-frequency Geodetic-Grade receiver connected to a Geodetic-Grade GPS/GLONASS antenna. The reference positions of the vehicle were obtained by using

carrier-phase measurements from the Geodetic-Grade GPS/GLONASS receiver and IMU measurements from the INS. The resulting position is accurate to several centimetres. The locations of the UWB radios were computed with similar accuracy using GPS carrier phase measurements made at these locations. Using the "known" locations of the vehicle and the UWB radios, the reference ranges between the vehicle and each UWB radio were computed for comparison with the actual UWB ranges measured by the UWB radios.

The integration algorithm described in Section 3.3 was implemented in software developed by the Positioning, Location And Navigation (PLAN) group at University of Calgary. Processing of the V2I data was done using the University of Calgary's existing GPS+UWB software. The software treats the velocity and clock drift states as first-order Gauss-Markov processes, position and clock offset are then driven by velocity and clock drift states (integrated Gauss-Markov processes) (Brown and Hwang 1997). The software is able to process the GPS data alone or augmented with UWB ranges. The key processing parameters used are obtained by analyzing the reference solution from the field data collection and are summarized in Table 4.2.

Table 4.2 Summary of Data Processing Parameters

Parameter	Value
Geodetic-grade GPS pseudorange standard deviation	0.8 m
Consumer-grade GPS pseudorange standard deviation	1.5 m
Doppler standard deviation (both receivers)	0.5 Hz
Carrier phase standard deviation (both receivers)	0.08 cycle
UWB standard deviation	0.42 m
Standard deviation of velocity system noise	15 m/s
Velocity system noise correlation time	2 s

For Scenario A, solutions were generated using five different strategies as listed below; the term in brackets will be used to denote the different tests throughout the thesis:

I. GPS-only ("GPS");

II. GPS + UWB estimating the UWB systematic errors using UWB measurements when the vehicle is within 100 m of the intersection ("GPS + UWB (≤100 m)");

III. GPS + UWB estimating the UWB systematic errors when the vehicle was within 200 m of

the intersection ("GPS + UWB (≤200 m)");

IV. GPS + UWB when the vehicle was within 100 m of the intersection but using UWB data corrected a priori with the estimates of the systematic errors computed from the reference solution ("GPS + Corrected UWB (≤100 m)");

V. GPS + UWB when the vehicle was within 200 m of the intersection but using UWB data corrected a priori with the estimates of the systematic errors computed from the reference solution ("GPS + Corrected UWB (≤200 m)").

The fourth and fifth strategies simulate the performance of a system without (or with smaller) systematic errors (details below). Although it represents an ideal case, it also provides a performance benchmark against which other UWB-based results can be compared.

Four travelling directions, each with several runs were performed in this test namely:

A. Travelling from the North to South and then turning at the intersection to the West (10 repeats);

B. Travelling from the East and going straight through the intersection to the West (10 repeats);

C. Travelling from the East to West and then turning at the intersection to the North (10 repeats);

D. Travelling from the West and going straight through the intersection to the East (20 repeats).

For the remainder of the thesis, the above runs are referred to as Trajectories A to D.

For Scenario B, C and D, solutions were generated using ten different strategies as listed below. The term in brackets will be used to denote the different tests throughout the thesis:

I. GPS-only when the vehicle is within 25 m from the first UWB radio ("GPS-only (baseline ≤25 m)");

II. GPS-only when the vehicle is within 50 m from the first UWB radio ("GPS-only (baseline ≤50 m)");

III. GPS-only when the vehicle is within 100 m from the first UWB radio ("GPS-only (baseline ≤100 m)");

IV. GPS-only when the vehicle is within 200 m from the first UWB radio ("GPS-only (baseline ≤200 m)");

V. GPS-only when the vehicle is within 300 m from the first UWB radio ("GPS-only (baseline ≤300 m)");

VI. GPS + UWB estimating the UWB systematic errors using UWB measurements when the vehicle is within 25 m from the first UWB radio ("GPS + UWB (baseline ≤25 m)");

VII. GPS + UWB estimating the UWB systematic errors when the vehicle was within 50 m from the first UWB radio ("GPS + UWB (baseline ≤50 m)");

VIII. GPS + UWB estimating the UWB systematic errors when the vehicle was within 100 m from the first UWB radio ("GPS + UWB (baseline ≤100 m)");

IX. GPS + UWB estimating the UWB systematic errors when the vehicle was within 200 m from the first UWB radio ("GPS + UWB (baseline ≤200 m)");

X. GPS + UWB estimating the UWB systematic errors when the vehicle was within 300 m from the first UWB radio ("GPS + UWB (baseline ≤300 m)");

For the remainder of the thesis, the above different strategies are referred to as Strategies I to X.

CHAPTER 5: RESULTS AND ANALYSIS

Four test scenarios were described and the corresponding data was collected as discussed in the previous chapter. To assess the performance of the proposed GPS/UWB integrated system for V2I application, the results of the four test scenarios are presented in this chapter. A performance comparison between the two types of receivers (i.e. Geodetic-Grade GPS and Consumer-Grade GPS) for Scenario B, C and D is made in terms of positioning accuracy, probability of correct fix and ambiguity resolution.

The results in this section are primarily presented as a function of distance. The reasons are that this research work is interested in assessing positioning accuracy relative to fixed infrastructure equipped with UWB radios and the distance to these infrastructure points is a more general parameter compared to time. In addition, by understanding the relationship of the results as a function of distance, the results can be easily scaled for different vehicle velocities. With this in mind, unless otherwise stated, the "distance" used for the x-axis of plots is the distance to the first UWB station. Furthermore, negative distances correspond to the vehicle is approaching the first UWB radio and positive distances correspond to the vehicle moving away from the radio.

5.1 Scenario A Results

The analysis begins by looking at the float solution quality. This information is useful for interpreting the benefits of the UWB data, especially given the different configurations. To the end, using corrected UWB ranging measurements vs. estimating UWB systematic errors and using uncorrected ranging UWB measurements up to 100 m vs. 200 m on the float solutions for

10 runs are shown in Figure 5.1 and Figure 5.2, where the vehicle is travelling from the North and turning at the intersection to the West. Similar results are shown for the East to West, North to West and West to East runs.

In each of these figures, the GPS only float error in the North direction is shown above and in the lower two subplots the corresponding float solution position estimates are shown for the four GPS + UWB cases (see Section 4.3). The results of east and vertical GPS-only float solution compared to GPS + UWB measurements (with errors estimated in run), GPS + corrected UWB measurements (with errors estimated in advance) up to 100 m and 200 m for Trajectory A (North to West) are shown in Figure A.1 to Figure A.4 in APPENDIX A.

It should be noted that in the 100 m UWB cases, the float solutions before -100 m (where negative represents approaching the intersection) are identical until UWB measurements are incorporated and change the solution. This is not seen in the two 200 m cases as UWB measurements are available immediately in some cases.

The best results are seen in the two corrected cases, where the UWB systematic errors are not being estimated and thus the full weight of the UWB ranging measurements can be applied to the position solution. In the two cases where UWB systematic errors are being estimated, in several runs the 100 m case outperforms the 200 m case. This is due to UWB visibility and multipath problems over longer ranges, and unlike the case where the systematic errors have been removed a priori, when the errors are being estimated, multipath errors can be misinterpreted as a bias or scale factor error by the filter. It is clear that the improvement of position solutions does not

occur until either around 75 metres before the intersection (two cases using corrected UWB ranges), or about 25 metres away after the vehicle has passed through the intersection (two cases estimating UWB errors). For the two cases estimating UWB errors, it confirms that the period during which a vehicle approaches an intersection is not sufficient to converge to a precise solution, even with assistance from UWB ranges (while with GPS alone a cm-level solution is impossible), which suggests that the UWB radios should be located some distances away from the intersection.

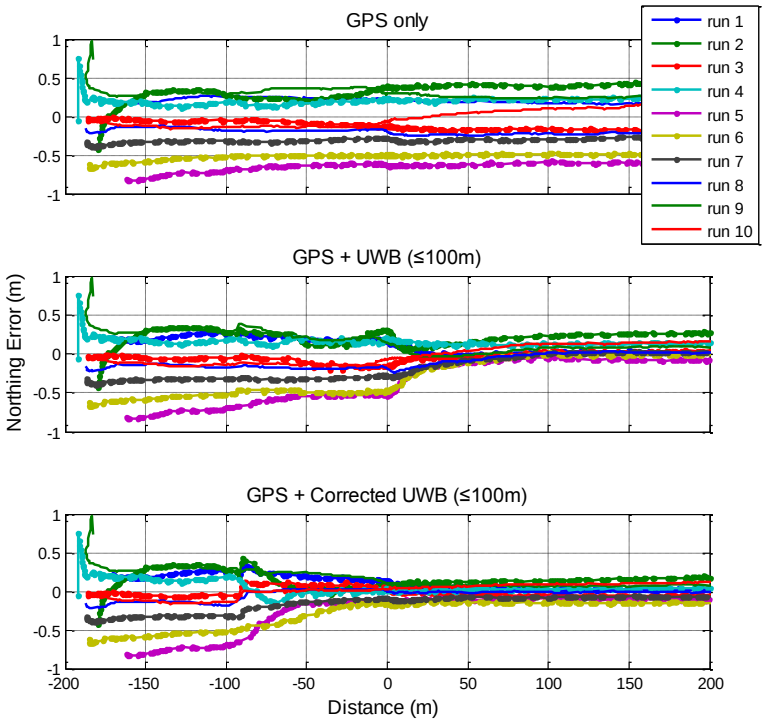

Figure 5.1 Northing float solution GPS-only compared to GPS + UWB measurements (with errors estimated in run), GPS + corrected UWB measurements (with errors estimated in advance) up to 100 m for Trajectory A (North to West)

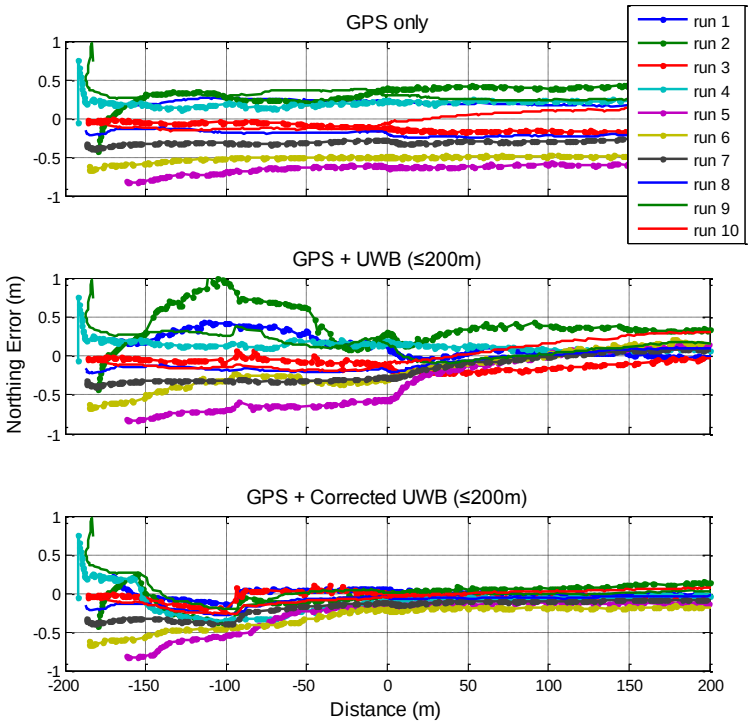

Figure 5.2 Northing float solution GPS-only compared to GPS + UWB measurements (with errors estimated in run), GPS + corrected UWB measurements (with errors estimated in advance) up to 200 m for Trajectory A (North to West)

The RMS position errors for all three components (i.e., North, East and vertical) as a function of distance to the intersection are shown in Figure 5.3 and Figure 5.4 shows the 2DRMS errors as a function of distance relative to the intersection for all the trajectories, namely, Trajectory A (North to West), Trajectory B (East to West), Trajectory C (East to North), and Trajectory D (West to East) (see Section 4.3).

Each of these figures show the RMS error computed over all runs of the particular vehicle approach geometry within 5 meter range intervals for each of the five processing strategies. Several patterns need to be noted. First, the RMS error improves as a function of distance for almost all cases, with some variability due to small sample size. Secondly, the vertical component has both the largest errors and the least improvement among all the components due to the UWB ranges contributing less in vertical direction. The five strategies show improvements in the following order. GPS alone consistently provides the poorest result, followed by 100 m UWB (with systematic errors being estimated), followed by 200 m UWB followed by 100 m UWB with a priori corrected ranges. 200 m UWB with corrected ranges is consistently the best performer, within the level of variability of the RMS estimates. Finally, the improvement is most noticeable in the horizontal direction of the approach to the intersection.

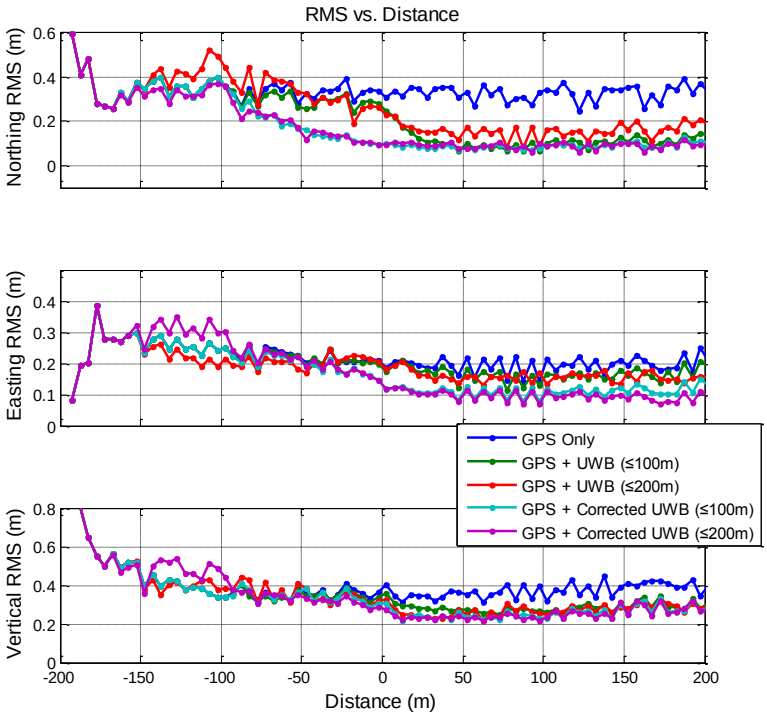

Figure 5.3 RMS position errors for all three components vs. distance to the intersection for Trajectory A (North to West)

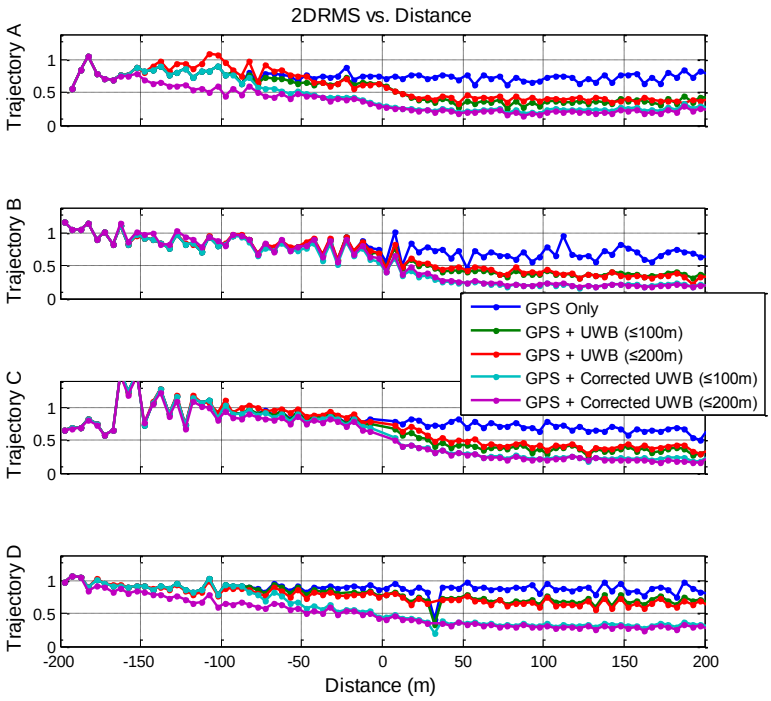

Figure 5.4 2DRMS position errors vs. distance to the intersection for all trajectories

The improvements in RMS and median errors of GPS + UWB compared to GPS-only (I) solution at intersection for all trajectories and travelling directions are shown in Table 5.1 and Table 5.2. Cases where an improvement occurs are positive values expressed as a percentage, while degradation is a negative value, for GPS + UWB solution with different trajectories and travelling directions. The percentage values are calculated by subtracting values between GPS + UWB and GPS-only solution (e.g. RMS and median errors in this case), and then divided by GPS-only solution. Of primary interest to this research is that adding the UWB ranges provides improvements in float solution.

For trajectory A (North to West), GPS and UWB integrated systems can improve RMS and median errors relative to the GPS-only case in all the data processing strategies (i.e. “GPS”, “GPS + UWB (≤100 m)”, “GPS + UWB (≤200 m)”, “GPS + Corrected UWB (≤100 m)”, “GPS + Corrected UWB (≤200 m)”) and directions (i.e. North, East, Vertical). Of all the five strategies for improvement in RMS errors, GPS + UWB (≤100 m) and UWB (≤200 m) (with systematic errors being estimated) provides less improvements than GPS + UWB with a priori corrected ranges. It is noted that the east median error is improved significantly (e.g. 2160.8% for GPS + UWB (≤200 m)), because the GPS-only results are already quite good, the improvement percentage (by subtracting GPS + UWB from GPS-only solution and then divided by GPS-only solution) will result in large percentage values, vice versa (e.g. median error of -490.9% and -515.9% for GPS + Corrected UWB (≤100 m) and GPS + Corrected UWB (≤200 m), respectively).

For trajectory B (East to West), it is shown that adding the UWB ranges provides improvements in RMS and median errors relative to the GPS-only case in most of the data processing strategies, however it is degraded in vertical RMS error for GPS + UWB (≤200 m), north median error for GPS + UWB (≤100 m), and east median error for GPS + UWB (≤200 m). Similar results are shown for trajectory C (East to North) and trajectory D (West to East).

Table 5.1 Improvement in RMS errors (positive values means improvement, negative means degradation) of GPS + UWB compared to GPS-only (I) solution at intersection for all trajectories and travelling directions

Trajectory	Direction	I (m)	II (%)	III (%)	IV (%)	V (%)
A (North to West)	Horizontal	0.360	17.3%	19.9%	59.6%	62.0%
	North	0.311	20.7%	26.7%	67.9%	70.2%
	East	0.187	6.8%	2.7%	37.2%	38.0%
	Vertical	0.403	11.2%	18.7%	23.9%	31.6%
B (East to West)	Horizontal	0.282	14.6%	15.9%	26.6%	25.4%
	North	0.254	13.9%	14.1%	23.8%	21.9%
	East	0.129	14.7%	8.8%	52.7%	47.3%
	Vertical	0.456	1.4%	-7.2%	2.5%	5.8%
C (East to North)	Horizontal	0.390	13.7%	7.6%	30.9%	34.5%
	North	0.360	14.1%	12.7%	27.2%	26.0
	East	0.247	10.1%	-18.6%	62.4%	70.6%
	Vertical	0.398	18.1%	3.5%	20.7%	18.3%
D (West to East)	Horizontal	0.443	5.0%	11.1%	50.2%	52.9%
	North	0.392	12.7%	15.8%	40.4%	38.1%
	East	0.246	-3.5%	6.2%	42.9%	48.5%
	Vertical	0.565	-3.3%	5.1%	18.8%	18.8%

I. GPS-only ("GPS");
II. GPS + UWB estimating the UWB systematic errors using UWB measurements when the vehicle is within 100 m of the intersection ("GPS + UWB (≤100 m)");
III. GPS + UWB estimating the UWB systematic errors when the vehicle was within 200 m of the intersection ("GPS + UWB (≤200 m)");
IV. GPS + UWB when the vehicle was within 100 m of the intersection but using UWB data corrected a priori with the estimates of the systematic errors computed from the reference solution ("GPS + Corrected UWB (≤100 m)");
V. GPS + UWB when the vehicle was within 200 m of the intersection but using UWB data corrected a priori with the estimates of the systematic errors computed from the reference solution ("GPS + Corrected UWB (≤200 m)").

Table 5.2 Improvement in median error (positive values means improvement, negative means degradation) of GPS + UWB compared to GPS-only (I) solution at intersection for all trajectories and travelling directions

Trajectory	Direction	I (m)	II (%)	III (%)	IV (%)	V (%)
A (North to West)	Horizontal	0.253	25.3%	17.1%	49.2%	48.9%
	North	0.216	42.8%	73.9%	79.0%	104.2%
	East	-0.003	603.7%	2160.8%	437.2%	452.2%
	Vertical	-0.339	9.1%	11.3%	22.6%	30.3%
B (East to West)	Horizontal	0.219	3.2%	14.7%	50.3%	44.3%
	North	0.117	-8.8%	68.9%	34.6%	28.6%
	East	-0.078	10.3%	-3.75%	52.4%	71.4%
	Vertical	-0.067	167.0%	337.5%	184.6%	184.6%
C (East to North)	Horizontal	0.216	54.3%	-86.7%	-27.0%	5.6%
	North	-0.033	68.8%	307.9%	42.9%	260.7%
	East	-0.110	24.2%	-113.0%	90.2%	116.5%
	Vertical	-0.171	7.0%	53.8%	16.5%	-14.2%
D (West to East)	Horizontal	0.070	-413.0%	22.0%	22.1%	1.9%
	North	0.027	353.2%	90.5%	-490.9%	-515.9%
	East	-0.132	25.6%	7.7%	85.5%	113.4%
	Vertical	-0.370	27.9%	3.9%	30.4%	26.0%

Now that all of the different float solutions have been discussed, the next step is to assess ambiguity resolution performance. In the remainder of this thesis, the "true" ambiguities are obtained by taking the last epoch estimates of the ambiguities. The time required to fix ambiguities for each run when the vehicle was travelling Trajectory A (North to West), Trajectory B (East to West), Trajectory C (East to North), and Trajectory D (West to East) can be seen in Appendix A from Table A.1 to Table A.4. Note that in these tables, improvements relative to the GPS-only case are highlighted in green, whereas degradations are highlighted in red. From these tables it can be seen that the addition of UWB ranges, regardless of the strategy results in more and faster ambiguity resolution. In addition, figures are provided later (starting with Figure 5.5) that summarize the main results of the tables more clearly.

The overall conclusion that can be drawn from these results is that the addition of UWB ranges, regardless of the strategy being used, results in an increase in ambiguity fixes for approaches to intersections. Specifically, only a very small number of incorrect fixes occur compared to GPS alone. More importantly, Table A.5 shows that the addition of UWB measurements speeds up the ambiguity resolution process and makes ambiguity resolution before or soon after the vehicle passes through the intersection more likely.

In order to make these results easier to view, the main results of these tables have been plotted as bar charts in Figure 5.5 and Figure 5.6. Figure 5.5 shows the number of times that correct, incorrect and no ambiguity fixes occur for each of the UWB strategies and Figure 5.6 shows the change in ambiguity resolution relative to GPS-only case for Trajectory A (North to West) approach geometry. The results of all the other trajectories (i.e. B, C and D) can be seen in Figure A.5 to Figure A.10. All four approaching geometries are shown in Figure 5.7. The addition of UWB increases the number of ambiguity fixes, though some incorrect fixes still do occur. Figure 5.6 and Figure 5.8 compare each of the UWB strategies to GPS-alone to show the changes resulting from the UWB measurements for Trajectory A and all the trajectories.

For Trajectory A, the addition of UWB measurements results in the correction of an incorrect GPS-only ambiguity fix in 2 cases out of 40 runs (4 UWB augmentation strategies for 10 runs) considered. There are 2 cases where an incorrect GPS-only fix is converted to a “no fix” result, while in 10 cases a “no fix” becomes a fix, and 10 cases an existing fix is fixed in a shorter amount of time, all the others are remaining the same. For all four trajectories (i.e. A, B, C and

D), the inclusion of UWB measurements results in 2 cases out of 200 runs where an incorrect GPS-only fix becomes correct fix, 5 cases incorrect to “no fix” result, 47 cases no fix” to correct fix and 62 cases an existing fix becomes more quickly, and all the other runs do not change.

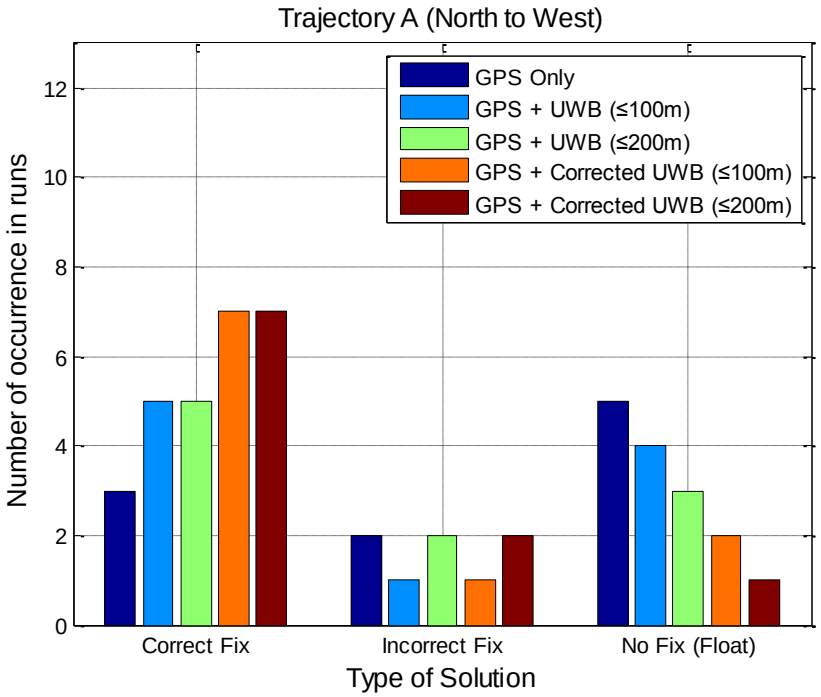

Figure 5.5 Ambiguity resolution for Trajectory A (North to West) approach geometry

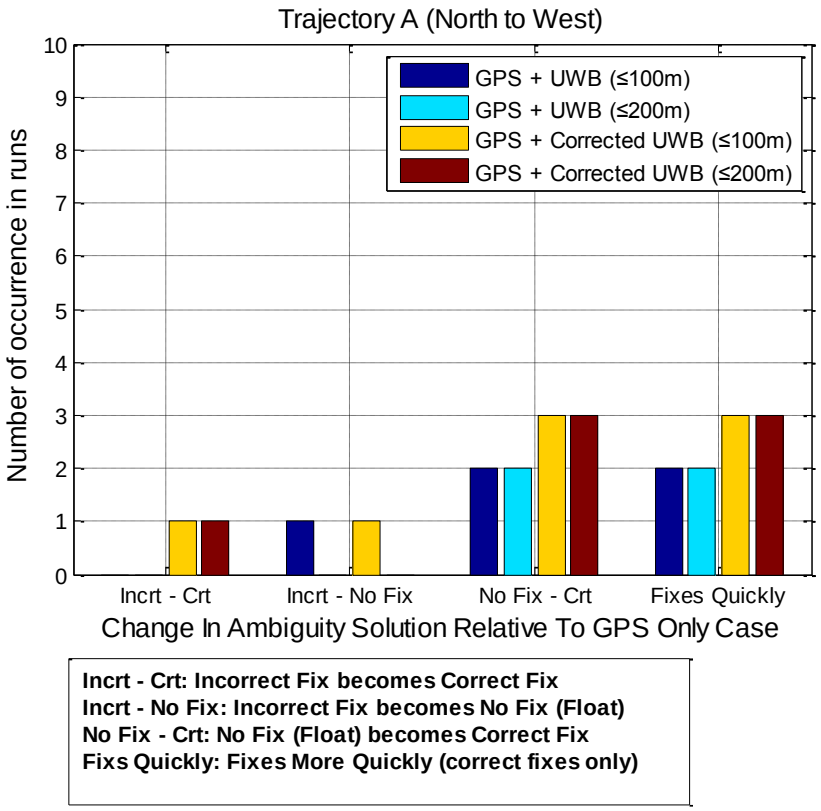

Figure 5.6 Change in ambiguity resolution relative to GPS-only case for Trajectory A (North to West) approach geometry

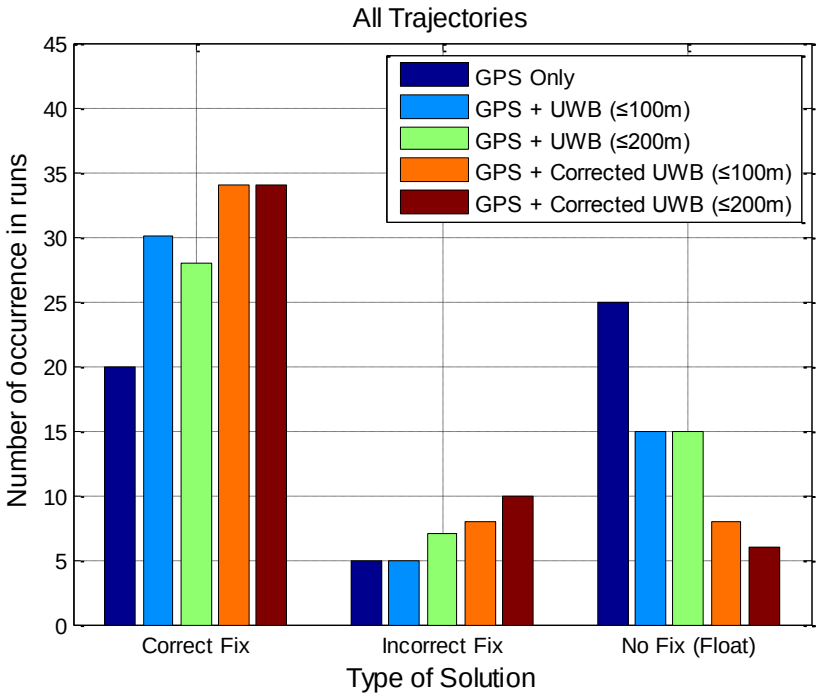

Figure 5.7 Ambiguity resolution for all the approach geometry (Trajectory A (North to West), Trajectory B (East to West), Trajectory C (East to North), and Trajectory D (West to East))

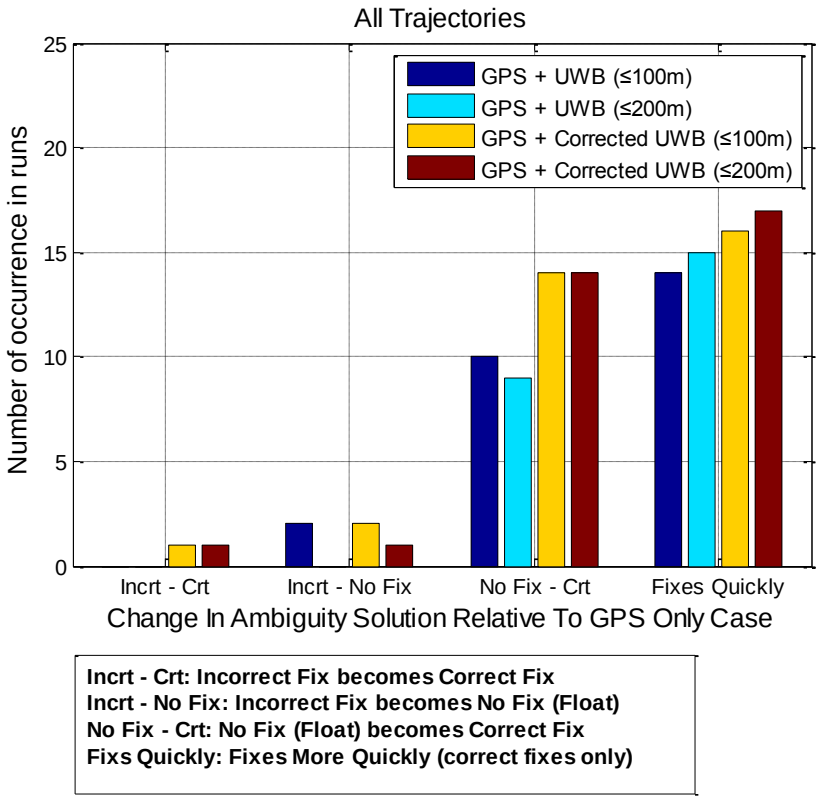

Figure 5.8 Change in ambiguity resolution relative to GPS-only case for all the approaches (Trajectory A (North to West), Trajectory B (East to West), Trajectory C (East to North), and Trajectory D (West to East))

Improvement in average time to first ambiguity fix of GPS + UWB fixed solution compared to GPS-only (I) fixed solution for all trajectories and travelling directions is shown in Table 5.3. The percentage values are computed by subtracting the values of average ambiguity fix time between GPS + UWB fixed solution and GPS-only fixed solution, and then divided by average fix time of GPS-only fixed solution. From the table, it is seen that the inclusion of UWB ranges provides improvements from 10.6% to 50.5% in average time of first ambiguity fix for all trajectories and travelling directions.

Of all the strategies, GPS + UWB (≤100 m) and UWB (≤200 m) (with systematic errors being estimated) provides less improvement than GPS + UWB with a priori corrected ranges. In addition, the solution with longer UWB ranges (with systematic errors being estimated) does not guarantee that ambiguity resolution will be resolved more quickly, which can be seen from the case trajectory A (North to West) and C (East to North).

Table 5.3 Improvement in average time of first ambiguity fix (in seconds) of GPS + UWB fix solution compared to GPS-only (I) fix solution for all trajectories and travelling directions

Trajectory	I (s)	II (%)	III (%)	IV (%)	V (%)
A(North to West)	22.9	24.5%	6.6%	41.5%	50.5%
B (East to West)	38.9	13.9%	29.1%	23.8%	25.5%
C(East to North)	29.9	30.0%	27.0%	30.7%	31.8%
D (West to East)	26.4	10.6%	11.6%	16.8%	24.0%

5.2 Scenario B Results

Scenario B consisted of a north-south rural road on the outskirts of Calgary as discussed in Section 4.2.2, where two infrastructure points (i.e., UWB radios) were deployed on the opposite sides of the road separated by about 10 m. The UWB radios were located approximately halfway along the length of the test trajectory. This setup was chosen in order to determine where to setup the UWB radios relative to an existing intersection based on the results of this scenario, and it

allows for characterizing the performance as the vehicle approaches and departs from the radio which provides useful information for how such a system should be deployed.

The results are presented by investigating the float solution quality, UWB systematic errors estimation and ambiguity resolution. In addition, the comparison between the two types of receivers (i.e. Geodetic-Grade GPS and Consumer-Grade GPS) is performed in this section.

5.2.1 Geodetic-Grade GPS Results

Figure 5.9 and Figure 5.10 show the horizontal position errors as a function of distance from the first UWB radio (i.e. infrastructure point 2 in Section 4.2.2) for all 10 trials for GPS+UWB and GPS-alone case, respectively. As shown in the two figures, there is a convergence in horizontal position accuracy as the vehicle passes the UWB radio (indicated as "0" on the x-axis). These results are similar to those presented in the previous section. North, east and vertical position errors as a function of distance from the first UWB radio for all 10 runs for GPS+UWB and GPS-alone solution are shown in Figure B.1 to Figure B.3. Since the trajectory is South to North, the largest improvement occurs in the North component, and due to horizontal geometry of the trajectory and the UWB range, there is little improvement in the vertical component.

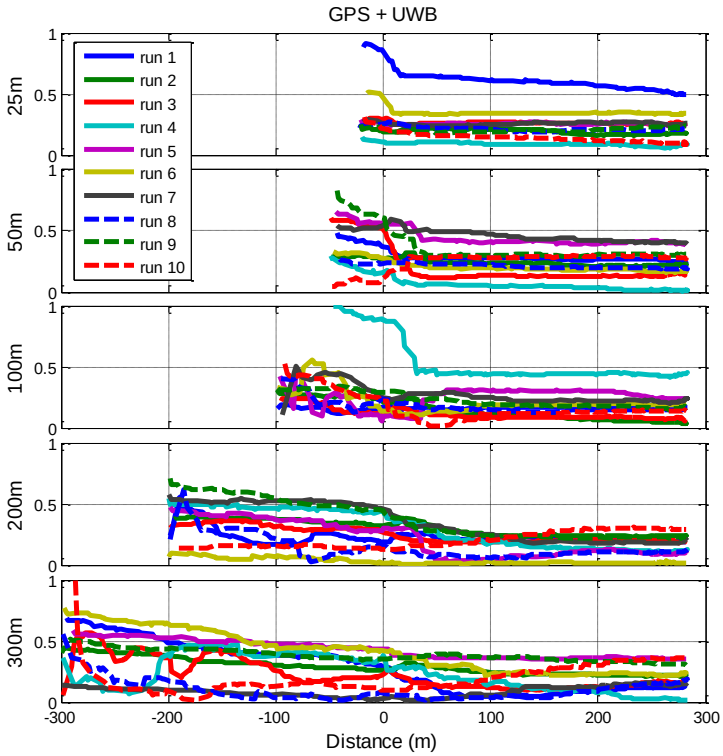

Figure 5.9 Horizontal error in metres vs. Distance for GPS + UWB solution under different initial baselines (25 m, 50 m, 100 m, 200 m, 300 m).

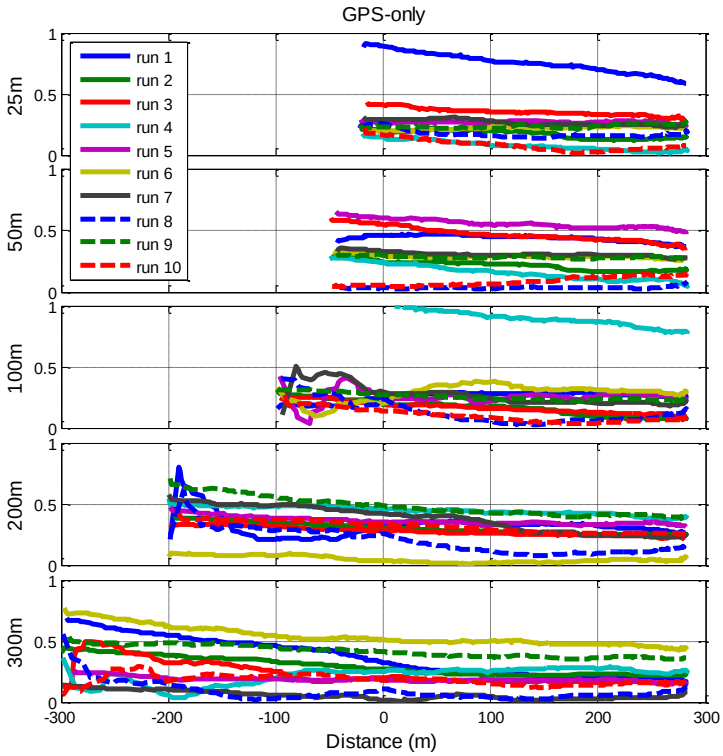

Figure 5.10 Horizontal error in metres vs. Distance for GPS-only solution under different initial baselines (25 m, 50 m, 100 m, 200 m, 300 m).

The northing, easting and vertical RMS errors as a function of distance with GPS-only compared to GPS + UWB under different initial baselines (25 m, 50 m, 100 m, 200 m, 300 m) are shown in Figure B.4 to Figure B.6. Figure 5.11 shows the horizontal RMS errors (DRMS) over the 10 runs as a function of distance for different starting distances with and without UWB ranges. In this case, the statistics are computed across 5 m wide bins. From this figure, it can be seen that improvement does not generally occur until after the vehicle passes the first UWB radio. As discussed in Section 4.2.2, this scenario tests different initial ranges (i.e. baselines) of UWB radios to investigate the usefulness of the UWB ranges. From the figures, it is shown that longer

initial ranges (e.g. the 200 m run) to the UWB radios result in early converge of the solution, however, it is not guaranteed to be better before arriving the intersection (e.g. the 300 m run). In addition, even shorter UWB ranges (e.g. the 25 m run) can improve the GPS-only solution after passing the UWB radios, which suggests that this system, even with shorter ranges, could also be used in practical applications.

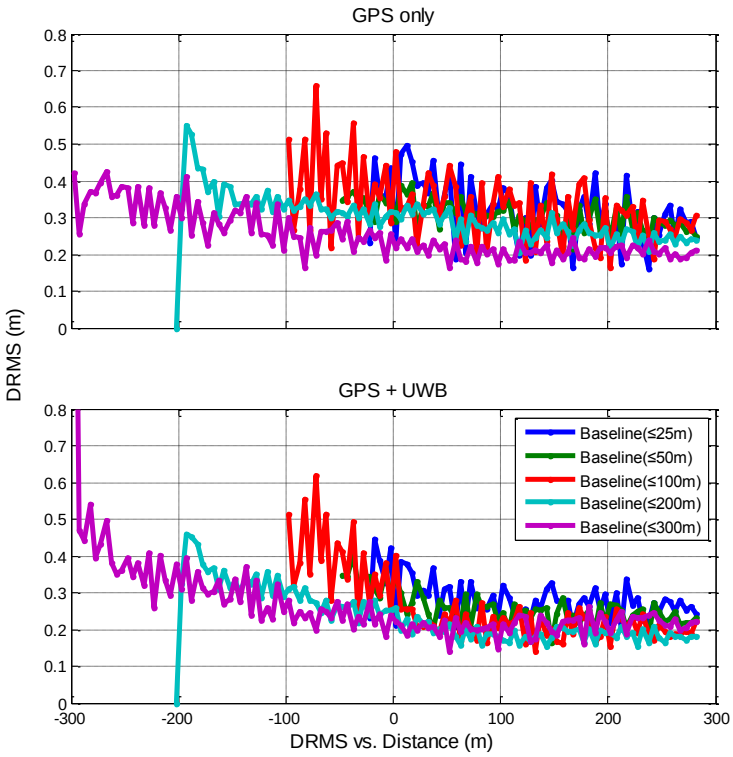

Figure 5.11 Horizontal RMS (DRMS) errors vs. distance, GPS-only compared to GPS + UWB under different initial baselines (25 m, 50 m, 100 m, 200 m, 300 m)

Improvement in RMS and median error of GPS + UWB compared to GPS-only solution just before passing the first UWB radio for all runs is shown in Table 5.4. Cases where an improvement occurs are positive values expressed as a percentage, while a degradation negative

values, for GPS-only and GPS + UWB solutions with different starting distance from the first UWB radios (i.e. infrastructure point 2). The percentage values are calculated by subtracting GPS + UWB from GPS-only solution (e.g. RMS and median errors in this case), and then divided by GPS-only solution.

It is noted that the east RMS errors for GPS-only cases (with all the baselines) are less than 18 centimetres, east median errors are less 7 centimetres. Since the results for the east are quite good, the north and vertical RMS and median errors are mainly presented in this table. It is shown that by adding the UWB ranges, the north RMS error for 4 out of 5 baselines (25 m, 100 m, 200 m and 300 m) are reduced with 31.5%, 11.0%, 16.7%, 16.4% improvement, respectively. The vertical RMS solutions for 3 (50 m, 100 m, and 200 m) out of 5 baselines improve 36.1%, 3.1%, 20.0%, respectively. Overall, 22 out of 40 cases (i.e. horizontal, north, east and vertical RMS and median errors for GPS + UWB with 5 baselines) are improved just before passing the first UWB radio.

Table 5.4 Improvement in RMS and median error of GPS + UWB compared to GPS-only solution just before passing the first UWB radio for all runs

strategies	RMS				Median			
	Horizontal	North	East	Vertical	Horizontal	North	East	Vertical
I (m)	0.229	0.207	0.124	0.749	0.232	-0.150	-0.061	-0.677
II (m)	0.290	0.246	0.153	0.750	0.292	-0.006	-0.025	-0.500
III (m)	0.481	0.498	0.156	1.046	0.229	-0.150	0.024	-0.144
IV (m)	0.313	0.340	0.177	0.370	0.330	-0.215	0.0	-0.053
V (m)	0.218	0.237	0.126	0.337	0.186	-0.165	-0.025	-0.022
VI (%)	8.1%	31.5%	-28.2%	-18.1%	-7.0%	82.6%	-94.6%	-2.7%
VII (%)	-18.7%	-38.2%	29.0%	36.1%	4.0%	2190.2%	-345.9%	17.7%
VIII (%)	16.6%	11.0%	8.6%	3.1%	1.3%	-34.9%	-11.8%	210.6%
IX (%)	17.2%	16.7%	17.7%	20.0%	18.1%	9.2%	-5650.0%	-93.0%
X (%)	-1.8%	16.4%	-36.9%	-22.7%	-42.4%	-11.1%	67.9%	-1510.8%

I. GPS-only when the vehicle is within 25 m from the first UWB radio ("GPS-only (baseline ≤25 m)");
II. GPS-only when the vehicle is within 50 m from the first UWB radio ("GPS-only (baseline ≤50 m)");
III. GPS-only when the vehicle is within 100 m from the first UWB radio ("GPS-only (baseline ≤100 m)");
IV. GPS-only when the vehicle is within 200 m from the first UWB radio ("GPS-only (baseline ≤200 m)");
V. GPS-only when the vehicle is within 300 m from the first UWB radio ("GPS-only (baseline ≤300 m)");
VI. GPS + UWB estimating the UWB systematic errors using UWB measurements when the vehicle is within 25 m from the first UWB radio ("GPS + UWB (baseline ≤25 m)");
VII. GPS + UWB estimating the UWB systematic errors when the vehicle was within 50 m from the first UWB radio ("GPS + UWB (baseline ≤50 m)");
VIII. GPS + UWB estimating the UWB systematic errors when the vehicle was within 100 m from the first UWB radio ("GPS + UWB (baseline ≤100 m)");
IX. GPS + UWB estimating the UWB systematic errors when the vehicle was within 200 m from the first UWB radio ("GPS + UWB (baseline ≤200 m)");
X. GPS + UWB estimating the UWB systematic errors when the vehicle was within 300 m from the first UWB radio ("GPS + UWB (baseline ≤300 m)");

Table 5.5 shows the improvement in RMS and median error of GPS + UWB compared to GPS-only solution 25 m away after passing the first UWB radio for all runs. By comparing Table 5.4 and Table 5.5, it is noted that 29 out of 40 cases (i.e. horizontal, north, east and vertical RMS and median errors for GPS + UWB with 5 baselines) comparing to GPS-only cases improved, while

22 out 40 cases just before passing the first UWB radio as discussed above. This is because the rapid changes in the measured range between vehicle and UWB radios are allowed to separate the UWB systematic errors (i.e. bias and scale factor), as a result, the ability to estimate each error improves. Once the UWB errors are well estimated, the UWB measurements can be used to better observe the position after passing the UWB radios.

Table 5.5 Improvement in RMS and median error of GPS + UWB compared to GPS-only solution 25 m away after passing the first UWB radio for all runs

strategies	RMS				Median			
	Horizontal	North	East	Vertical	Horizontal	North	East	Vertical
I (m)	0.394	0.363	0.126	0.620	0.233	-0.196	-0.031	-0.072
II (m)	0.335	0.306	0.178	0.678	0.287	-0.033	-0.138	-0.468
III (m)	0.333	0.305	0.148	0.801	0.269	-0.126	-0.027	-0.130
IV (m)	0.309	0.281	0.175	0.458	0.335	-0.155	-0.035	0.092
V (m)	0.226	0.263	0.123	0.469	0.190	-0.153	-0.029	-0.033
VI (%)	22.3%	26.8%	-46.2%	-84.7%	-5.6%	113.3%	-286.9%	48.1%
VII (%)	14.2%	10.3%	12.2%	-16.2%	2.5%	-270.8%	26.4%	66.3%
VIII (%)	37.1%	39.4%	12.7%	6.4%	12.5%	23.6%	-7.3%	160.4%
IX (%)	29.8%	29.3%	14.8%	15.5%	25.1%	0.9%	36.2%	30.3%
X (%)	2.7%	24.1%	-33.9%	-38.2%	25.2%	-16.7%	32.1%	-311.9%

Figure 5.12 shows the estimated horizontal standard deviations and HDOP as a function of distance for one certain run (i.e. Run# 2) for GPS+UWB and for GPS only solution. The addition of the UWB range reduces the horizontal error primarily in the north direction as discussed above. The instantaneous HDOP also improves from around 1.1 for GPS-alone, to approximately 0.8 when UWB ranges are available. It should be noted that the estimated accuracy is obtained from the output of a Kalman filtered solution (as opposed to the HDOP, which is a single epoch value) and this filter also has to estimate the UWB systematic errors before the UWB measurement can aid the solution. These two facts explain why the estimated standard deviation

is not just a scaled version of the HDOP, and also why the UWB measurements do not improve the solution instantaneously.

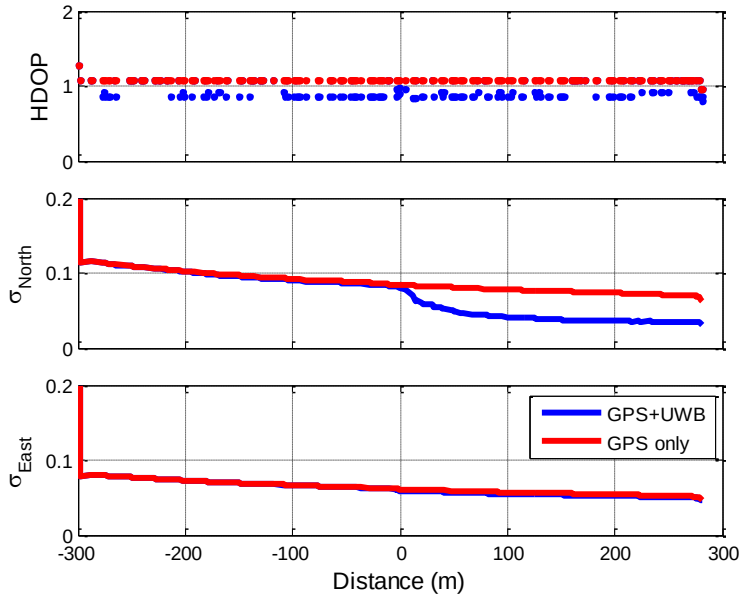

Figure 5.12 Run #2, HDOP and North & East standard deviations vs. Distance for GPS-only and GPS + UWB with distances of up to 300 m.

The estimated standard deviation of the UWB bias, scale factor and the corresponding UWB error standard deviation (for two radio pairs) is shown in Figure 5.13. From this, it can be seen that the two systemic errors become well estimated at the same time that the UWB-aided position solution starts to outperform the GPS-only solution, namely as the vehicle passes the first UWB radio. Indeed this makes sense because changes in the measured range are what allow for the separation of the bias and scale factor errors; this happens more rapidly as the vehicle passes the UWB radios. In turn, the ability to estimate each error improves, as shown by the estimated standard deviation in Figure 5.13. Once the UWB errors are well estimated using

Equation (2.10), the UWB measurements can be used to determine position more accurately, as shown in Figure 5.12.

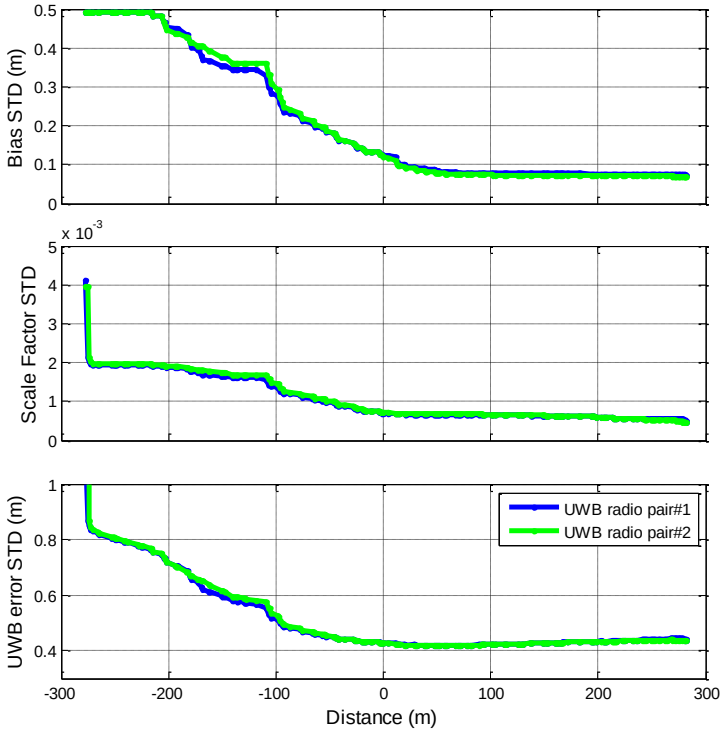

Figure 5.13 Run #2, Estimated Bias and Scale Factor Standard Deviations for each UWB radio pair vs. Distance using GPS + UWB with 300 m baseline

It is noted that in many of the references (Cao, 2009; O'Keefe et al., 2006) and in the remainder of this thesis, the PCF is quantified in terms of PIF (Probability of Incorrect Fix), which is equal to one minus PCF. Likewise, the lower bound of probability of correct fix becomes an upper bound on the probability of incorrect fix. In this case "good" performance is represented as a small upper bound (far less than 1) while "poor" performance is represented by an upper bound that is close to unity.

As an example, Figure 5.14 shows the PIF obtained from the method described above for Run #2 for five different initial distances. It is noted that the y-axis is on a log scale and that each of the plots starts at 100% (1.0) and decreases during the run as the float ambiguity solution improves and the probability of incorrect fix decreases. Also near the bottom of the graph, the probabilities of incorrect fix become very small ($<10^{-10}$). Small values are not necessarily meaningful, as the PCF/PIF is the evaluation of several areas under the normal distribution with extra small values multiplied together. More importantly, it is observed that the distance (or time) at which the upper bound on the PIF passes below a certain threshold (10^{-8} for example). When this occurs, we can be 99.999999% confident that the ambiguities are resolved correctly. In the particular case shown, the addition of the UWB ranges makes this occur faster for the 25, 50 and 100 m baseline cases while for the 200 and 300 m cases the advantage is less obvious.

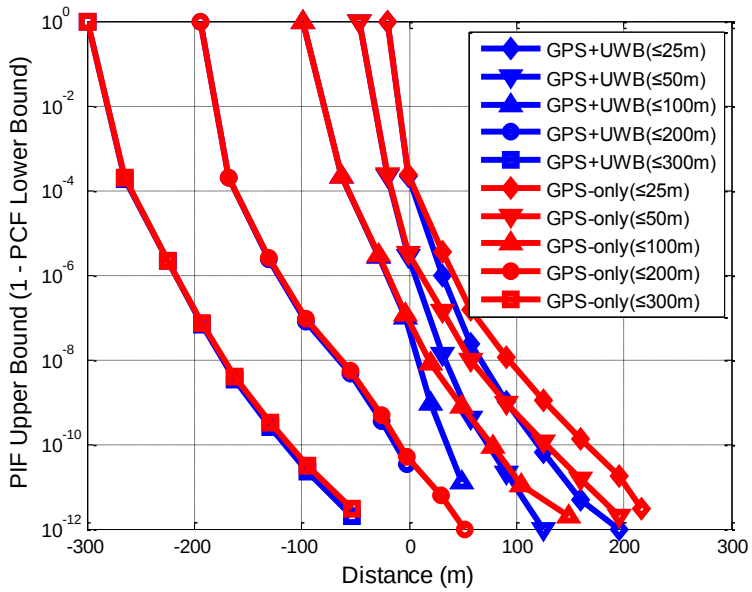

Figure 5.14 Run #2, PIF vs. Distance, GPS-only compared to GPS + UWB measurements (with errors estimated in run) up to 300 m

To further demonstrate the improvement by adding the UWB measurement to this particular run, the ratio between the two PIF values (with and without UWB) at each distance is shown in Figure 5.15. From this, it is obvious that adding the UWB ranges can improve the probability of correct fix by factors between 10 and 100 in the 25, 50, 100 and 200 m cases after the vehicle passes the UWB radios while the improvement for the 300 m case only really occurs just as the vehicle passes the radio. The declines in the ratio at the end of each line are numerical effects resulting from dividing two very small numbers. By extension, once the GPS-only PIF value falls below 10^{-12}, the improvement in PIF is no longer computed.

Although the results shown in Figure 5.15 are for the case when the UWB bias, scale factors and UWB errors are estimated on the fly, very similar results are obtained when using UWB ranges that are corrected a priori, which are shown in Figure 5.16. This can be explained as follows. First, referring back to Figure 5.13, when the vehicle is starting its approach, for example at 250 m, the uncertainty in the bias and scale factor are 0.5 m and 0.002 respectively. Converting the scale factor value into distance by multiplying the distance (i.e., 250 m) and then adding the variances of the bias, scale factor and measurement noise (from Table 4.2) gives a total range uncertainty of approximately 0.82 m. This is approximately double the value when the UWB measurements are already corrected (i.e., when only consider measurement noise). However, when the vehicle is 100 m from the intersection, the total error is only 0.51 m or 9 cm worse than for the corrected case. In other words, the difference in range measurement is small (9 cm in this case), especially as time passes (and distance decreases). Second, as the vehicle passes the UWB radio, the unit vector from the vehicle to the radio, which is used in the design matrix, changes by nearly 180 °. This rapid change in measurement geometry is very important for ambiguity

resolution. Considering these two points together means, that by the time the measurement geometry changes (which benefits ambiguity resolution) the corrected and uncorrected UWB range uncertainties are effectively the same (in fact, at 50 m the difference is less than 3 cm), hence it results in the similar results for both using corrected and uncorrected UWB ranges. In other words, based on this analysis, estimating the UWB errors in this scenario has only limited effect on performance.

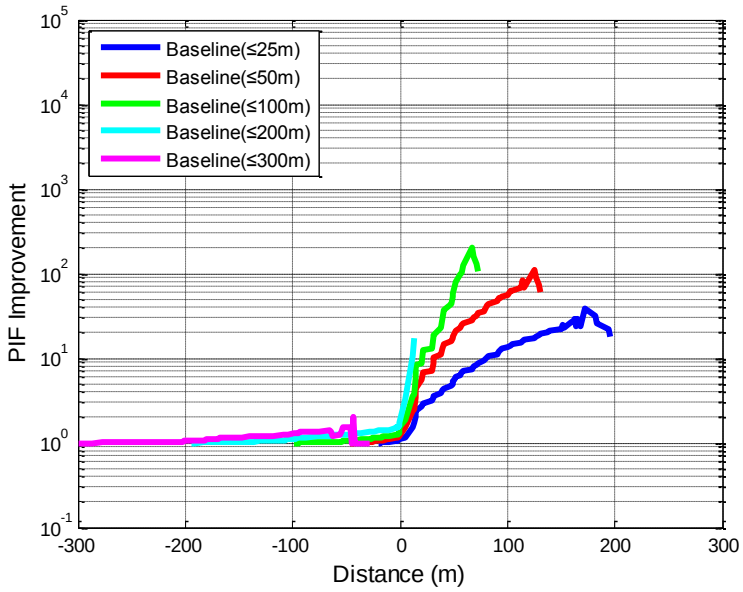

Figure 5.15 Run #2, PIF Improvement vs. Distance, GPS-only compared to GPS + UWB measurements (with errors estimated in run) up to 300 m

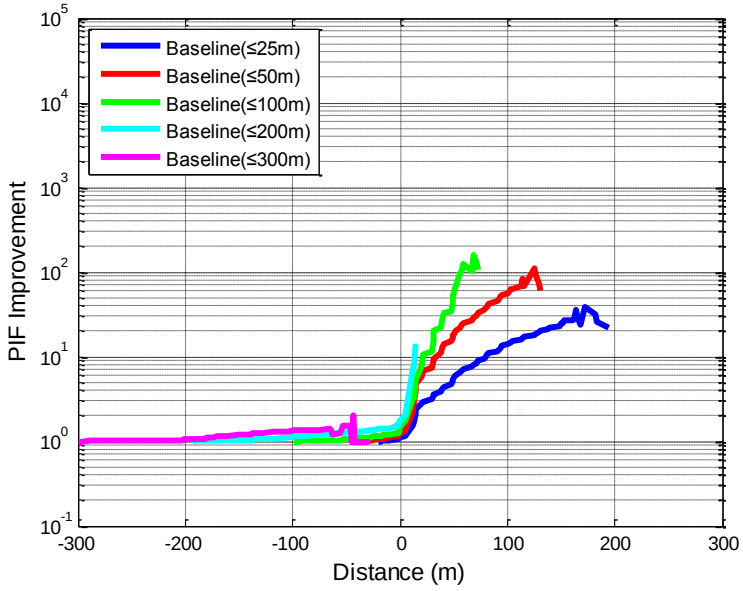

Figure 5.16 Run #2, PIF Improvement vs. Distance, GPS-only compared to GPS + UWB measurements (with errors corrected in advance) up to 300 m

The above analysis looked at one particular run but it is desirable to assess the overall improvement offered by UWB ranges. The upper plot in Figure 5.17 shows the minimum, mean and median improvement in PIF values across all 10 runs for the case when UWB ranges of up to 300 m are used. The minimum improvement is included as a "worst case" run (based on the data processed). The lower plot shows the number of runs (data points) used to compute the results in the upper plot, this trails off with increasing distance because the GPS-only PIF values become overly small.

It is noted that the minimum improvement can actually be a degradation (i.e., value less than one). This is because when processing GPS-only data, one or more measurements are temporarily rejected. In addition, it has been observed that these degradations are only observed

when the GPS-only PIF value is already very small and in these cases where differences in selection of base satellites is causing a sufficiently large change in the computed bound to make it appear as though the GPS-only results are better.

In contrast to the minimum improvement, the mean and median improvement are always positive (not only in the mathematical sense, but in the sense that the results get better). More importantly, the performance is improved most after the vehicle passes the UWB radios. This is consistent with the results of the single run shown above.

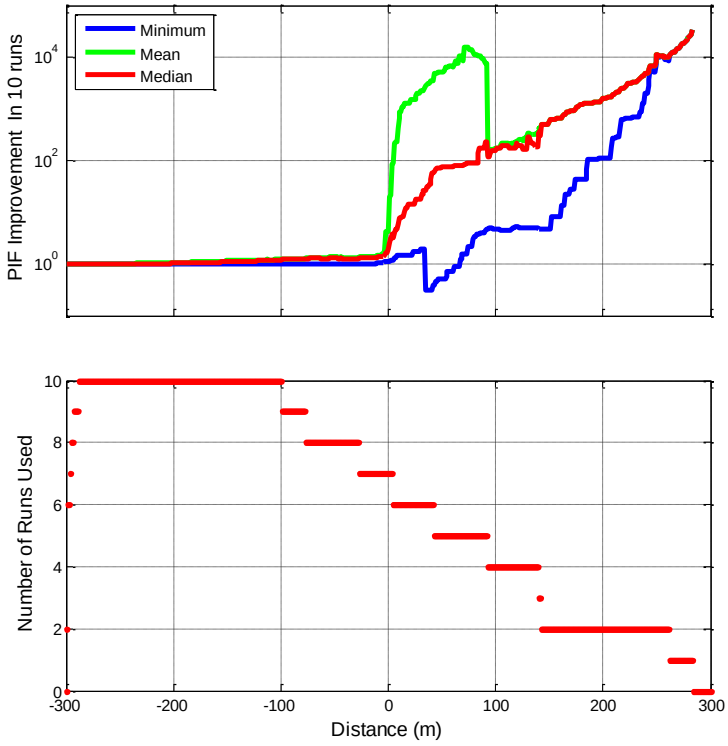

Figure 5.17 Minimum, Mean, Median PIF Improvement vs. Distance to first UWB station using GPS + UWB relative to GPS-only under 300m baseline

Finally, Figure 5.18 and Figure 5.19 show the minimum and mean values computed across all runs for different initial UWB baseline lengths. In general, the longer initial baselines receive the largest PIF improvements when adding UWB, especially for the minimum improvement case. This is because the GPS-only PIF values are already very small and thus the marginal (in terms of magnitude) benefit offered by the UWB measurements manifests as a large ratio. Nevertheless, these results suggest that improvement of between a factor of about 10 and 100 are reasonable, on average, before the vehicle approaches the intersection, regardless of initial baseline length.

Even if the improvements are smaller for shorter baselines, they still mean the difference between resolving the ambiguities or not. For example, for a longer baseline, the PIF may improve by a ratio of 100 from 10^{-10} to 10^{-12}, the correct ambiguity resolution is almost assured in both cases. However, for a shorter baseline, the improvement may only be a factor of 10 but may change the PIF from 10^{-4} to 10^{-5}. In this case, a factor of 10 may be all that is needed to make the system practically feasible. The PCF/PIF analysis is usually optimistic because the statistical models used for estimation are usually not correct; specifically, the noise is assumed to be white, which usually does not hold.

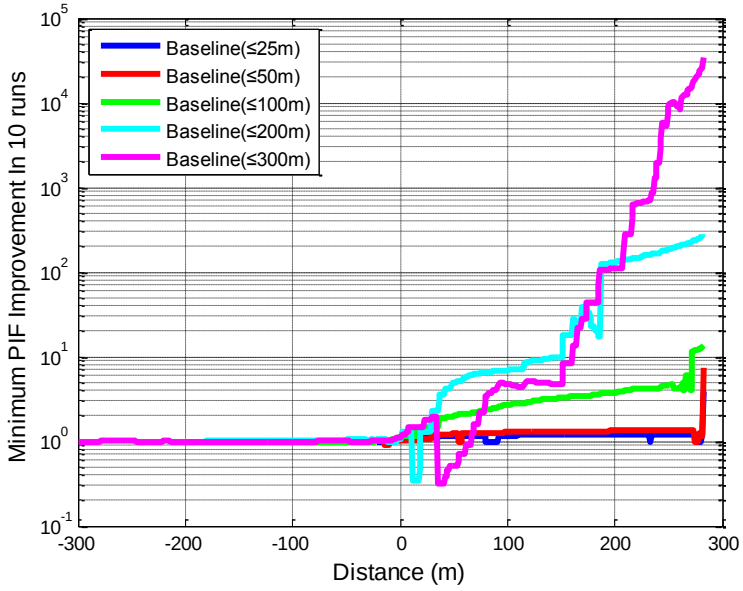

Figure 5.18 Minimum PIF Improvement vs. Distance for different initial baseline lengths

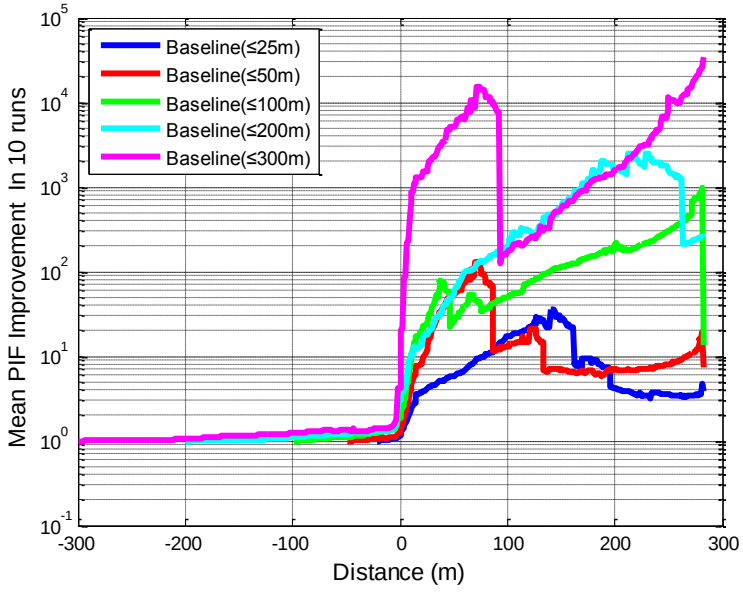

Figure 5.19 Mean PIF Improvement vs. Distance for different initial baseline lengths

Table B.3 shows the number of runs for which including UWB measurements improved the GPS-only result and in what way. Results from Table B.1 and Table B.2 are summarized graphically in Figure 5.20 and Figure 5.21 respectively.

Overall, adding the UWB ranges provides improvements in ambiguity resolution. 22 of 50 cases (5 different initial distance in 10 runs), which is 44%, are able to resolve ambiguities more quickly and 12% of all the cases are able to produce an ambiguity fix when GPS alone was only able to provide a float solution.

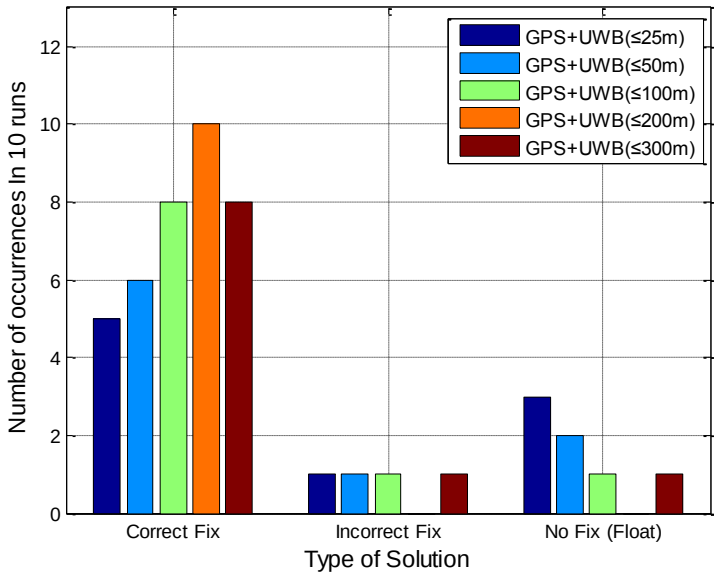

Figure 5.20 Ambiguity Resolution for GPS + UWB under different initial baselines (25 m, 50 m, 100 m, 200 m, 300 m)

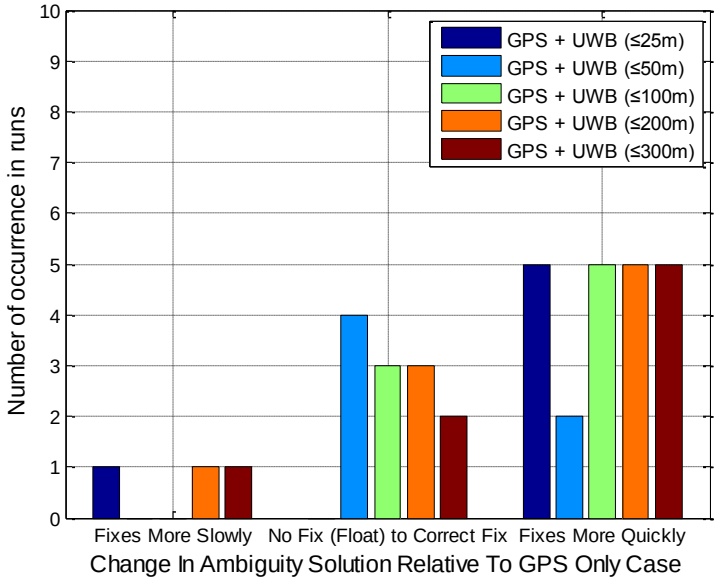

Figure 5.21 Change in Ambiguity Solution when Adding UWB Relative to GPS-only case under different initial baselines (25 m, 50 m, 100 m, 200 m, 300 m)

Improvement in average time of first ambiguity fix (in seconds) of GPS + UWB fix solution compared to GPS-only fix solution for all runs is shown in Table 5.6. The percentage values are computed by subtracting the values of average ambiguity fix time between GPS + UWB fix solution and GPS-only fix solution, and then divided by average fix time of GPS-only fix solution. From the table, it is seen that the inclusion of UWB ranges provides improvements in first ambiguity fix for with 9.4%, 10.5%, 21.4%, 18.3% and 1.1% for all runs, respectively.

Table 5.6 Improvement in average time of first ambiguity fix (in seconds) of GPS + UWB fix solution compared to GPS-only fix solution for all runs

Solution	Strategies	Time Improvement
GPS-only	I	10.6 s
	II	9.6 s
	III	14.4 s
	IV	18.8 s
	V	23.2 s
GPS+UWB	VI (%)	9.4%
	VII (%)	10.5%
	VIII (%)	21.4%
	IX (%)	18.3%
	X (%)	1.1%

I. GPS-only when the vehicle is within 25 m from the first UWB radio ("GPS-only (baseline ≤25 m)");
II. GPS-only when the vehicle is within 50 m from the first UWB radio ("GPS-only (baseline ≤50 m)");
III. GPS-only when the vehicle is within 100 m from the first UWB radio ("GPS-only (baseline ≤100 m)");
IV. GPS-only when the vehicle is within 200 m from the first UWB radio ("GPS-only (baseline ≤200 m)");
V. GPS-only when the vehicle is within 300 m from the first UWB radio ("GPS-only (baseline ≤300 m)");
VI. GPS + UWB estimating the UWB systematic errors using UWB measurements when the vehicle is within 25 m from the first UWB radio ("GPS + UWB (baseline ≤25 m)");
VII. GPS + UWB estimating the UWB systematic errors when the vehicle was within 50 m from the first UWB radio ("GPS + UWB (baseline ≤50 m)");
VIII. GPS + UWB estimating the UWB systematic errors when the vehicle was within 100 m from the first UWB radio ("GPS + UWB (baseline ≤100 m)");
IX. GPS + UWB estimating the UWB systematic errors when the vehicle was within 200 m from the first UWB radio ("GPS + UWB (baseline ≤200 m)");
X. GPS + UWB estimating the UWB systematic errors when the vehicle was within 300 m from the first UWB radio ("GPS + UWB (baseline ≤300 m)");

5.2.2 Consumer-Grade GPS Results

This section looks at results obtained with the Consumer-Grade GPS receivers. The structure is similar to the Geodetic-Grade GPS results.

Figure 5.22 shows a plot of horizontal RMS error as a function of distance with different initial baseline length. Since the Consumer-Grade GPS data rate was less than that of the Geodetic-Grade GPS receivers, the bin sizes in this case were increased to 10 m (from 5 m) in order to have more points per bin for computing statistics.

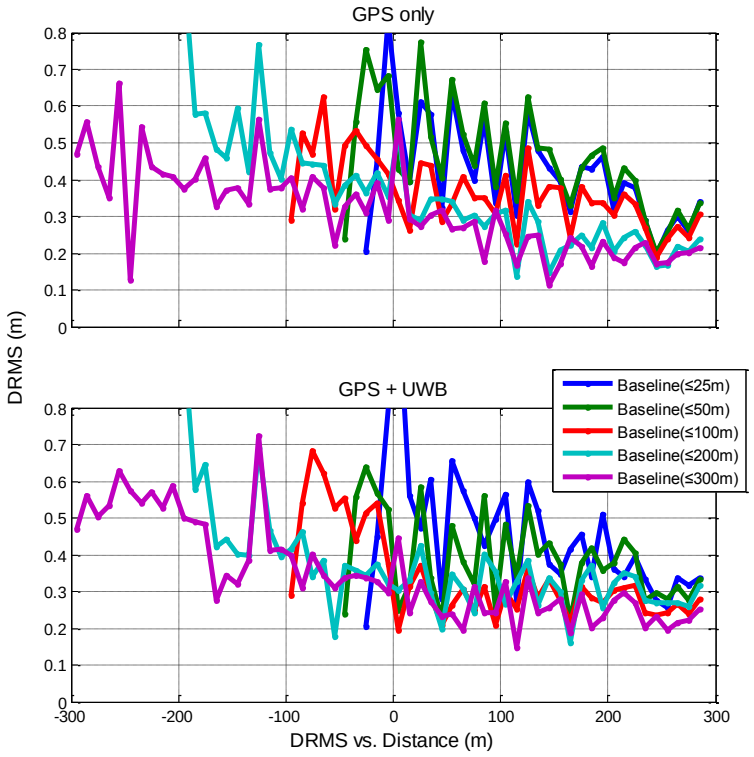

Figure 5.22 Horizontal RMS (DRMS) errors vs. Distance for GPS-only and GPS + UWB under different initial baselines (25 m, 50 m, 100 m, 200 m, 300 m)

In general, the results are only slightly worse – and noticeably more variable – than those obtained with the Geodetic-Grade GPS receiver. The decreased performance is expected because of the poorer quality pseudorange measurements of the Consumer-Grade GPS receivers (see from Table 4.2). The increased variability from bin to bin is because of the small number of points used to compute the statistics (typically only 4-8 from bin to bin).

It is also noted that – as with the Geodetic-Grade GPS receivers – the positioning accuracy was very similar with and without applying corrections to the UWB data in advance of processing. Again, this suggests that having these errors present is not a limiting factor in terms of positioning accuracy. Improvement in RMS and median error of GPS + UWB compared to GPS-only solution at the intersection for all runs is shown in Table B.4 in APPENDIX B. It is noted that by adding the UWB ranges, the 25 m and 100 m baselines perform best with 19 out of 40 cases (i.e. horizontal, north, east and vertical RMS and median errors for GPS + UWB with 5 baselines) are improved.

For the Consumer-Grade GPS solution, the PIF values are considerably larger than that of the Geodetic-Grade GPS receivers. As an example, Figure 5.23 shows PIF as a function of distance for the same run as shown in Figure 5.14 for the Geodetic-Grade GPS receivers. Comparing these two plots shows that the Consumer-Grade GPS PIF values are larger by several orders of magnitude.

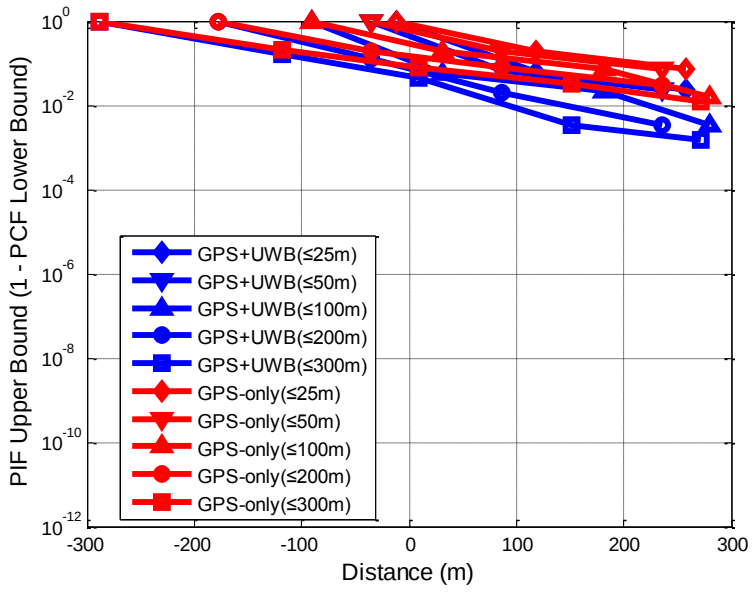

Figure 5.23 Run #2, PIF vs. Distance, GPS-only compared to GPS + UWB measurements (with errors estimated in run) up to 300 m

The main reason for this is that the Consumer-Grade GPS receivers have an effective data rate of 1 Hz, compared to 10 Hz for the Geodetic-Grade GPS receivers. The increased number of measurements with the Geodetic-Grade GPS receivers results in smaller PIF values. When using fewer measurements with the Geodetic-Grade GPS receiver, the PIF values increase considerably as can be shown in Figure 5.24.

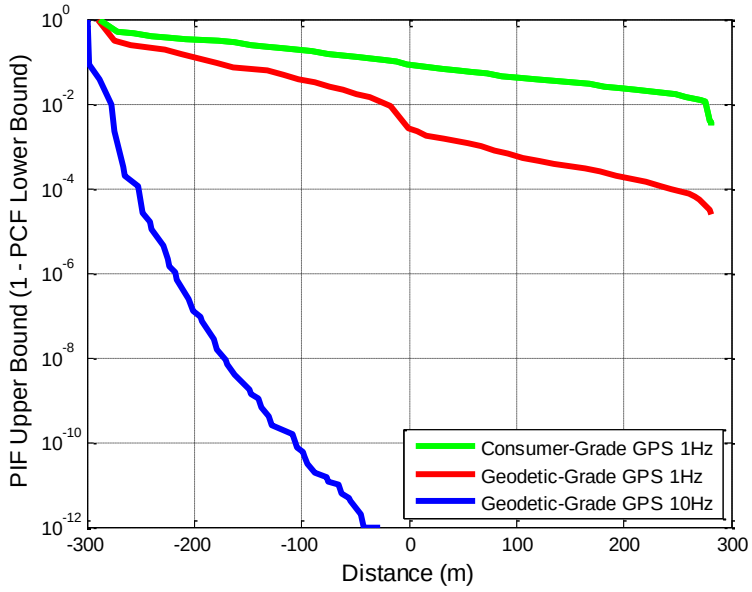

Figure 5.24 Run #2, PIF vs. Distance using GPS-only with 1 Hz data rate relative to 10 Hz for the 300 m baseline case

Given the relatively poor GPS-only PIF values, adding UWB data does not offer considerable benefits due to the poor quality pseudorange measurements of the Consumer-Grade GPS receivers. These are shown in Figure 5.25 and Figure 5.26 where the PIF improvement is shown to be limited to a factor of less than 10 for all baselines, regardless of where the vehicle is located relative to the intersection.

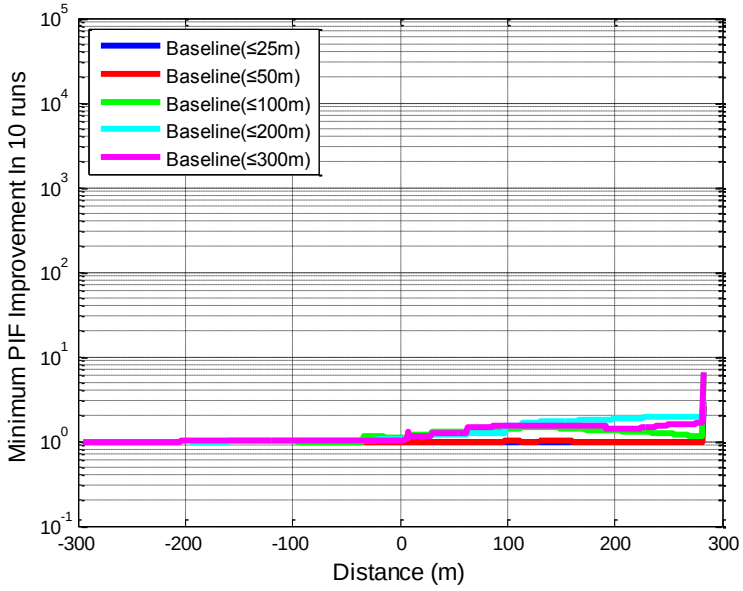

Figure 5.25 Minimum PIF Improvement vs. Distance for different initial baseline lengths

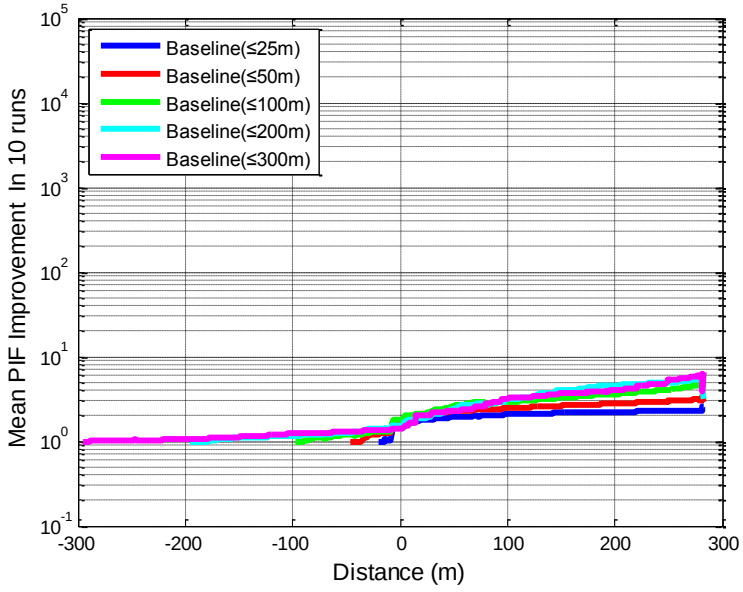

Figure 5.26 Mean PIF Improvement vs. Distance for different initial baseline lengths

According to the poor PIF results shown above, none of the runs were able to resolve ambiguities either for GPS alone or for GPS + UWB. As such, there are no results to show in this section.

5.2.3 Geodetic-Grade GPS with 1 Hz Data Rate Results

The results of Geodetic-Grade GPS receivers with 1Hz data rate are presented in this section in order to have a comparison between Geodetic-Grade GPS and Consumer-Grade GPS with the same data rate. The structure is similar to the Geodetic-Grade GPS results.

Figure 5.27 shows the horizontal RMS error as a function of distance for this setup. The results are generally similar to those of the other setup shown in Figure 5.22, which suggest that the GPS type (i.e. Geodetic-Grade GPS or Consumer-Grade GPS) does not affect position accuracy much.

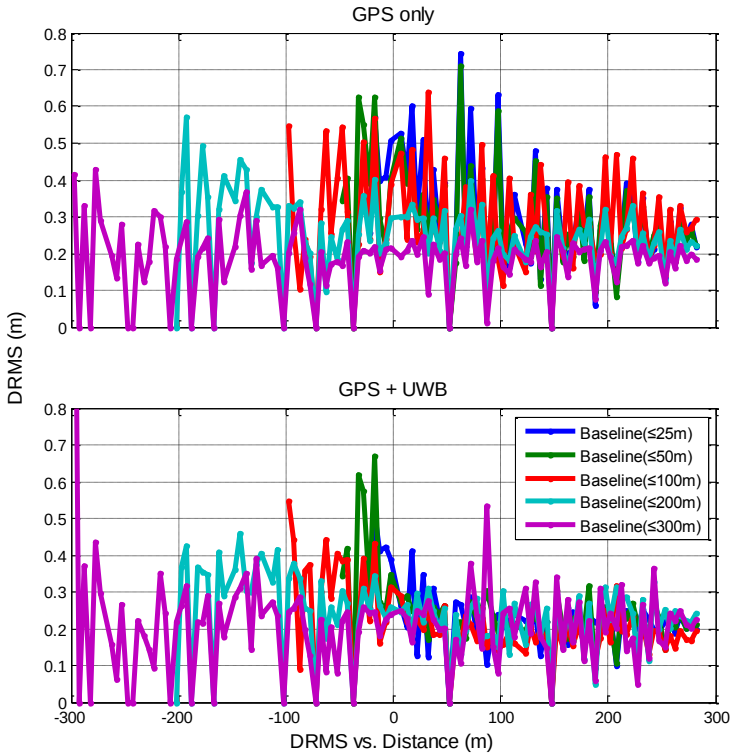

Figure 5.27 Horizontal RMS (DRMS) errors vs. Distance for 1 Hz GPS-only and 1 Hz GPS + UWB under different initial baselines (25 m, 50 m, 100 m, 200 m, 300 m)

Improvement in RMS and median error of 1 Hz GPS + UWB compared to 1 Hz GPS-only solution at the intersection for all runs is shown in Table B.5 in APPENDIX B. It indicates that with the inclusion of the UWB ranges, the 100 m baseline performed best with 27 out of 40 cases (i.e. horizontal, north, east and vertical RMS and median errors for GPS + UWB with 5 baselines) improved compared 22 cases for 10Hz Geodetic-Grade GPS receivers and 19 cases for 1Hz Consumer-Grade GPS receivers.

For the 1Hz Geodetic-Grade GPS results, the PIF values are considerably larger than that of the Consumer-Grade GPS receivers, however they were smaller than that of the 10Hz Geodetic-Grade GPS receivers as discussed in Section 5.2.2. As an example, Figure 5.28 shows PIF as a function of distance for 1Hz Geodetic-Grade GPS receivers for the same run as shown in Figure 5.14 for the 10 Hz Geodetic-Grade GPS receivers and Figure 5.23 for the Consumer-Grade GPS receivers.

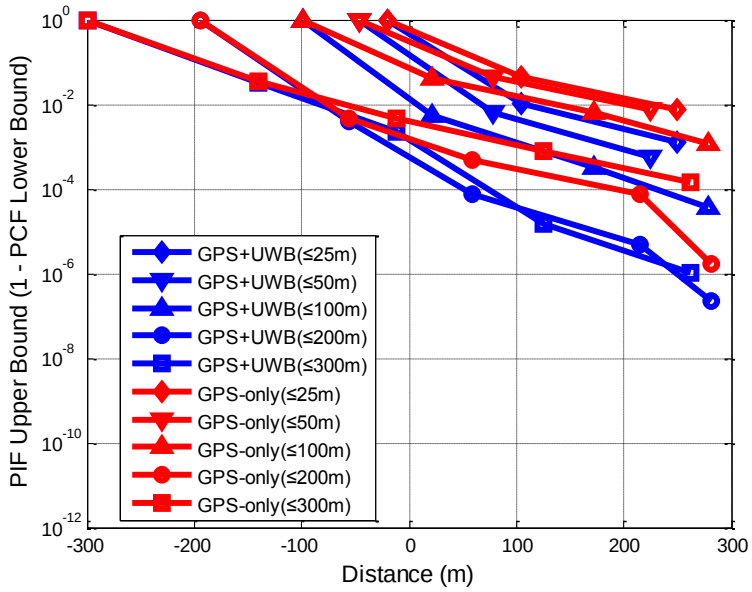

Figure 5.28 Run #2, PIF vs. Distance, 1 Hz GPS-only compared to 1 Hz GPS + UWB measurements (with errors estimated in run) up to 300 m

Minimum and mean values computed across all runs for different initial UWB baseline lengths are shown in Figure 5.29 and Figure 5.30. In general, the longer initial baselines receive the largest PIF improvements when adding UWB. These results suggest that mean improvement of between a factor of about 1 and 100 are reasonable, before the vehicle approaches the intersection, regardless of initial baseline length. The results are generally similar to Consumer-

Grade GPS results but slightly better than that shown in Figure 5.25 and Figure 5.26, which suggest that the GPS type (Geodetic-Grade and Consumer-Grade GPS) slightly affect PCF/PIF performance (improvement performance for Geodetic-Grade GPS is a factor of 1-100, Consumer-Grade GPS a factor of 1-10).

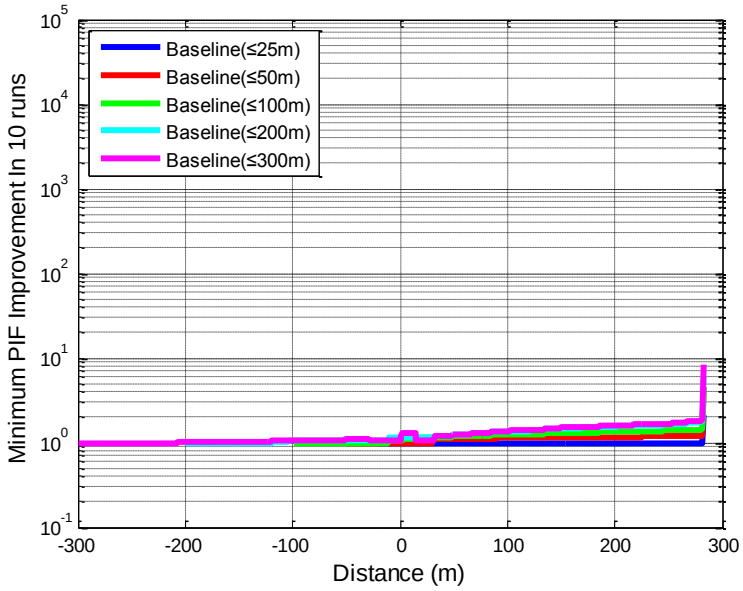

Figure 5.29 Minimum PIF Improvement vs. Distance for different initial baseline lengths with 1 Hz GPS data rate

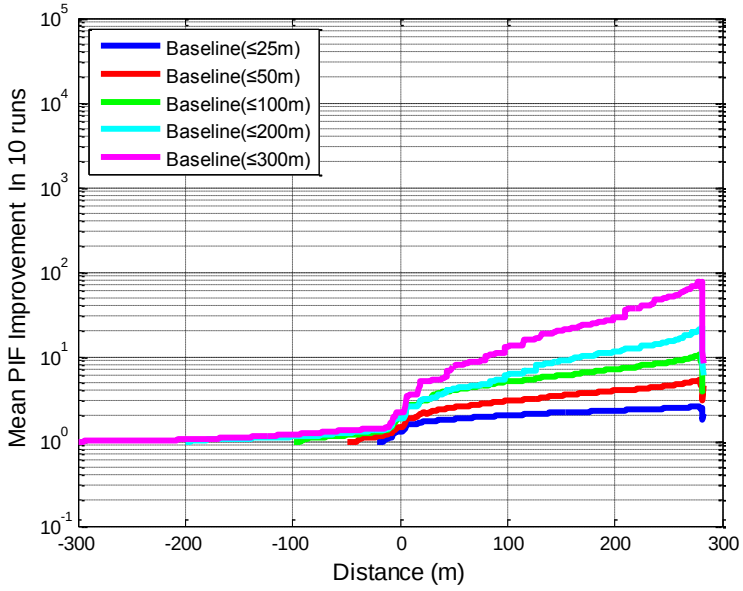

Figure 5.30 Mean PIF Improvement vs. Distance for different initial baseline lengths with 1 Hz GPS data rate

Similar to the Consumer-Grade GPS ambiguity resolution results as shown in Section 5.2.2, none of the runs were able to resolve ambiguities either for GPS alone or for GPS + UWB cases.

5.3 Scenario C Results

Scenario C used the same data used for Scenario B as discussed in Section 4.2.3, but only one infrastructure point was deployed locating approximately halfway along the length of the test trajectory. This setup was chosen to determine how many radios need to be deployed relative to an existing intersection. The data processing of Scenario C is the same as that for Scenario B, except it only process the measurements from only one UWB radio. Not all of the plots shown in the previous section are included since they only reduplicate the previous conclusions.

5.3.1 Geodetic-Grade GPS Results

Figure 5.31 shows the horizontal RMS errors as a function of distance from the UWB radio for all 10 trials for this setup. The results are generally similar to those of the setup shown in Figure 5.11, which indicates that the even with one UWB radio, the solution is similar in terms of position accuracy to Scenario B.

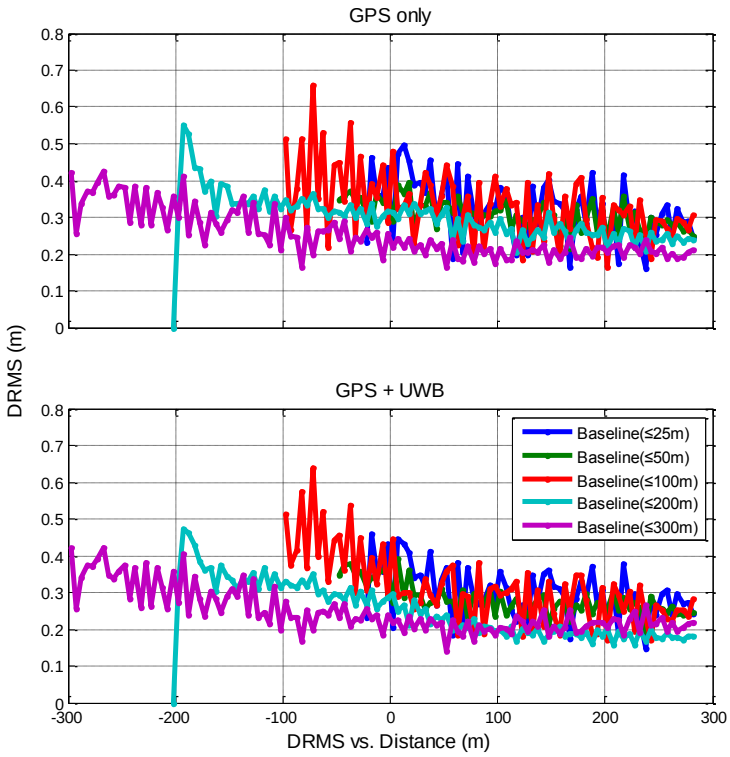

Figure 5.31 Horizontal (DRMS) errors vs. distance, GPS-only compared to GPS + UWB under different initial baselines (25 m, 50 m, 100 m, 200 m, 300 m)

Improvement in RMS and median error of GPS + UWB compared to GPS-only solution at intersection for all runs is shown in Table C.1. It is seen that adding the UWB ranges, the 200 m

baseline performed best with 29 out of 40 cases (i.e. horizontal, north, east and vertical RMS and median errors for GPS + UWB with 5 baselines) improved compared to 22 cases for Geodetic-Grade GPS receivers for Scenario B.

For the PCF/PIF analysis, the GPS + UWB results are similar to previous scenario B results. As an example, Figure 5.32 shows PIF as a function of distance for Geodetic-Grade GPS receivers with one UWB radio for the same run as shown in Figure 5.14 for the Geodetic-Grade GPS receivers but with two UWB radios, which suggests that the PIF performance does not change too much by using only one UWB radio for Scenario C.

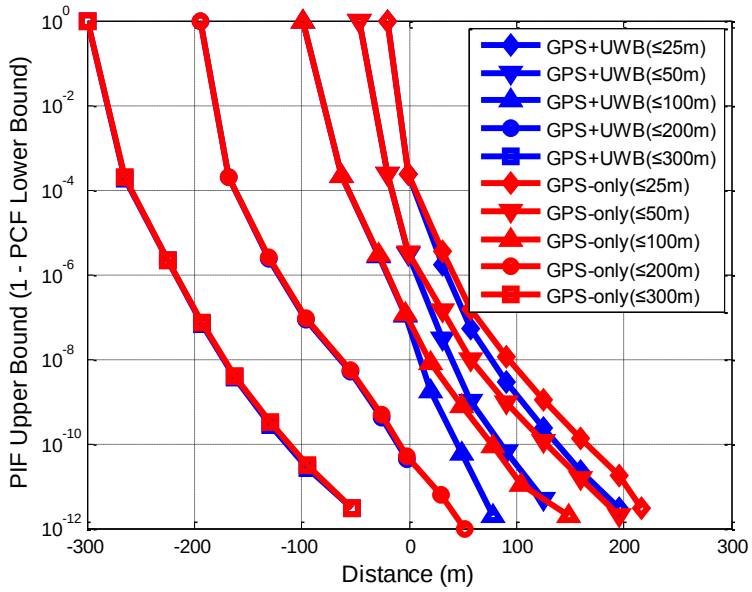

Figure 5.32 Run #2, PIF vs. Distance, GPS-only compared to GPS + UWB measurements (with errors estimated in run) up to 300 m

Minimum and mean values computed across all runs for different initial UWB baseline lengths are shown in Figure 5.33 and Figure 5.34. As with Scenario B, the longer initial baselines

provide the larger PIF improvements when adding UWB ranges before approaching the intersection. The results are generally slightly worse than Figure 5.18 and Figure 5.19 from Scenario B, but indeed provide the PIF improvements relative to the GPS-only case for all initial baselines.

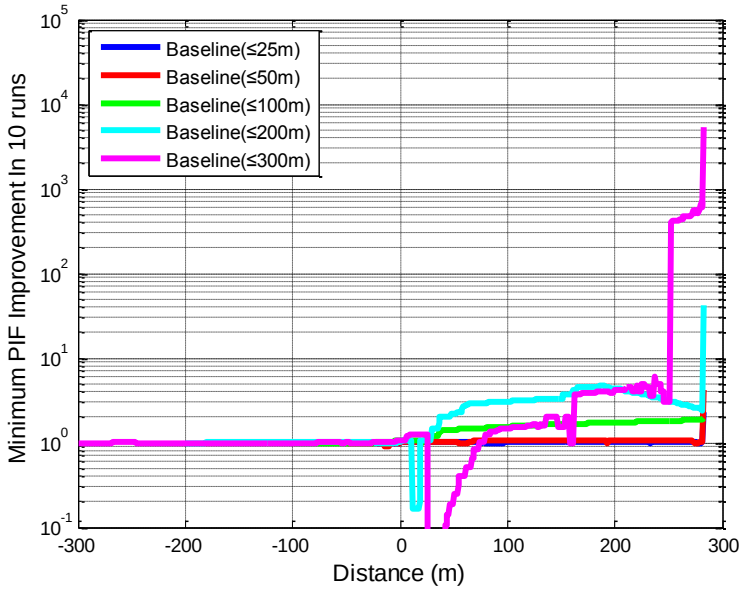

Figure 5.33 Minimum PIF Improvement vs. Distance for different initial baseline lengths

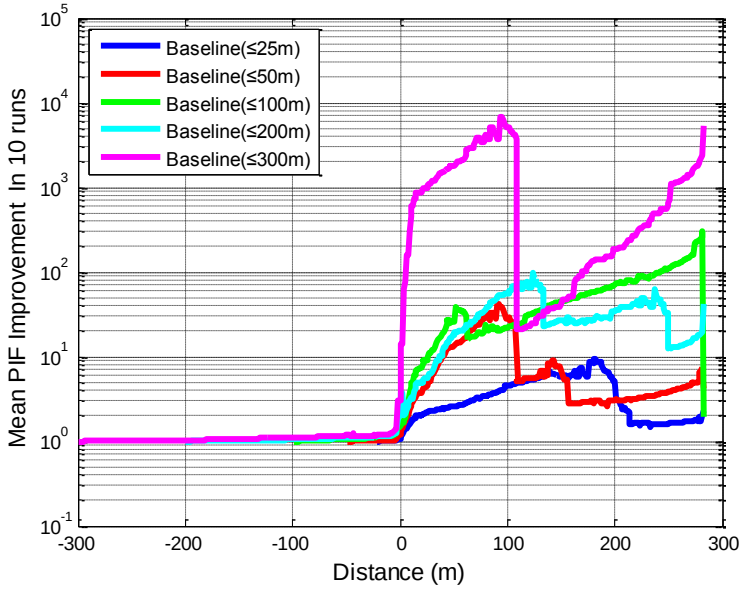

Figure 5.34 Mean PIF Improvement vs. Distance for different initial baseline lengths

For the ambiguity resolution, the inclusion of UWB ranges, regardless of the different starting baseline being used, results in an increase in ambiguity fixes before approaching the intersection. Time to first fix for ambiguity resolution, distance from the intersection at time of first fix and ambiguity fixing performance of GPS+UWB compared to GPS alone results are shown in Table C.2 through Table C.4 in APPENDIX C. In order the make these results easier to view, the main results of these tables are summarized as bar charts in Figure 5.35 and Figure 5.36. Overall, 23 of 50 cases (5 different initial distance in 10 runs), which is 46%, are able to resolve ambiguities more quickly (29 of 50 cases in Scenario B), and 14% of all the cases are able to produce an ambiguity fix when GPS alone was only able to provide a float solution (12% in Scenario B). From Table 5.7, it is seen that the by adding UWB ranges, improvements in first ambiguity fix range from 4.1% to 16.9% across all runs.

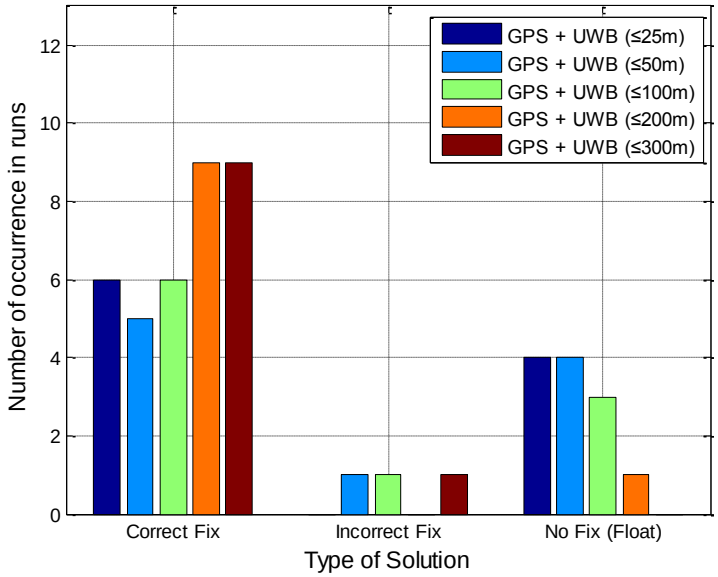

Figure 5.35 Ambiguity Resolution for GPS + UWB under different initial baselines (25 m, 50 m, 100 m, 200 m, 300 m)

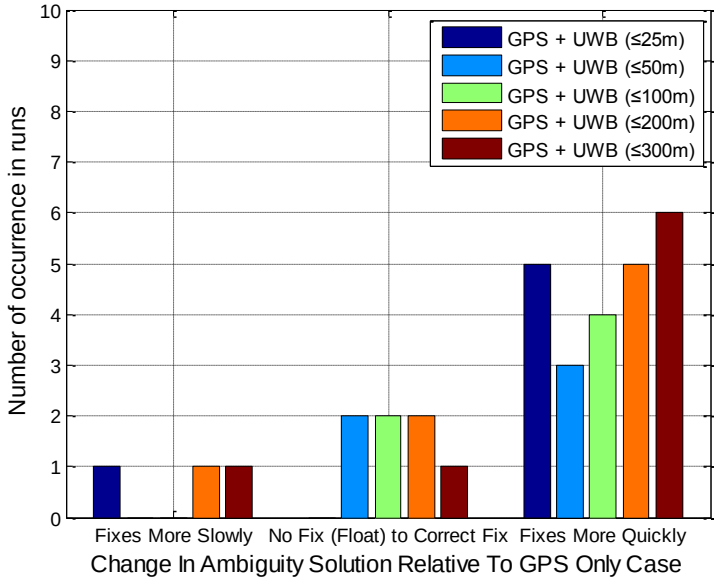

Figure 5.36 Change in Ambiguity Solution when Adding UWB Relative to GPS-only case under different initial baselines (25 m, 50 m, 100 m, 200 m, 300 m)

Table 5.7 Improvement in average time of first ambiguity fix (in seconds) of GPS + UWB fix solution compared to GPS-only fix solution for runs

Solution	Strategies	Time Improvement
GPS-only	I	10.6 s
	II	9.6 s
	III	14.3 s
	IV	18.8 s
	V	26.5 s
GPS+UWB	VI	4.1%
	VII	9.4%
	VIII	16.8%
	IX	16.9%
	X	15.0%

I. GPS-only when the vehicle is within 25 m from the first UWB radio ("GPS-only (baseline ≤25 m)");
II. GPS-only when the vehicle is within 50 m from the first UWB radio ("GPS-only (baseline ≤50 m)");
III. GPS-only when the vehicle is within 100 m from the first UWB radio ("GPS-only (baseline ≤100 m)");
IV. GPS-only when the vehicle is within 200 m from the first UWB radio ("GPS-only (baseline ≤200 m)");
V. GPS-only when the vehicle is within 300 m from the first UWB radio ("GPS-only (baseline ≤300 m)");
VI. GPS + UWB estimating the UWB systematic errors using UWB measurements when the vehicle is within 25 m from the first UWB radio ("GPS + UWB (baseline ≤25 m)");
VII. GPS + UWB estimating the UWB systematic errors when the vehicle was within 50 m from the first UWB radio ("GPS + UWB (baseline ≤50 m)");
VIII. GPS + UWB estimating the UWB systematic errors when the vehicle was within 100 m from the first UWB radio ("GPS + UWB (baseline ≤100 m)");
IX. GPS + UWB estimating the UWB systematic errors when the vehicle was within 200 m from the first UWB radio ("GPS + UWB (baseline ≤200 m)");
X. GPS + UWB estimating the UWB systematic errors when the vehicle was within 300 m from the first UWB radio ("GPS + UWB (baseline ≤300 m)");

5.3.2 Consumer-Grade GPS Results

Figure 5.37 shows horizontal RMS error as a function of distance with different initial baseline length. These results are similar to scenario B results as shown in Figure 5.22.

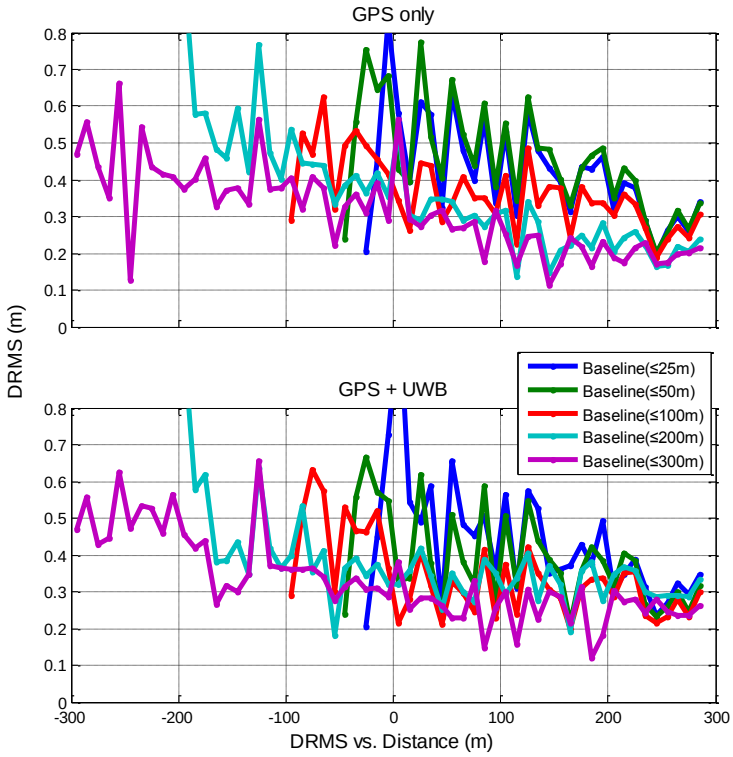

Figure 5.37 Horizontal RMS (DRMS) errors vs. Distance for GPS-only and GPS + UWB under different initial baselines (25 m, 50 m, 100 m, 200 m, 300 m)

Improvement in RMS and median error of GPS + UWB compared to GPS-only solution at intersection for all runs is shown in Table C.5 in APPENDIX C. It is seen that adding the UWB ranges, only 17 out of 40 cases (i.e. horizontal, north, east and vertical RMS and median errors for GPS + UWB with 5 baselines) improved compared to 19 cases for Consumer-Grade GPS receivers for Scenario B.

For the PCF/PIF analysis, the GPS + UWB results are slightly worse than those from scenario B. As an example, Figure 5.38 shows PIF as a function of distance for Consumer-Grade GPS receivers with one UWB radio for the same run as shown in Figure 5.23 for the Consumer-Grade GPS receivers but with two UWB radios, which suggests that, for the Consumer-Grade GPS receivers, PIF performance does not change too much when only using one UWB radio.

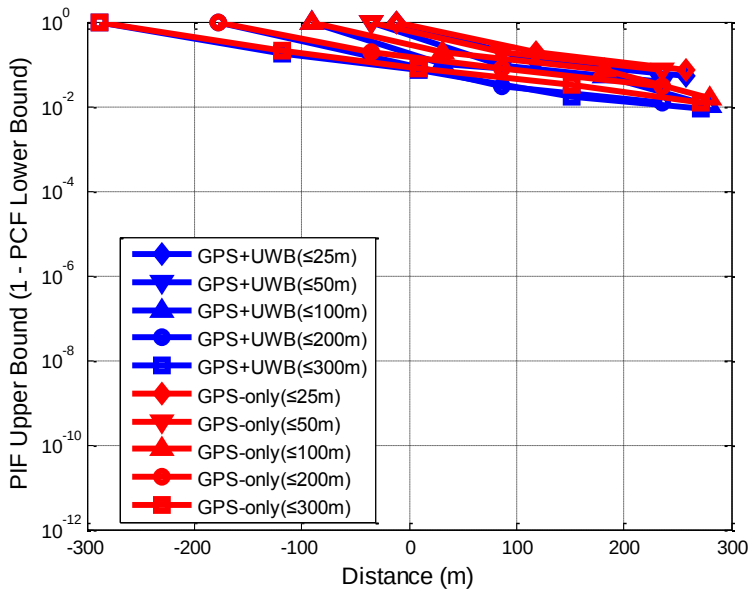

Figure 5.38 Run #2, PIF vs. Distance, GPS-only compared to GPS + UWB measurements (with errors estimated in run) up to 300 m

Given the poor PIF values, the inclusion of UWB ranges does not provide benefit due to the poor quality pseudorange measurements of the Consumer-Grade GPS receivers. Figure 5.39 and Figure 5.40 show the PIF improvement is limited to a factor for less than 10 for all baselines, regardless of where the vehicle is located relative to the intersection.

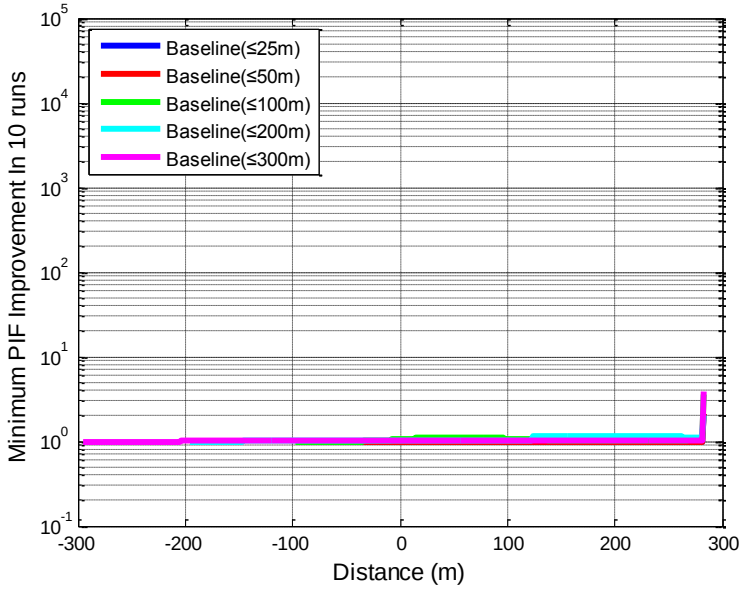

Figure 5.39 Minimum PIF Improvement vs. Distance for different initial baseline lengths

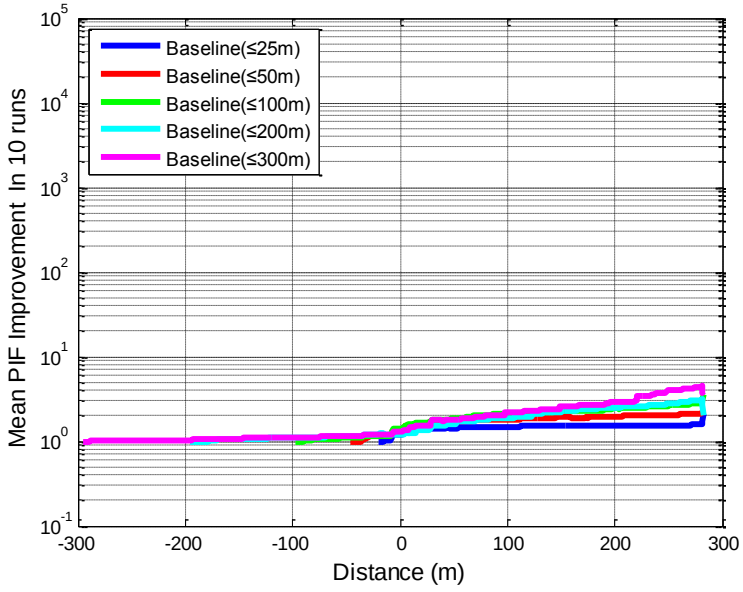

Figure 5.40 Mean PIF Improvement vs. Distance for different initial baseline lengths

However, none of the runs were able to resolve ambiguities either for GPS-alone or for GPS + UWB cases due to the poor PIF results shown above.

5.4 Scenario D Results

This section looks at the results for the case where one of the two UWB radios is moved next to the (fictitious) intersection while the other one remains the same location as that of Scenario B and C. It is noted that not all of the plots shown in the previous section are included since they only serve to re-enforce the previous conclusions.

5.4.1 Geodetic-Grade GPS Results

Figure 5.41 shows the horizontal RMS error as a function of distance for this setup. The results are similar to those of the other setup shown in Figure 5.11 and Figure 5.31 suggesting that the UWB geometry does not affect position accuracy too much.

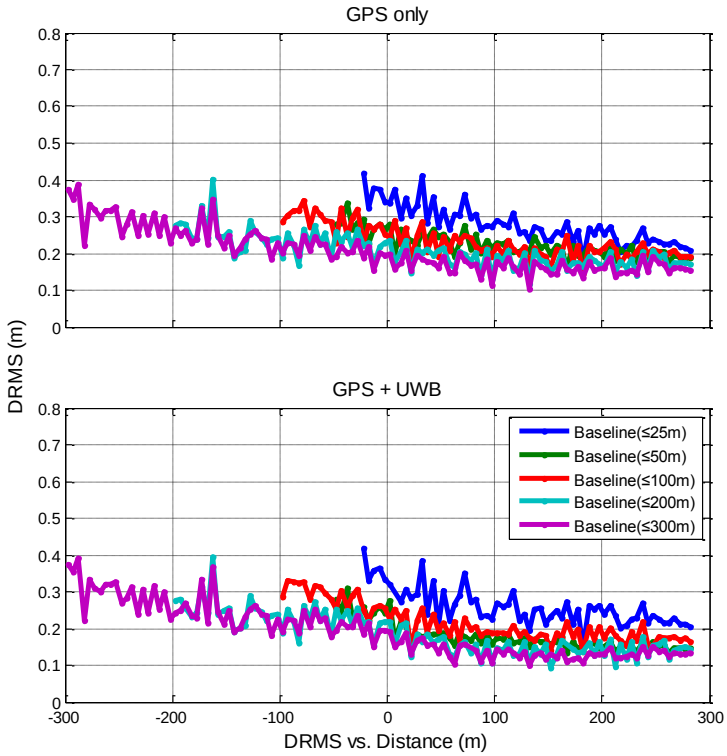

Figure 5.41 Horizontal RMS (DRMS) errors vs. Distance for GPS-only and GPS + UWB under different initial baselines (25 m, 50 m, 100 m, 200 m, 300 m)

Improvement in RMS and median error of GPS + UWB compared to GPS-only solution at intersection for all runs is shown in Table D.1 in APPENDIX D. It is seen that by adding the UWB ranges, the 25 m baseline performed best with 35 out of 40 cases (i.e. horizontal, north, east and vertical RMS and median errors for GPS + UWB with 5 baselines) improved.

For the PCF/PIF analysis, the GPS-only results are much better than in the previous scenarios due to an improved GPS constellation during the test. For this test setup, nine satellites were in view for most of the runs. In contrast, for the other test setup, six to eight satellites were in view.

As such, for longer initial baselines, the PIF values are already extremely low by the time the vehicle reaches the intersection. An example of this is shown in Figure 5.42.

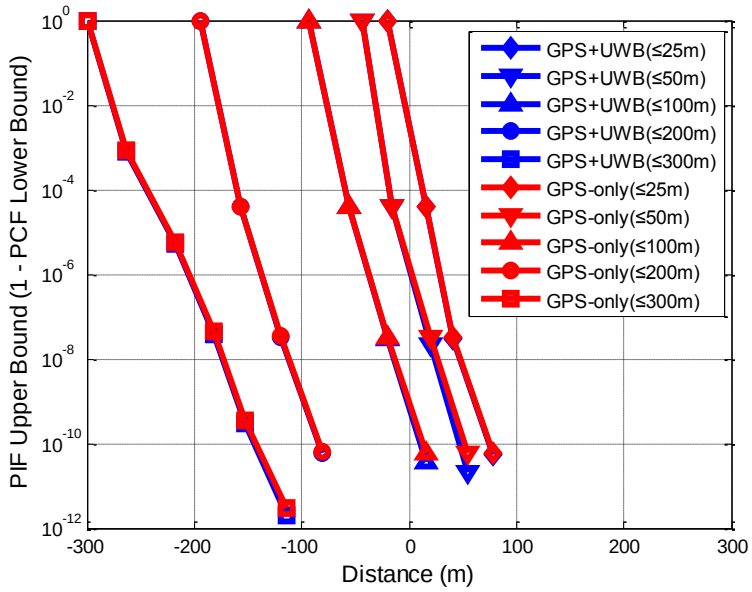

Figure 5.42 Run #4, PIF vs. Distance, GPS-only compared to GPS + UWB measurements (with errors estimated in run) up to 300 m

The improvement is seen when adding UWB data is negligible – if it is even observable – for most cases. However, even in these cases the PIF improvement is modest, especially compared to previous scenarios. To illustrate, Figure 5.43 and Figure 5.44 show the minimum and mean PIF improvement as a function of distance for different initial baseline lengths.

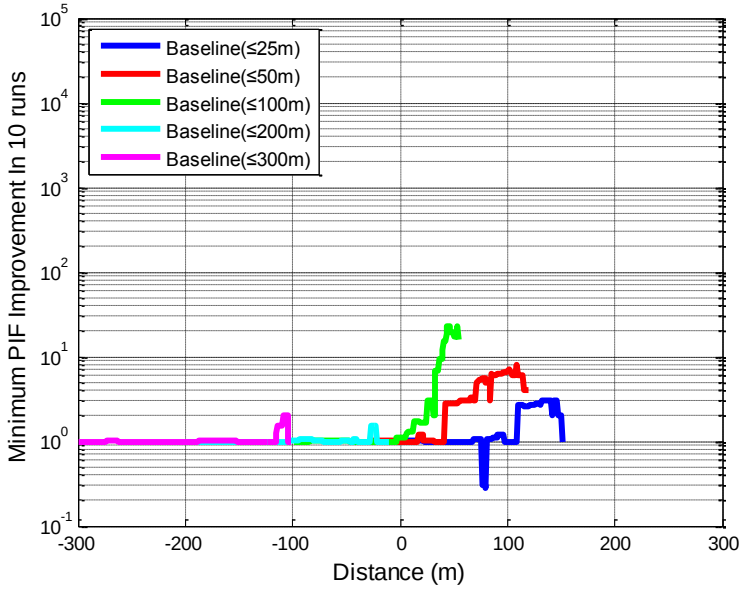

Figure 5.43 Minimum PIF Improvement vs. Distance for different initial baseline lengths

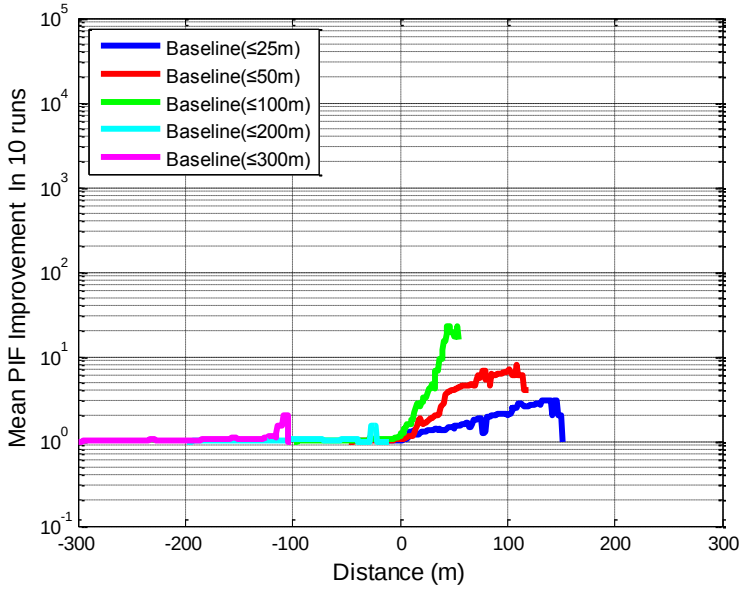

Figure 5.44 Mean PIF Improvement vs. Distance for different initial baseline lengths

Ambiguity resolution results are shown in Table D.2 to Table D.4 in APPENDIX D, they are summarized graphically in Figure 5.45 and Figure 5.46 respectively. In this case, the

performance is less improved because the GPS-only results are already quite good. Overall, 15 of 50 cases (5 different initial distance in 10 runs), which is 30%, are able to resolve ambiguities more quickly. Nevertheless, including UWB data does provide better ambiguity resolution for 25 m, 50 m and 200 m cases as shown in Table 5.8 with 6.1%, 10.5% and 9.1% improvements, respectively.

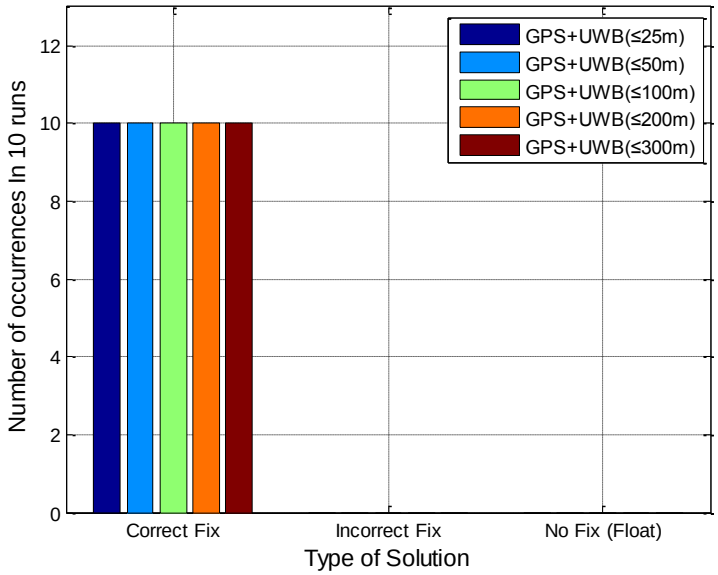

Figure 5.45 Ambiguity Resolution for GPS + UWB under different initial baselines (25 m, 50 m, 100 m, 200 m, 300 m)

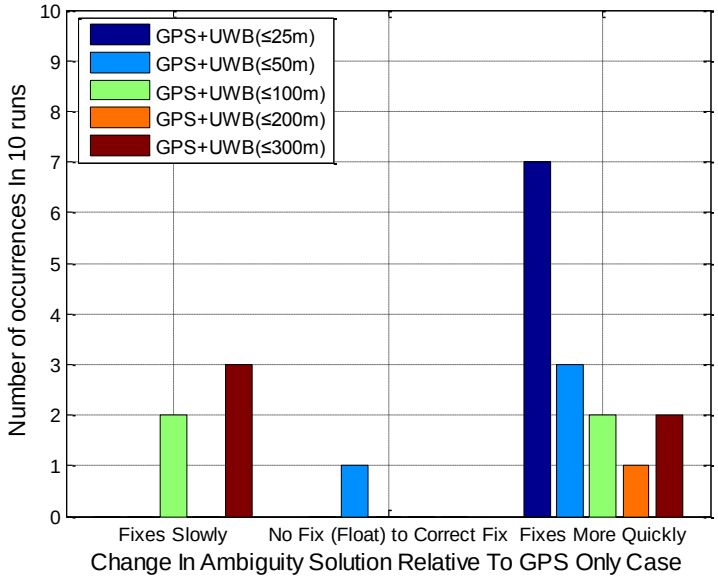

Figure 5.46 Change in Ambiguity Solution when Adding UWB Relative To GPS-only case under different initial baselines (25 m, 50 m, 100 m, 200 m, 300 m)

Table 5.8 Improvement in average time of first ambiguity fix (in seconds) of GPS + UWB fix solution compared to GPS-only fix solution for runs

Solution	Strategies	Time Improvement
GPS-only	I	8.2 s
	II	4.1 s
	III	4.0 s
	IV	5.9 s
	V	4.9s
GPS+UWB	VI	6.1%
	VII	10.5%
	VIII	-28.8%
	IX	9.1%
	X	-9.3%

I. GPS-only when the vehicle is within 25 m from the first UWB radio ("GPS-only (baseline ≤25 m)");
II. GPS-only when the vehicle is within 50 m from the first UWB radio ("GPS-only (baseline ≤50 m)");
III. GPS-only when the vehicle is within 100 m from the first UWB radio ("GPS-only (baseline ≤100 m)");
IV. GPS-only when the vehicle is within 200 m from the first UWB radio ("GPS-only (baseline ≤200 m)");
V. GPS-only when the vehicle is within 300 m from the first UWB radio ("GPS-only (baseline ≤300 m)");
VI. GPS + UWB estimating the UWB systematic errors using UWB measurements when the vehicle is within 25 m from the first UWB radio ("GPS + UWB (baseline ≤25 m)");
VII. GPS + UWB estimating the UWB systematic errors when the vehicle was within 50 m from the first UWB radio ("GPS + UWB (baseline ≤50 m)");
VIII. GPS + UWB estimating the UWB systematic errors when the vehicle was within 100 m from the first UWB radio ("GPS + UWB (baseline ≤100 m)");
IX. GPS + UWB estimating the UWB systematic errors when the vehicle was within 200 m from the first UWB radio ("GPS + UWB (baseline ≤200 m)");
X. GPS + UWB estimating the UWB systematic errors when the vehicle was within 300 m from the first UWB radio ("GPS + UWB (baseline ≤300 m)");

5.4.2 Consumer-Grade GPS Results

Figure 5.47 shows the horizontal RMS error as a function of distance. These results are slightly better than in the previous scenarios (i.e. B and C), because of the improved satellite visibility. Compared to the Geodetic-Grade GPS receiver, the results are slightly worse due to the poor pseudorange measurement quality.

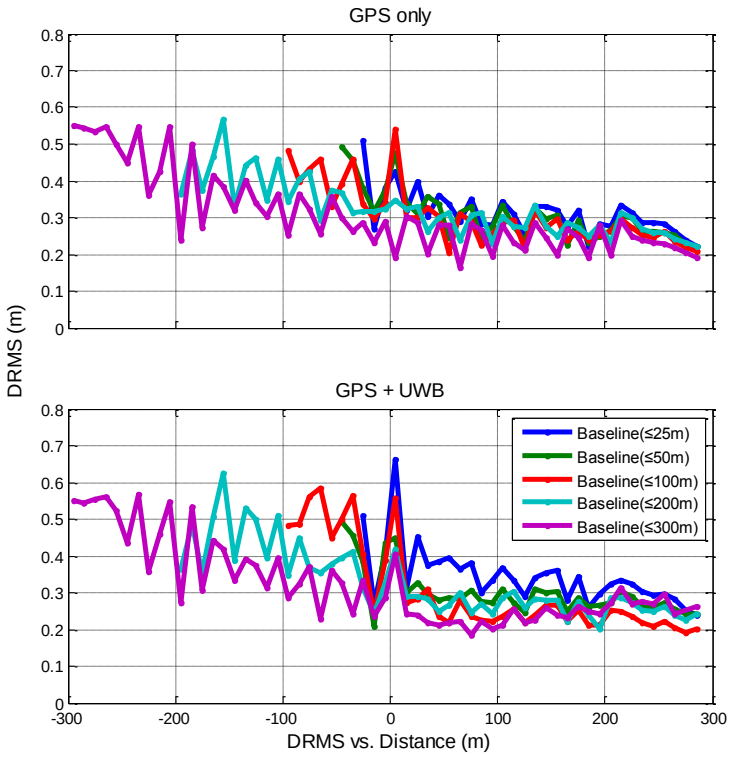

Figure 5.47 Horizontal RMS (DRMS) errors vs. Distance for GPS-only and GPS + UWB under different initial baselines (25 m, 50 m, 100 m, 200 m, 300 m)

Improvement in RMS and median error of GPS + UWB compared to GPS-only solution at intersection for all runs is shown in Table D.5 in APPENDIX D. It is seen that the only 13 out of 40 cases (i.e. horizontal, north, east and vertical RMS and median errors for GPS + UWB with 5

baselines) improved due to the poorer quality pseudorange measurements of the Consumer-Grade GPS receivers (see from Table 4.2)

Unlike the previous scenarios B and C, the improved satellite visibility in this case yielded better PIF results – even for GPS alone – as shown in Figure 5.48. These results are for the same run as in Figure 5.42 which shows the corresponding Geodetic-Grade GPS results. Although the PIF values are still much larger, they are considerably better than the Consumer-Grade GPS results in the other scenarios as shown in Figure 5.23 whose best case PIF is approximately 10^{-2} and Geodetic-Grade GPS results with 1Hz data rate shown in Figure 5.28 approximately 10^{-7}.

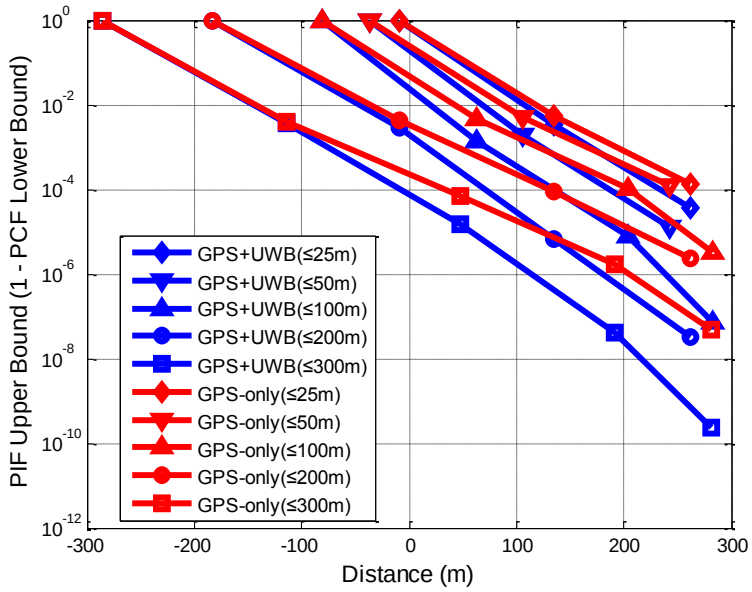

Figure 5.48 Run #4, PIF vs. Distance, GPS-only compared to GPS + UWB measurements (with errors estimated in run) up to 300 m

Figure 5.49 and Figure 5.50 respectively show the minimum and average PIF improvements after adding UWB data. In this case, the improvements are much more noticeable and similar to the Geodetic-Grade GPS results in Section 5.4.1, and the longest initial baseline gives the largest minimum and mean PIF improvement. In addition, less than 10^4 times improvement is achieved for all the baselines for the mean PIF improvements.

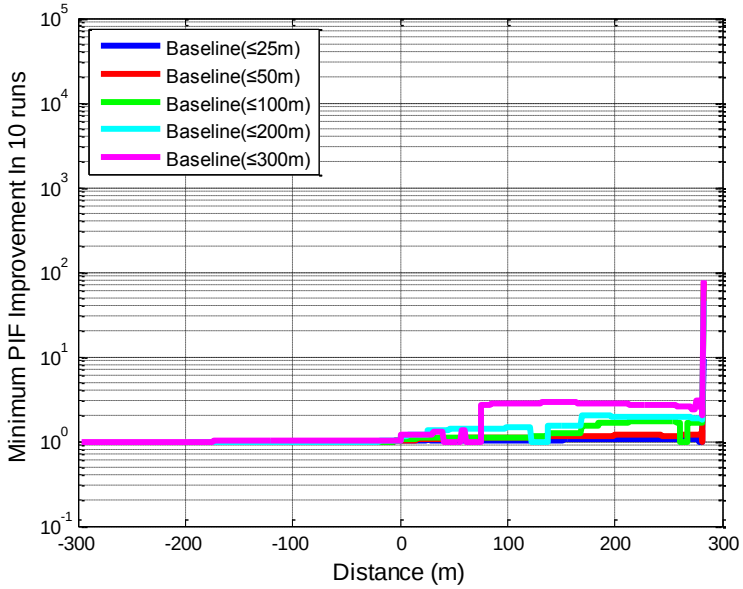

Figure 5.49 Minimum PIF Improvement vs. Distance for different initial baseline lengths with UWB errors estimated in filter

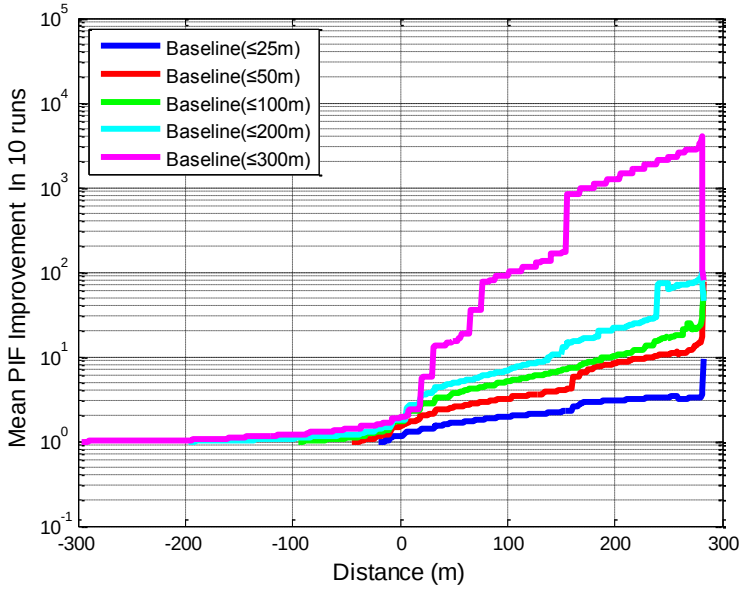

Figure 5.50 Mean PIF Improvement vs. Distance for different initial baseline lengths with UWB errors estimated in filter

The ambiguity resolution results are shown in Table D.6 to Table D.8 in APPENDIX D, and they are summarized graphically Figure 5.51 and Figure 5.52, respectively. As with the other cases, UWB measurements improve ambiguity resolution performance, if only slightly. Overall, 9 of 50 cases (5 different initial distance in 10 runs), which is 18%, are able to resolve ambiguities more quickly and 14% of all the cases are able to produce an ambiguity fix when GPS alone was only able to provide a float solution. Nevertheless, adding UWB data does provide better ambiguity resolution for 100 m, 200 m and 300 m cases as shown in Table 5.9 with 3.2%, 17.0% and 16.4% improvements, respectively.

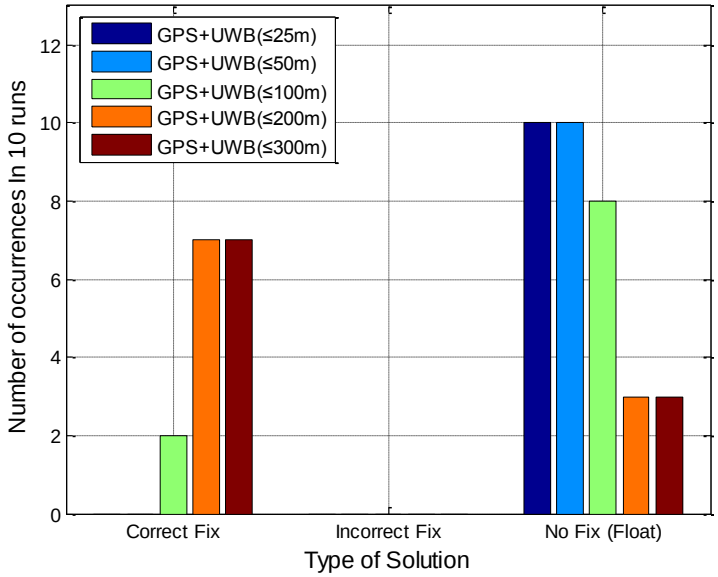

Figure 5.51 Ambiguity Resolution for GPS + UWB under different initial baselines (25 m, 50 m, 100 m, 200 m, 300 m)

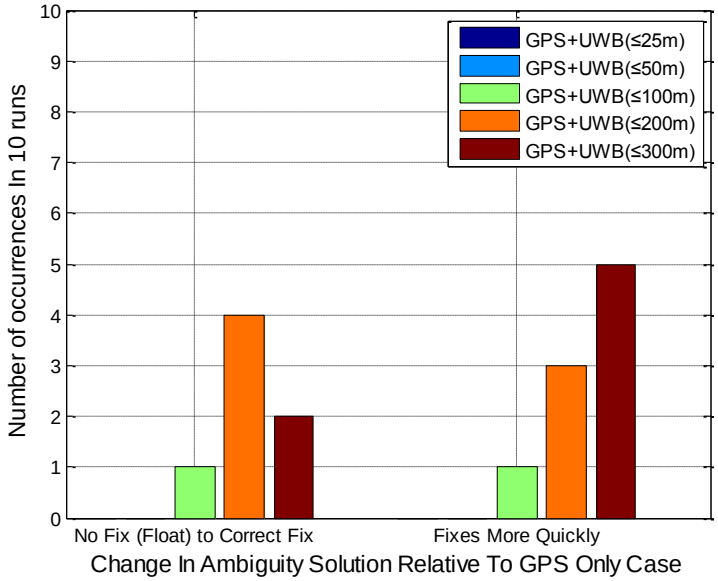

Figure 5.52 Change in Ambiguity Solution when Adding UWB Relative To GPS-only case under different initial baselines (25 m, 50 m, 100 m, 200 m, 300 m)

Table 5.9 Improvement in average time of first ambiguity fix (in seconds) of GPS + UWB fix solution compared to GPS-only fix solution for runs

Solution	Strategies	Time Improvement
GPS-only	I	N/A
	II	N/A
	III	31.0 s
	IV	31.3 s
	V	33.0 s
GPS+UWB	VI	N/A
	VII	N/A
	VIII	3.2%
	IX	17.0%
	X	16.4%

I. GPS-only when the vehicle is within 25 m from the first UWB radio ("GPS-only (baseline ≤25 m)");
II. GPS-only when the vehicle is within 50 m from the first UWB radio ("GPS-only (baseline ≤50 m)");
III. GPS-only when the vehicle is within 100 m from the first UWB radio ("GPS-only (baseline ≤100 m)");
IV. GPS-only when the vehicle is within 200 m from the first UWB radio ("GPS-only (baseline ≤200 m)");
V. GPS-only when the vehicle is within 300 m from the first UWB radio ("GPS-only (baseline ≤300 m)");
VI. GPS + UWB estimating the UWB systematic errors using UWB measurements when the vehicle is within 25 m from the first UWB radio ("GPS + UWB (baseline ≤25 m)");
VII. GPS + UWB estimating the UWB systematic errors when the vehicle was within 50 m from the first UWB radio ("GPS + UWB (baseline ≤50 m)");
VIII. GPS + UWB estimating the UWB systematic errors when the vehicle was within 100 m from the first UWB radio ("GPS + UWB (baseline ≤100 m)");
IX. GPS + UWB estimating the UWB systematic errors when the vehicle was within 200 m from the first UWB radio ("GPS + UWB (baseline ≤200 m)");
X. GPS + UWB estimating the UWB systematic errors when the vehicle was within 300 m from the first UWB radio ("GPS + UWB (baseline ≤300 m)");

CHAPTER 6: CONCLUSIONS AND RECOMMENDATIONS

This chapter draws conclusions from the preceding chapters and summarizes the findings of the research. Ideas for future investigation are also recommended.

6.1 Conclusions

This work investigates a system integrating UWB measurements with GPS for Vehicle-to-Infrastructure (V2I) applications with the goal of providing a reliable carrier-phase differential GPS position solution while a vehicle is within a limited communication service area centered at an intersection. The GPS position solution and ambiguity resolution performance were analyzed for different UWB integration strategies and approach trajectories. The key findings that can be drawn are as follows:

For Scenario A with two stationary UWB radios deployed at the corners of the intersection, GPS and UWB integrated positioning systems can improve GPS float position solutions relative to the GPS-only case. 115 out of 128 cases (i.e. horizontal, north, east and vertical RMS and median errors for all trajectories, travelling directions and data processing strategies), which is 89.8% in percentage, improved. Furthermore, UWB measurements generally improve the position accuracy along track direction due to improved geometry.

The improvement of position solutions does not occur until about 25 metres after the vehicle has passed through the intersection (two cases estimating UWB errors), which confirms that the period during which a vehicle approaches an intersection is not sufficient to converge to a good solution, even with assistance from UWB ranges (while with GPS alone a cm-level solution is

impossible), which suggests that the UWB radios could be located some distances away from the intersection.

For ambiguity resolution, the inclusion of UWB measurements results in 2 cases (i.e. 1%) out of 200 runs (4 UWB augmentation strategies for 10 runs for all 4 trajectories) where an incorrect GPS-only fix becomes correct fix, 5 cases (i.e. 2.5%) incorrect to "no fix" result, and 47 cases (i.e. 23.5%) "no fix" to correct fix and 62 cases (i.e. 31%) an existing fix becomes more quickly.

For ambiguity fix solution, the use of UWB measurements can provide improved fix time relative to the GPS-only case. The addition of UWB measurements results in 30.8% (7.0 seconds) improvement on average for Trajectory A (North to West) for all 4 data processing strategies, 23.1% (8.9 seconds) improvement for Trajectory B (East to West), 30% (9.0 seconds) improvement for Trajectory C (East to North), and 15.8% (4.2 seconds) improvement for Trajectory D (West to East).

For scenario B, it consisted of a north-south rural road with two UWB radios located on either side of the road roughly 300 m north of a fictitious intersection. For float position solution, the largest improvement occurs in the north component, and due to horizontal geometry of the trajectory and the UWB range, there is little improvement in the vertical component.

In addition, improvement does not generally occur until after the vehicle passes the first UWB radio. Longer initial ranges (e.g. the 200 m run) of UWB radios could converge the solution earlier, and even with shorter UWB ranges (e.g. the 25 m run) it could also augment GPS after

passing the UWB radios, which suggests that this system implementing even shorter ranges could also be used in the practical applications.

Overall, 29 out of 40 cases (i.e. horizontal, north, east and vertical RMS and median errors for GPS + UWB with 5 baselines) compared with GPS-only cases improved, while 22 out 40 cases just before passing the first UWB radio. This is due to the rapid changes in the measured range between vehicle and UWB radios are able to separate the UWB systematic errors (i.e. bias and scale factor), the ability to estimate each error improves. Once the UWB errors are well estimated, the UWB measurements can be used better observe the position after passing the UWB radios.

The two UWB systemic errors become well estimated at the same time that the UWB-aided position solution starts to outperform the GPS-only solution, namely as the vehicle passes the first UWB radio.

Results are similar for both using corrected and uncorrected UWB ranges. This is because when the vehicle is approaching to the intersection, the total error is only slightly worse than that of the corrected case. The total error is calculated by converting the scale factor value into a distance by multiplying the distance and then adding the variances of the bias, scale factor and measurement noise (discussed in Section 5.2.1). In other words, the difference in range measurement is small, especially as time passes (and distance decreases). Based on these results, estimating the UWB errors in this scenario did not affect performance too much.

For PCF/PIF analysis, the results suggest that improvement of between a factor of about 10 and 100 occur, on average, before the vehicle approaches the intersection, regardless of initial baseline length.

For ambiguity resolution, 22 of 50 cases (5 different initial distances in 10 runs) in total, which is 44%, are able to resolve ambiguities more quickly and 12% of all the cases are able to produce an ambiguity fix when GPS alone was only able to provide a float solution. For ambiguity fix solution, inclusion of UWB ranges provides improvements in fix time with 9.4% (1.0 seconds), 10.5% (1.1 seconds), 21.4% (3.1 seconds), 18.3% (3.4 seconds) and 1.1% (0.3 seconds) for different initial baselines (25 m, 50 m, 100 m, 200 m, 300 m), respectively.

This Scenario also investigates the performance by comparing two types of receivers (i.e. Geodetic-Grade GPS and Consumer-Grade GPS) with different data rate. The float solution performance is decreased because of the poorer quality pseudorange measurements of the Consumer-Grade GPS receivers. Overall, 19 out of 40 cases (i.e. horizontal, north, east and vertical RMS and median errors for GPS + UWB with 5 baselines) are improved at intersection.

By comparing the results for Geodetic-Grade GPS with 1Hz and Consumer-Grade GPS, it suggests that the GPS type (i.e. Geodetic-Grade GPS or Consumer-Grade GPS) does not affect position accuracy too much. 27 out of 40 cases (i.e. horizontal, north, east and vertical RMS and median errors for GPS + UWB with 5 baselines) improved compared to 29 cases for 10Hz Geodetic-Grade GPS receivers and 19 cases for 1Hz Consumer-Grade GPS receivers.

For the 1Hz Geodetic-Grade GPS results, the PIF values are considerably larger than that of the Consumer-Grade GPS receivers, however smaller than that of 10Hz Geodetic-Grade GPS receivers.

In general, the longer initial baselines of Geodetic-Grade GPS with 1Hz data rate receive the largest PIF improvements when adding UWB. The mean improvement of between a factor of about less 100 occur before the vehicle approaches the intersection with different initial baseline length, which are generally similar to Consumer-Grade GPS results but slightly better. Thus it can be concluded that the GPS type (i.e. Geodetic-Grade GPS or Consumer-Grade GPS) does not affect PCF/PIF performance too much.

Scenario C used the same data with Scenario B but only one infrastructure point was deployed locating approximately halfway along the length of the test trajectory. For RMS and median error performance, the results are generally similar to those of Scenario B setup, which indicates that the even with one UWB radio, the solution performs similar with regard to position accuracy to that of Scenario B. Overall, 25 out of 40 cases (i.e. horizontal, north, east and vertical RMS and median errors for GPS + UWB with 5 baselines) improved compared to 29 cases for Geodetic-Grade GPS receivers for Scenario B.

For the PCF/PIF analysis, the results are similar to those of scenario B, which shows that the PIF performance does not change substantially when using only one UWB radio.

For ambiguity resolution, 23 of 50 cases (5 different initial distances in 10 runs), which is 46%, were able to resolve ambiguities more quickly (29 of 50 cases in Scenario B), 14% of all the cases are able to produce an ambiguity fix when GPS alone was only able to provide a float solution (12% in Scenario B). For ambiguity fix solution, inclusion of UWB ranges provides improvements in fix time with 4.1% (0.4 seconds), 9.4% (0.9 seconds), 16.8% (2.4 seconds), 16.9% (3.2 seconds) and 15% (4.0 seconds) for different initial baselines (25 m, 50 m, 100 m, 200 m, 300 m), respectively.

Scenario D is the setup where one of the two UWB radios is moved next to the intersection while the other one remains the same location as that of Scenario B and C.
The results are generally similar to those of the other setup (i.e. Scenario B and C) suggesting that the UWB geometry does not affect position accuracy too much. 35 out of 40 cases (i.e. horizontal, north, east and vertical RMS and median errors for GPS + UWB with 5 baselines) improved when the vehicle is approaching the intersection.

For the PCF/PIF analysis, the GPS-only results are much better than in the previous scenarios due to an improved GPS constellation during the test.

The improvements in ambiguity resolution are less than GPS-only results because the GPS-only results are already quite good. Overall, 15 of 50 cases (5 different initial distance in 10 runs), which is 30%, are able to resolve ambiguities more quickly. For ambiguity fix solution, inclusion of UWB ranges provides improvements in fix time with 6.1% (0.5 seconds), 10.5% (0.4 seconds) and 9.1% (0.5 seconds) for different initial baselines (25 m, 50 m, 200 m), respectively.

For Consumer-Grade GPS receivers, 9 of 50 cases (5 different initial distance in 10 runs), which is 18%, are able to resolve ambiguities more quickly and quickly and 14% of all the cases are able to produce an ambiguity fix when GPS alone was only able to provide a float solution. For ambiguity fix solution, inclusion of UWB ranges provides improvements in fix time with 3.2% (1.0 seconds), 17% (5.3 seconds) and 16.4% (5.4 seconds) for different initial baselines (100 m, 200 m, 300 m), respectively.

6.2 Recommendations

Though this thesis has done a lot of work to study the benefit of integrating UWB ranges with GPS for the different V2I configurations, there are still many years of work to do related to this topic to exploit the full benefits of UWB technology. Further implementation in hostile environments (e.g. urban canyon and dense foliage) is needed to fully investigate the benefits of the integrated system. More work is regard to estimate and correct for the scale factor and bias errors OTF for real-time applications. GPS L2, GLONASS and Galileo satellites measurements could also be included in the integrated system to improve the ambiguity resolution performance.

REFERENCES

Arslan, H., Chen, Z., & Di Benedetto, M. (2006). Ultra Wideband Wireless Communications. *Wiley-Interscience*.

Axelrad, P., & Brown, R. G. (1996). *The Global Positioning System: Theory and Applications, Chapter 9 GPS Navigation Algorithms*: American Institute of Aeronautics and Astronautics.

Basnayake, C., Lachapelle, G. & Bancroft, J (2011). *Relative Positioning for Vehicle-to-Vehicle Communications-Enabled Vehicle Safety Applications,*. 18th ITS World Congress, Orlando Florida.

Brown, R. G., & Hwang, P. Y. C. (1997). *Introduction to Random Signals and Applied Kalman Filtering*: John Wiley & Sons.

Cai, C. (2009). *Precise Point Positioning Using Dual-Frequency GPS and GLONASS Measurements.* MSc Thesis, Univerisity of Calgary.

Cao, W. (2009). *Multi-frequency GPS and Galileo Kinematic Positioning with Partial Ambiguity Fixing.* MSc Thesis, University of Calgary.

Chen, D., & Lachapelle, G. (1994). *A Comparison of the FASF and Least-Squares Search Algorithms for Ambiguity Resolution On The Fly.* Paper presented at the International Symposium on Kinematic Systems in Geodesy, Geomatics and Navigation, Banff, Alberta, Canada.

Chiu, D. (2008). *Ultra Wideband Augmented GPS.* MSc Thesis, University of Calgary, Canada.

Chiu, D., & O'Keefe, K. (2008). *Seamless Outdoor-to-Indoor Pedestrian Navigation using GPS and UWB.* Paper presented at the ION GNSS 2008, Savannah, GA.

Cobb, H. (1997). *GPS Pseudolites: Theory, Design and Applications.* Ph.D Thesis, Standford University.

Conley, R., Cosentino, R., Hegarty, C., Kaplan, E., Leva, J., Haag, M. U. d., & Dyke, K. V. (2006). *Understanding GPS: Principles and Applications, Chapter 7Performance of Stand-Alone GPS*: Artech House.

Cosentino, R., Diggle, D., Haag, M. U. d., Hegarty, C. J., Milbert, D., & Nagle, J. (2006). *Understanding GPS: Principles and Applications, Chapter 8 Differential GPS*: Artech House.

FCC. (2002). Revision of Part 15 of the Commissions Rules Regarding Ultra-Wideband Transmission Systems. First Report and Order in ET Docket No. 98-153.

Fernandez-Madrigal, J. A., Cruz-Martin, E., Gonzalez, J., Galindo, C., & Blanco, J. L. (2007). *Application of UWB and GPS technologies for vehicle localization in combined indoor-outdoor environments.* Paper presented at the Signal Processing and Its Applications, 2007. ISSPA 2007. 9th International Symposium on.

Fontana, R. (2002). Experimental Results from an Ultra Wideband Precision Geolocation System. *Short Pulse Electromagnetics*, Pages 215-223.

Fukushima, M., & Seto, M. (2006). *Field Operational Test Plan of Vehicle Infrastructure Cooperative System for Intersection Collision Avoidance in Kanagawa, Japan.* Paper presented at the Proceedings of the 13th ITS World Congress, London.

Gelb, A. (1974). *Applied Optimal Estimation*: Analytical Sciences Corporation.

Gezici, S., & Poor, H. V. (2009). Position Estimation via Ultra-Wide-Band Signals. *In Proceedings of the IEEE*.

Gezici, S., Tian, Z., Giannakis, G. B., Kobayashi, H., Molisch, A. F., Poor, H. V., & Sahinoglu, Z. (2005). Localization via ultra-wideband radios. *IEEE Signal Processing Magazine*.

Gonzalez, J., Blanco, J., Galindo, C., Ortiz-de-Galisteo, A., Fernández-Madrigal, J., Moreno, F., & Martinez, J. (2007). *Combination of UWB and GPS for indoor-outdoor vehicle localization.* Paper presented at the Intelligent Signal Processing, 2007. WISP 2007. IEEE International Symposium on.

Grewal, S. M., Weill, L. R., & Andrews, A. P. (2001). *Global Positioning Systems, Inertial Navigation and Integration*: John Wiley and Sons.

Han, S. (1997). Quality Control Issues Relating to Instantaneous Ambiguity Resolution for Real-time GPS Kinematic Positioning. *Journal of Geodesy*.

Hatch, R. R. (1990). *Instantaneous Ambiguity Resolution.* Paper presented at the Proc. of KIS'90, Banff, Canada.

Hofmann-Wellenhof, B., Lichtenegger, H., & Collins, J. (2001). *GPS Theory and Practice* (Fifth revised ed.). New York: Springer-Verlag Wien

IEEE802-15.4a. (2007). Part 15.4: Wireless Medium Access Control and Physical Layer Specifications for Low-Rate Wireless Personal Area Networks, IEEE Standards.

Jiang, Y., Petovello, M., O'Keefe, K., & Basnayake, C. (2012). *Augmentation of Carrier-Phase DGPS with UWB Ranges for Relative Vehicle Positioning.* Paper presented at the Proceedings of ION GNSS 2012, Nashville, TN.

Kaplan, E. D., Hegarty, C. J., & (2006). *Understanding GPS: Principles and Applications.* (2nd ed.): Artech House.

Kaplan, E. D., Leva, J., Milbert, D., & Pavloff, M. S. (2006). *Understanding GPS: Principles and Applications, Chapter 2 Fundamentals of Satellite Navigation*: Artech House.

Kay, S. (1993). *Fundamentals of Statistical Signal Processing Estimation Theory*: Prentice-Hall Inc.

Lachapelle, G. (2010). *Advanced GNSS Theory And Application, ENGO 625 Course Notes*. Department of Geomatics Engineering, University of Calgary, Canada.

MacGougan, G., O'Keefe, K., & Chiu, D. (2008). *Multiple UWB Range Assisted GPS RTK in Hostile Environments.* Paper presented at the ION GNSS 2008, Savannah, GA.

MacGougan, G., & O'Keefe, K. (2009). Real time UWB error estimation in a tightly-coupled GPS/UWB positioning system. *Proceedings of ION ITM*, 26-28.

MacGougan, G. D. (2009). *Real-Time Kinematic Surveying using Tightly-Coupled GPS and Ultra-Wideband Ranging.*

MacGougan, G. D., & Klukas, R. (2009). *Method and Apparatus for High Precision GNSS/UWB Surveying.* Paper presented at the Proceedings of the 22nd International Technical Meeting of The Satellite Division of the Institute of Navigation (ION GNSS 2009), Savannah, GA.

Maybeck, P. (1979). *Stochastic Models, Estimation and Control*: Academic Press.

Misra, P., & Enge, P. (2006). *Global Positioning System: Signals, Measurements, and Performance*: Ganga-Jamuna Press

O'Keefe, K., Petovello, M., Lachapelle, G., & Cannon, M. E. (2006). Assessing Probability of Correct Ambiguity Resolution in the Presence of Time-Correlated Errors. *Journal of The Institute of Navigation*.

O'Keefe, K., Sharma, J., Cannon, M., & Lachapelle, G. (1999). *Pseudolite-Based Inverted GPS Concept for Local Area Positioning.* Paper presented at the ION GPS 99, Nashville, TN.

Olynik, M. (2002). *Temporal Characteristics of GPS Error Sources and Their Impact on Relative Positioning.* MSc. Thesis, The University of Calgary.

Opshaug, G. R., & Enge, P. (2002). *Integrated GPS and UWB navigation system:(Motivates the necessity of non-interference).* Paper presented at the Ultra Wideband Systems and Technologies, 2002. Digest of Papers. 2002 IEEE Conference on.

Pahlavan, K., Akgul, F., Dovis, F., Ye, Y., Morgan, T., Alizadeh-Shabdiz, F., . . . Steger, C. (2010). Taking Positioning Indoors Wi-Fi Localization and

GNSS. *Inside GNSS*.

Petovello, M., Cannon, M., & Lachapelle, G. (2003). *Quantifying Improvements from the Integration of GPS and a Tactical Grade INS in High Accuracy Navigation Applications.* Paper presented at the ION NTM, Anaheim, CA.

Petovello, M., O'Keefe, K., Chan, B., Spiller, S., Pedrosa, C., & Basnayake, C. (2010). *Demonstration of Inter-Vehicle UWB Ranging to Augment DGPS for Improved Relative Positioning.* Paper presented at the Proceedings of the 23rd International Technical Meeting of The Satellite Division of the Institute of Navigation (ION GNSS 2010), Portland, OR.

Petovello, M. G. (2010). Estimation for Navigation, ENGO 699 Course notes. *Department of Geomatics Engineering, The University of Calgary, Canada.*

Sahinoglu, Z., Gezici, S., & Guvenc, I. (2008). Ultra-Wideband Positioning Systems: Theoretical Limits, Ranging Algorithms, and Protocols. *Cambridge University Press*.

Shafiee, M., O'Keefe, K., & Lachapelle, G. (2011). *Context-aware Adaptive Extended Kalman Filtering Using Wi-Fi Signals for GPS Navigation.* Paper presented at the ION GNSS 2011, Portland, OR.

Shen, Y., & Xu, G. (2008). Simplified Equivalent Representation of GPS Observation Equations. *GPS Solutions*.

Skone, S. (2011). *Atmosphere Effects on Satellite Navigation Systems. ENGO 633 Course notes.* Department of Geomatics Engineering, The University of Calgary, Canada.

Spilker, J. J. (1996). *The Global Positioning System: Theory and Applications, Chapter 4 GPS Navigation Data*: American Institute of Aeronautics and Astronautics.

Tanigawa, M., Hol, J. D., Dijkstra, F., Luinge, H., & Slycke, P. (2004). Augmentation of low-cost GPS/MEMS INS with UWB positioning system for seamless outdoor/indoor positioning. *ION GNSS, Savannah, Georgia, Session C*.

Tao, W. Y. (2008). *Near Real-time GPS PPP-inferred Water Vapor System Development and Evaluation.* MSc Thesis, The University of Calgary, Canada.

Teunissen, P. (2000). *Adjustment theory; an introduction.* . Delft: Delft University Press.

Teunissen, P., & Tiberius, C. (1994). *Integer Least-Squares Estimation of The GPS Phase Ambiguities.* Paper presented at the International Symposium on Kinematic Systems in Geodesy, Geomatics and Navigation, Banff, Alberta, Canada.

Tiberius, C. C. J. M., Jonkman, N., & Kenselaar, F. (1999). The Stochastics of GPS Observables. *GPS World*.

US National Research Council, Committee on the Future of the Global Positioning System. (1995). *The global positioning system : a shared national asset : recommendations for technical improvements and enhancements*. Washington, D.C.: National Academy Press.

Verhagen, A. (2005). *The GNSS integer ambiguities: estimation and validation.* PhD thesis, Delft University of Technology.

Wan, X., Zhai, C., & Zhan, X. (2010). The pseudolite-based indoor navigation system using Ambiguity Resolution On The Fly. *Systems and Control in Aeronautics and Astronautics (ISSCAA)*, Page 212 - 217.

Wang, J. (2002). Pseudolite Applications in Positioning and Navigation: Progress and Problems. *Journal of Global Positioning Systems*, Page 48 - 56.

Wang, S., & Zhong, W. (2007). *Analyze and research the integrated navigation technique for GPS and pseudolite*. Paper presented at the Second International Conference on Space Information Technology, Wuhan, China.

Ward, P., Betz, J., & Hegarty, C. (2006). *Understanding GPS: Principles and Applications, Chapter 6 Interference, Multipath, and Scintillation*: Artech House.

Win, M., Dardari, D., Molisch, A., Wiesbeck, W., & Zhang, J. (2009). History and Applications of UWB. *Institute of Electrical and Electronics Engineers*.

Zhang, Q., Zhang, S., Bian, H., & Liu, W. (2010). *Research on GPS signal ambiguity resolution aided by INS*. Paper presented at the Image and Signal Processing (CISP), 2010 3rd International Congress.

Zhang, Y., & Gao, Y. (2007). Integration of INS and Un-Differenced GPS Measurements for Precise Position and Attitude Determination. *The Journal of Navigation, The Royal Institute of Navigation*.

APPENDIX A

This appendix includes additional results for Scenario A, which was analyzed in Section 5.1.

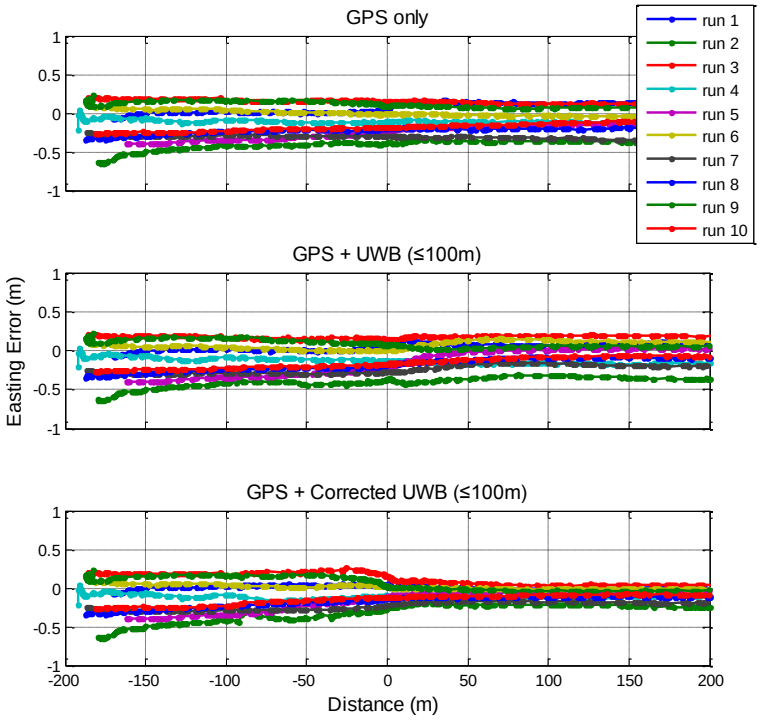

Figure A.1 Easting float solution GPS-only compared to GPS + UWB measurements (with errors estimated in run), GPS + corrected UWB measurements (with errors estimated in advance) up to 100 m for Trajectory A (North to West)

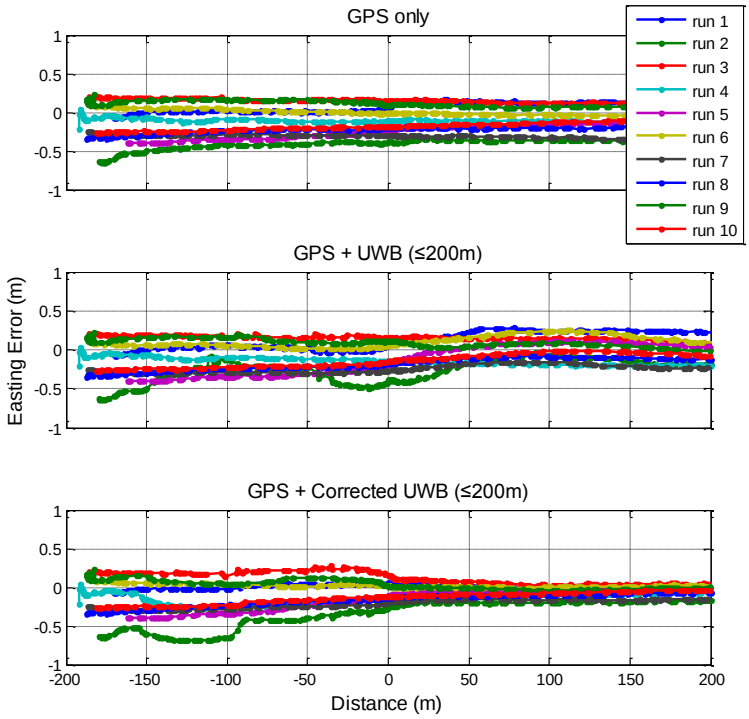

Figure A.2 Easting float solution GPS-only compared to GPS + UWB measurements (with errors estimated in run), GPS + corrected UWB measurements (with errors estimated in advance) up to 200 m for Trajectory A (North to West)

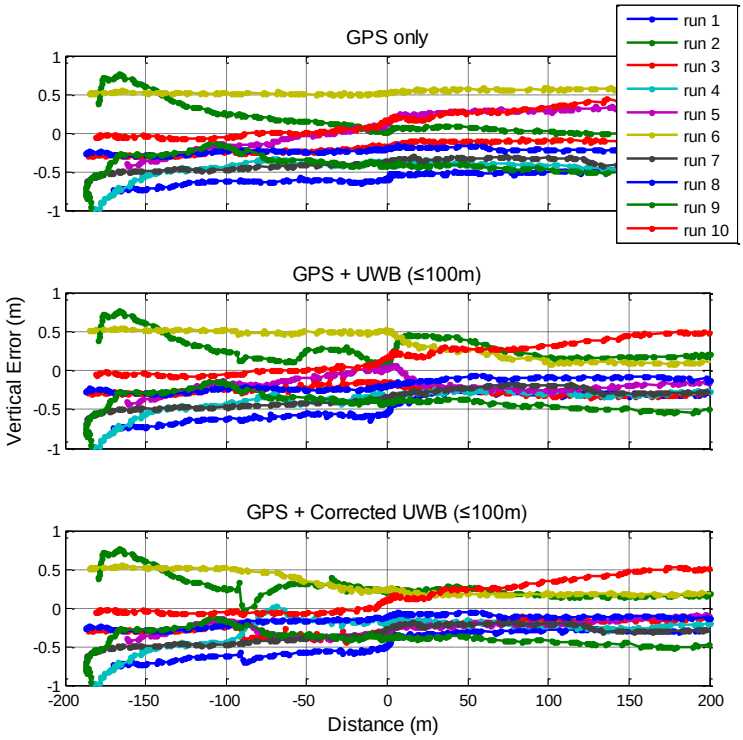

Figure A.3 Vertical float solution GPS-only compared to GPS + UWB measurements (with errors estimated in run), GPS + corrected UWB measurements (with errors estimated in advance) up to 100 m for Trajectory A (North to West)

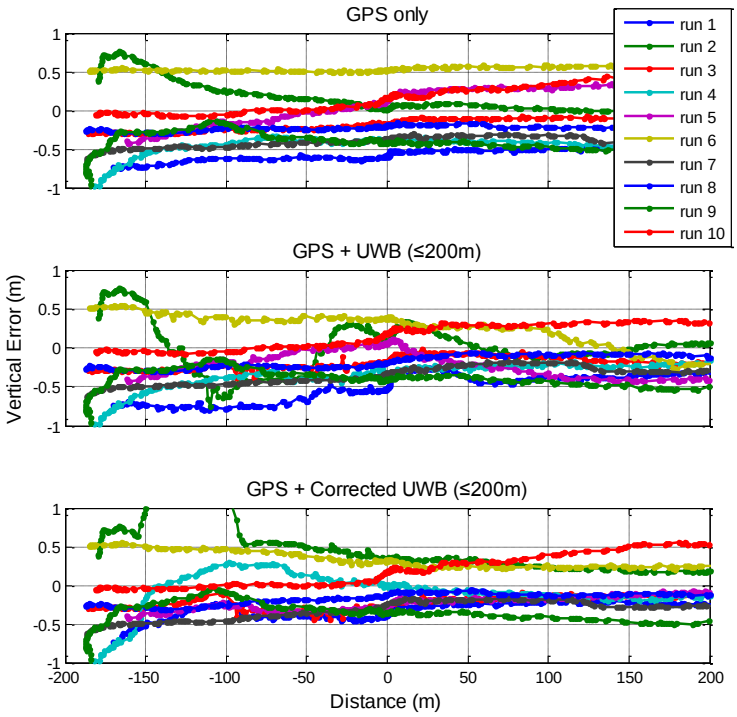

Figure A.4 Vertical float solution GPS-only compared to GPS + UWB measurements (with errors estimated in run), GPS + corrected UWB measurements (with errors estimated in advance) up to 200 m for Trajectory A (North to West)

Table A.1 Trajectory A (North to West) Time to First Fix by Run

Run #	Time to First Fix (s)				
	GPS only	GPS+UWB 100m	GPS+UWB 200m	GPS+UWB 100m Crt	GPS+UWB 200m Crt
1	19.9	18.4	18.2	18.4	11.9
2	N/A	N/A	N/A	N/A	11.7
3	35.6	20.4	33	10.9	9.9
4	N/A	N/A	N/A	14.3	17.9
5	13.5 (wrong fix)	13.4 (wrong fix)	13 (wrong fix)	11.9	13
6	N/A	27.9	27.9	22	N/A
7	N/A	29.8	29.9	24.7 (wrong fix)	24.7 (wrong fix)
8	29.7 (wrong fix)	N/A	13.9 (wrong fix)	N/A	10.1 (wrong fix)
9	N/A	N/A	N/A	26	26.8
10	13.1	13.1	14.5	11	12.2

Table A.2 Trajectory B (East to West) Time to First Fix by Run

Run #	Time To First Fix (s)				
	GPS only	GPS+UWB 100m	GPS+UWB 200m	GPS+UWB 100m Crt	GPS+UWB 200m Crt
1	21.8	18.5	21.4	15.8	13
2	N/A	30.6 (wrong fix)	N/A	23.6 (wrong fix)	22 (wrong fix)
3	33.4	29.6	23.9	21	21.5
4	29.4	21.3	20.7	19.1	18.6
5	29	21.3	20.6	18.8	19.8
6	N/A	51.6	43.8	28.6	26.5
7	57.3	56.7	32	55.8	55
8	23.7	20.1	19.4	17.8	17.1
9	N/A	N/A	29.7	N/A	18.7
10	N/A	26.1 (wrong fix)	25.9 (wrong fix)	25.4 (wrong fix)	25.3 (wrong fix)

Table A.3 Trajectory C (East to North) Time to First Fix by Run

Run #	Time to First Fix (s)				
	GPS only	GPS+UWB 100m	GPS+UWB 200m	GPS+UWB 100m Crt	GPS+UWB 200m Crt
1	29.5	24.5	24.3	23.8	24
2	N/A	29.9	30.3	29.6	29.5
3	33.2	22.1	21.5	21.6	21.6
4	N/A	16.6	24.9	14.4	17.3
5	26.9	19.8	19.7	16.8	15.6
6	N/A	28.8	28.1	24.8	24.6
7	N/A	N/A	N/A	40	36.3
8	27 (wrong fix)	N/A	26.7 (wrong fix)	N/A	N/A
9	9.8	9.8	N/A	9.6	8.8
10	N/A	N/A	N/A	31	23.5

Table A.4 Trajectory D (West to East) Time to First Fix by Run

Run #	Time To First Fix (s)				
	GPS only	GPS+UWB 100m	GPS+UWB 200m	GPS+UWB 100m Crt	GPS+UWB 200m Crt
1	N/A	24.3	24.7	22.9	23.7
2	19.4	19.2	19.1	15.4	8.6
3	N/A	N/A	N/A	11.6 (wrong fix)	9 (wrong fix)
4	N/A	N/A	N/A	15.7	12.1 (wrong fix)
5	34.1 (wrong fix)	29.7 (wrong fix)	35.5 (wrong fix)	24.4 (wrong fix)	48.9 (wrong fix)
6	14.5	14.5	14.5	14.5	14.3
7	40.9	23.9	22.9	21.5	21.4
8	18.5	18.8	18.3	15.2	9.5
9	N/A	N/A	N/A	N/A	N/A
10	N/A	22.3	22.1	18.3	19.1
11	N/A	N/A	N/A	26.8	N/A
12	N/A	49.5	N/A	36.8	27.9
13	N/A	N/A	N/A	N/A	35.8
14	6 (wrong fix)	6 (wrong fix)	6 (wrong fix)	6 (wrong fix)	5.3 (wrong fix)
15	48.6	48.6	48.6	48.6	48.6
16	16.5	16.6	16.6	16.6	18
17	N/A	N/A	N/A	N/A	N/A
18	N/A	N/A	N/A	N/A	N/A
19	N/A	18.9	18.6 (wrong fix)	16.9 (wrong fix)	16.9 (wrong fix)
20	13.3	12.6	12.5	10.3 (wrong fix)	8.3 (wrong fix)

Table A.5 Distance from intersection at time of first ambiguity fix for Trajectory A (North to West)

	Distance from intersection at time of first fix (m)				
Run #	**GPS only**	**GPS+UWB 100m**	**GPS+UWB 200m**	**GPS+UWB 100m Crt**	**GPS+UWB 200m Crt**
1	0.69	-0.27	-0.62	-0.23	-50.48
2	N/A	N/A	N/A	N/A	-69.88
3	163.77	5.11	127.80	-76.42	-89.44
4	N/A	N/A	N/A	-58.04	-18.88
5	-7.42	-8.16	-11.01	-21.41	-11.40
6	N/A	49.12	49.08	5.49	N/A
7	N/A	61.11	62.34	15.07	15.08
8	63.88	N/A	-49.40	N/A	-97.63
9	N/A	N/A	N/A	-0.38	2.82
10	-49.69	-49.69	-33.65	-77.10	-61.21

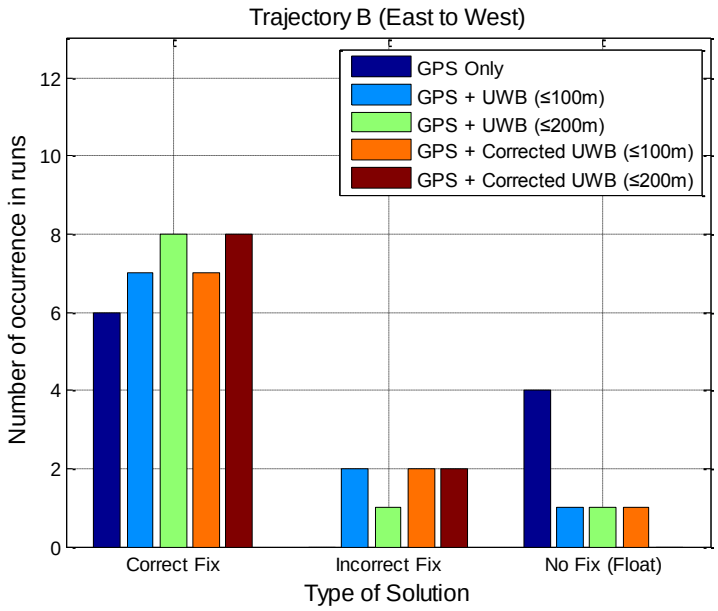

Figure A.5 Ambiguity resolution for Trajectory B (East to West) approach geometry

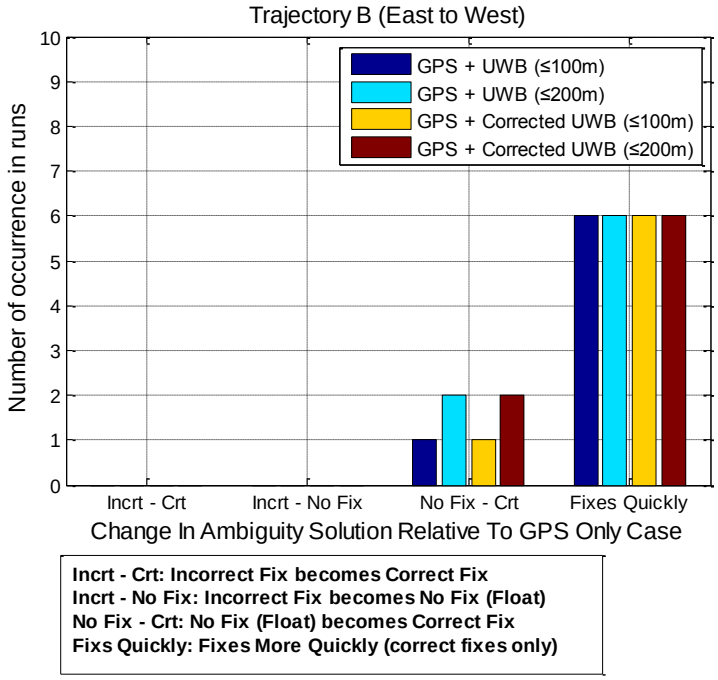

Figure A.6 Change in ambiguity resolution relative to GPS-only case for Trajectory B (East to West) approach geometry

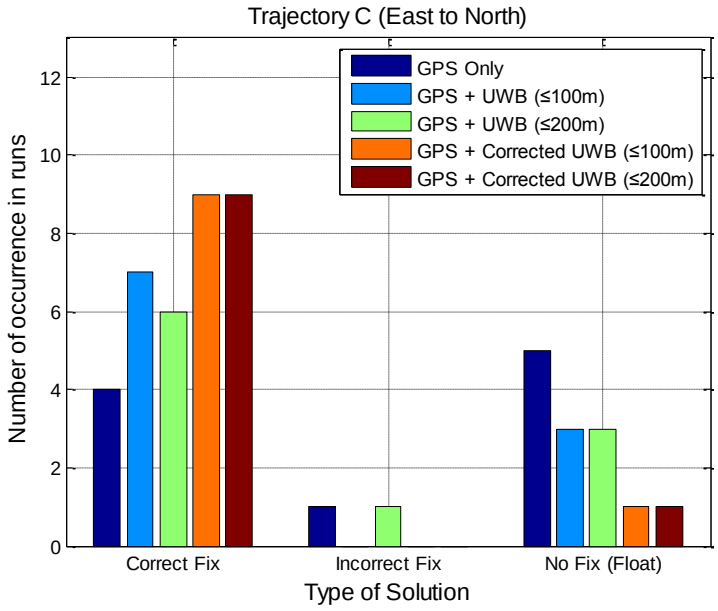

Figure A.7 Ambiguity resolution for Trajectory C (East to North) approach geometry

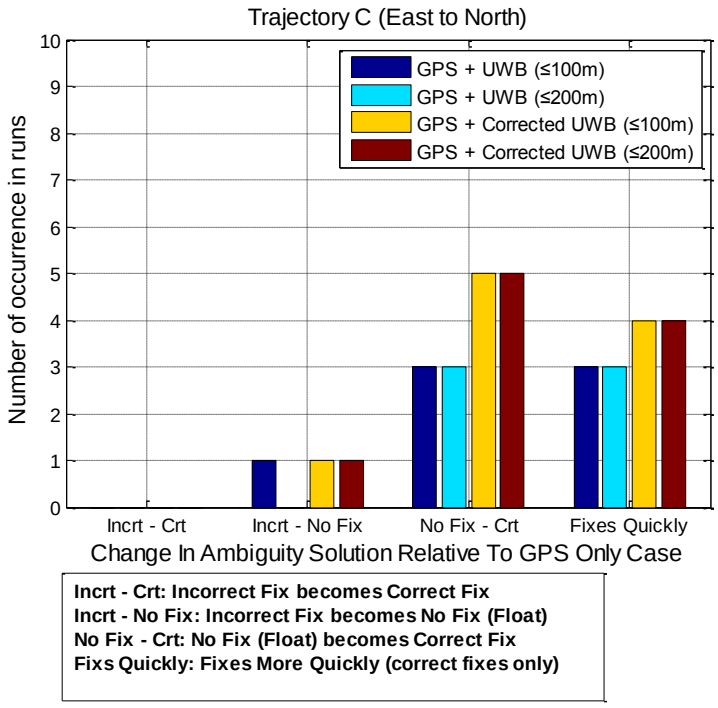

Figure A.8 Change in ambiguity resolution relative to GPS-only case for Trajectory C (East to North) approach geometry

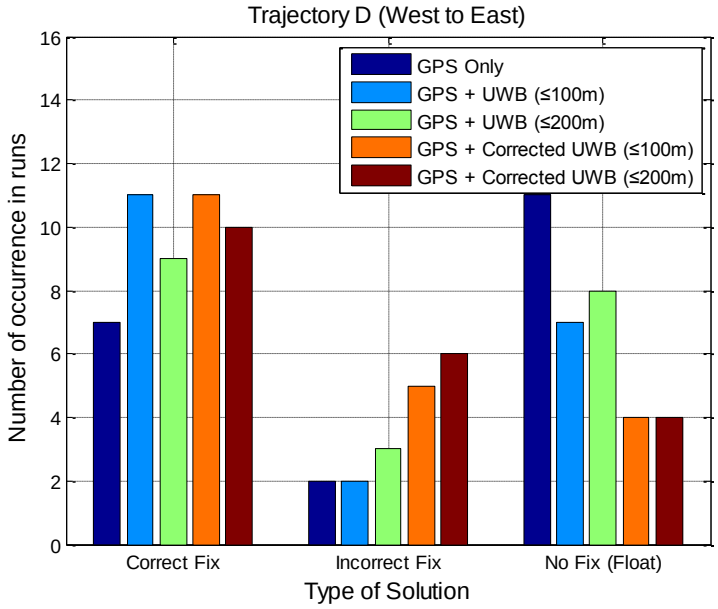

Figure A.9 Ambiguity resolution for Trajectory D (West to East) approach geometry

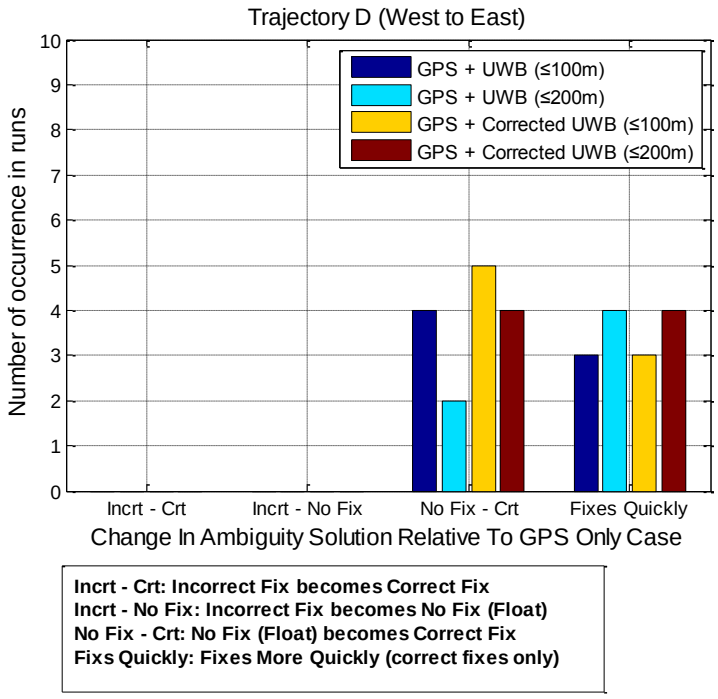

Figure A.10 Change in ambiguity resolution relative to GPS-only case for Trajectory D (West to East) approach geometry

APPENDIX B

This appendix includes additional results for Scenario B, which was analyzed in Section 5.2.

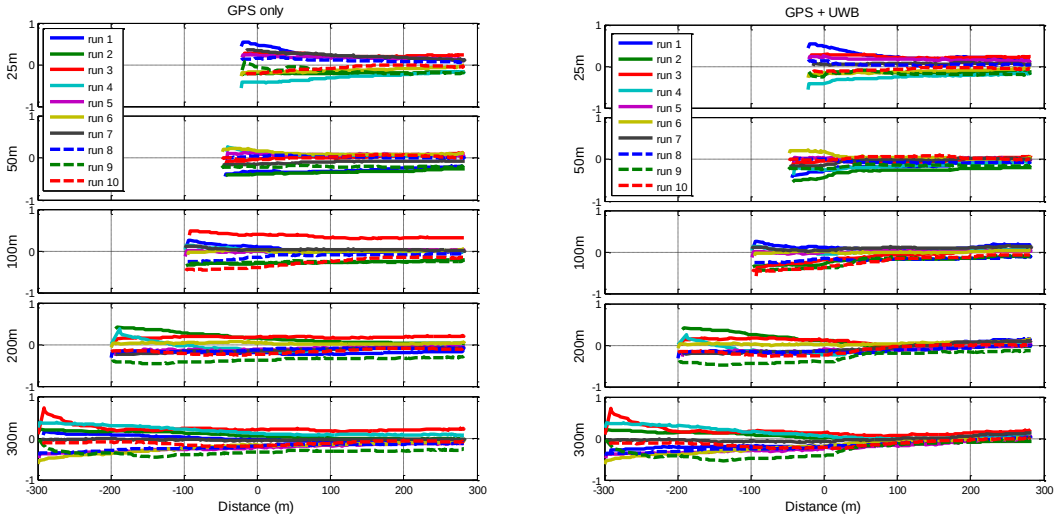

Figure B.1 Northing Errors vs. Distance to first UWB station using GPS along (left) and GPS + UWB (right) for different initial baselines (25 m, 50 m, 100 m, 200 m, 300 m)

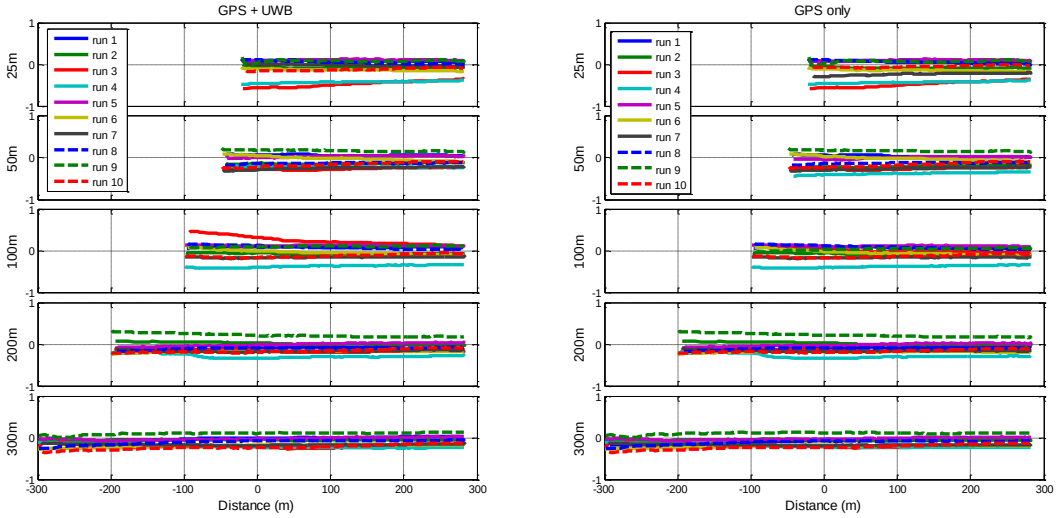

Figure B.2 Easting Errors vs. Distance to first UWB station using GPS along (left) and GPS + UWB (right) for different initial baselines (25 m, 50 m, 100 m, 200 m, 300 m)

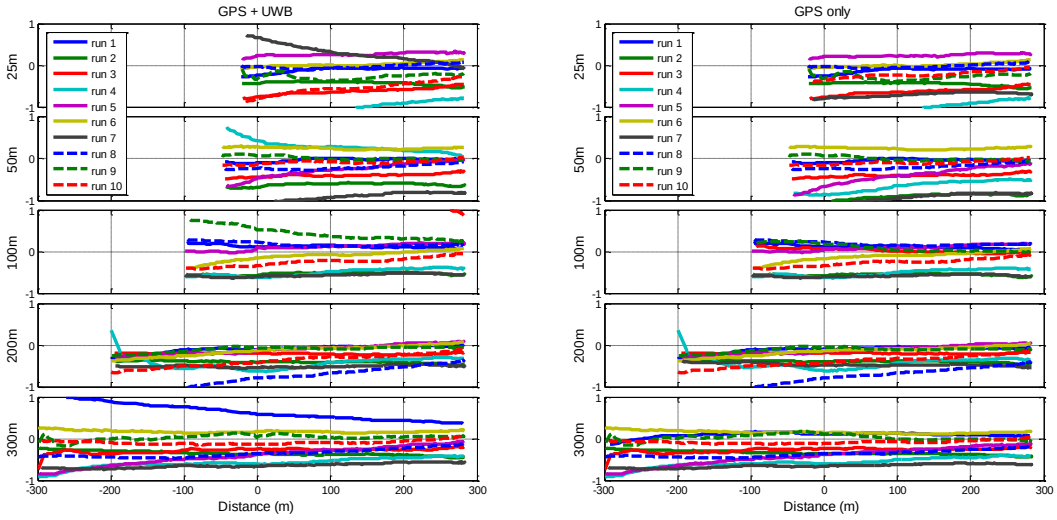

Figure B.3 Vertical Errors vs. Distance to first UWB station using GPS along (left) and GPS + UWB (right) for different initial baselines (25 m, 50 m, 100 m, 200 m, 300 m)

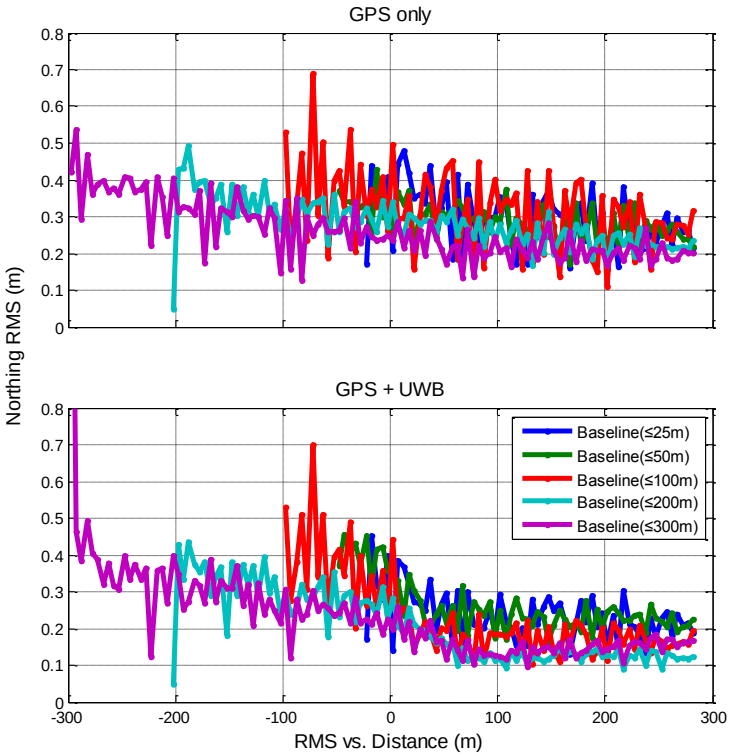

Figure B.4 Northing RMS errors vs. distance, GPS-only compared to GPS + UWB under different initial baselines (25 m, 50 m, 100 m, 200 m, 300 m)

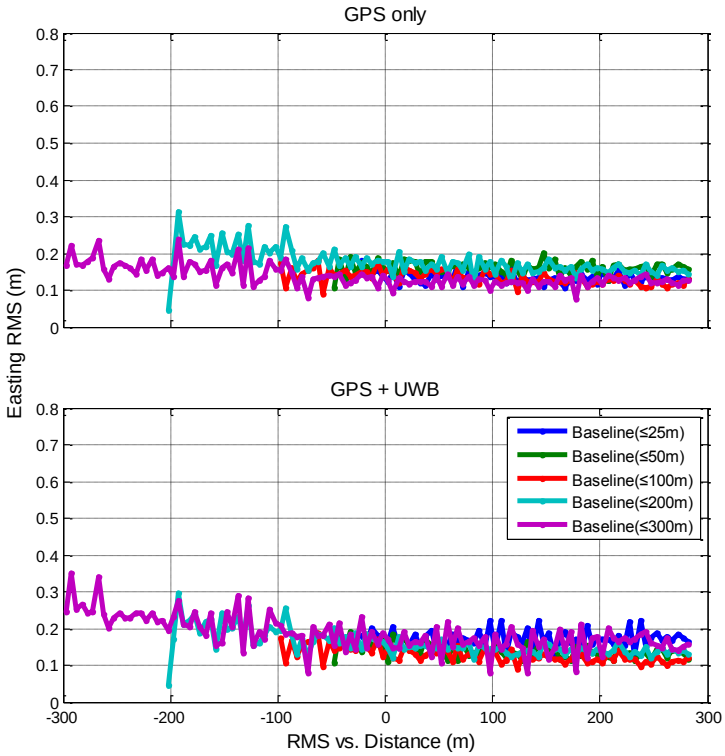

Figure B.5 Easting RMS errors vs. distance, GPS-only compared to GPS + UWB under different initial baselines (25 m, 50 m, 100 m, 200 m, 300 m)

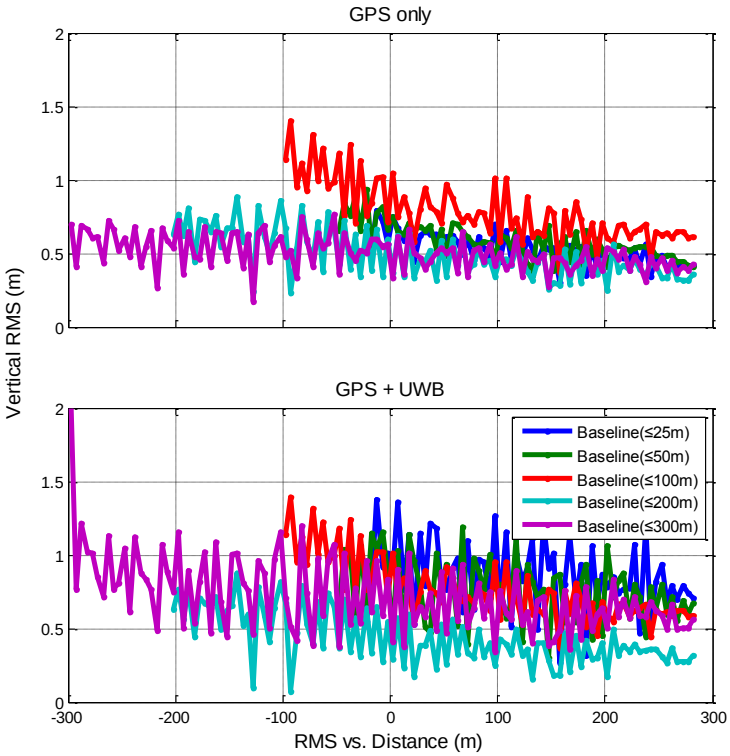

Figure B.6 Vertical RMS errors vs. distance, GPS-only compared to GPS + UWB under different initial baselines (25 m, 50 m, 100 m, 200 m, 300 m)

Table B.1 Time to First Fix by Run where UWB improves results are highlighted green and runs were UWB degrades results are highlighted in red. Red text indicates an incorrect fix.

Run #	Time to First Fix (s)									
	GPS 25m	G+U 25m	GPS 50m	G+U 50m	GPS 100m	G+U 100m	GPS 200m	G+U 200m	GPS 300m	G+U 300m
1	N/A	25.0	N/A	13.3	N/A	13.8	N/A	20.3	37.1	26.6
2	7.7	6.7	8.2	6.9	14	12.6	8.9	8.9	12.4	12.3
3	N/A	N/A	N/A	26.7	22.8	13.9	22	19.1	39	31.8
4	N/A	N/A	N/A	N/A	N/A	N/A	30.3	21.6	N/A	27.3
5	16.8	16.7	17.0	16.2	N/A	21.6	N/A	26.5	29.5	N/A
6	N/A	N/A	N/A	7.4	N/A	19	20.3	13.7	N/A	25.7
7	8.1	4.5	6.7	N/A	17.6	12.7	17.1	18.6	16.4	16.4
8	6.6	7.6	6.2	4.5	13.2	9.6	13.5	13.2	12.5	12.4
9	9.4	7.9	N/A	8.1	12.5	9.7	19.6	12.5	10.5	30.4
10	14.9	14.2	14.3	14.3	14.7	12.0	N/A	14.2	27.9	24.4

Table B.2 Distance from intersection at time of first fix (m)

Run #	Distance from Intersection at Time to First Fix (m)									
	GPS 25m	G+U 25m	GPS 50m	G+U 50m	GPS 100m	G+U 100m	GPS 200m	G+U 200m	GPS 300m	G+U 300m
1	N/A	N/A	N/A	181.22	N/A	226.90	N/A	226.90	82.98	225.8
2	199.10	213.23	222.71	239.41	193.26	213.23	335.73	335.73	378.32	379.75
3	N/A	N/A	N/A	21.54	N/A	N/A	203.48	238.55	92.77	182.44
4	N/A	N/A	N/A	N/A	N/A	N/A	14.63	142.09	N/A	142.09
5	46.48	47.71	N/A	N/A	N/A	44.04	N/A	54.07	86.31	N/A
6	N/A	N/A	N/A	211.65	N/A	83.16	165	264.52	N/A	177.63
7	156.44	216.97	205.38	N/A	69.51	152.99	176.95	151.26	N/A	N/A
8	212.18	198.22	237.34	258.30	192.5	241.15	264.15	267.59	348.85	350.43
9	168.07	190.33	N/A	213.44	212.03	249.81	213.44	301.72	417.42	154.40
10	75.03	84.38	113.69	113.69	150.96	192.85	N/A	246.79	128.34	181.94

Table B.3 Ambiguity fixing performance of GPS+UWB compared to GPS alone

Change in Solution	Baseline within 25m	Baseline within 50m	Baseline within 100m	Baseline within 200m	Baseline within 300m	Total
Incorrect to Correct	0/10	0/10	0/10	0/10	0/10	0/50
Incorrect to N/A	0/10	0/10	0/10	0/10	0/10	0/50
Correct to N/A	0/10	1/10	0/10	0/10	1/10	2/50
Correct to Incorrect	0/10	0/10	0/10	0/10	0/10	0/50
N/A to Incorrect	1/10	0/10	0/10	0/10	0/10	1/50
N/A to Correct	0/10	4/10	3/10	3/10	2/10	12/50
Slower to Faster	5/10	2/10	5/10	5/10	5/10	22/50
Faster to Slower	1/10	0/10	0/10	1/10	1/10	3/50
No Change	3/10	3/10	2/10	1/10	1/10	10/50

Table B.4 Improvement in RMS and median error (in metres) of GPS + UWB compared to GPS-only solution at intersection for all runs

strategies	RMS				Median			
	Horizontal	North	East	Vertical	Horizontal	North	East	Vertical
I (m)	0.340	0.258	0.205	0.444	0.203	0.032	0.071	0.175
II (m)	0.336	0.266	0.191	0.472	0.207	0.003	0.083	0.094
III (m)	0.307	0.230	0.190	0.499	0.185	-0.030	0.106	0.113
IV (m)	0.238	0.185	0.145	0.460	0.174	0.009	0.074	0.233
V (m)	0.214	0.156	0.149	0.399	0.209	0.024	0.076	0.014
VI (%)	1.0%	-4.5%	0.4%	3.9%	8.2%	384.7%	56.7%	-7.9%
VII (%)	1.3%	-2.9%	6.0%	18.7%	-27.8%	2043.6%	59.8%	-36.2%
VIII (%)	8.8%	10.6%	6.0%	1.9%	-27.7%	136.7%	26.9%	-18.1%
IX (%)	-32.6%	-50.6%	-2.5%	-16.3%	-24.8%	-120.2%	27.8%	73.7%
X (%)	-18.1%	-51.6%	-42.4%	-31.0%	-40.3%	-698.1%	-55.2%	-975.1%

I. GPS-only when the vehicle is within 25 m from the first UWB radio ("GPS-only (baseline ≤25 m)");
II. GPS-only when the vehicle is within 50 m from the first UWB radio ("GPS-only (baseline ≤50 m)");
III. GPS-only when the vehicle is within 100 m from the first UWB radio ("GPS-only (baseline ≤100 m)");
IV. GPS-only when the vehicle is within 200 m from the first UWB radio ("GPS-only (baseline ≤200 m)");
V. GPS-only when the vehicle is within 300 m from the first UWB radio ("GPS-only (baseline ≤300 m)");
VI. GPS + UWB estimating the UWB systematic errors using UWB measurements when the vehicle is within 25 m from the first UWB radio ("GPS + UWB (baseline ≤25 m)");
VII. GPS + UWB estimating the UWB systematic errors when the vehicle was within 50 m from the first UWB radio ("GPS + UWB (baseline ≤50 m)");
VIII. GPS + UWB estimating the UWB systematic errors when the vehicle was within 100 m from the first UWB radio ("GPS + UWB (baseline ≤100 m)");
IX. GPS + UWB estimating the UWB systematic errors when the vehicle was within 200 m from the first UWB radio ("GPS + UWB (baseline ≤200 m)");
X. GPS + UWB estimating the UWB systematic errors when the vehicle was within 300 m from the first UWB radio ("GPS + UWB (baseline ≤300 m)");

Table B.5 Improvement in RMS and mean error (in metres) of 1 Hz Geodetic-Grade GPS + UWB compared to 1 Hz GPS-only solution at intersection for all runs

strategies	RMS				Median			
	Horizontal	North	East	Vertical	Horizontal	North	East	Vertical
I (m)	0.218	0.167	0.138	0.346	0.189	-0.061	-0.074	0.017
II (m)	0.223	0.175	0.151	0.331	0.223	-0.123	-0.044	-0.072
III (m)	0.294	0.268	0.158	0.499	0.208	-0.069	-0.091	0.073
IV (m)	0.221	0.158	0.158	0.358	0.239	-0.031	-0.059	0.118
V (m)	0.186	0.144	0.133	0.352	0.187	-0.065	-0.055	0.195
VI (%)	8.8%	24.1%	-11.9%	-69.0%	10.9%	30.8%	26.4%	38.8%
VII (%)	4.7%	12.5%	-0.3%	-0.5%	-4.0%	37.0%	54.4%	-93.8%
VIII (%)	34.1%	52.1%	8.5%	6.2%	17.5%	163.7%	26.8%	113%
IX (%)	-9.6%	-38.6%	1.9%	9.6%	7.2%	243.7%	109.3%	53.7%
X (%)	-8.7%	-80.2%	20.4%	22.9%	-23.3%	385.7%	-2.0%	175.3%

I. GPS-only when the vehicle is within 25 m from the first UWB radio ("GPS-only (baseline ≤25 m)");
II. GPS-only when the vehicle is within 50 m from the first UWB radio ("GPS-only (baseline ≤50 m)");
III. GPS-only when the vehicle is within 100 m from the first UWB radio ("GPS-only (baseline ≤100 m)");
IV. GPS-only when the vehicle is within 200 m from the first UWB radio ("GPS-only (baseline ≤200 m)");
V. GPS-only when the vehicle is within 300 m from the first UWB radio ("GPS-only (baseline ≤300 m)");
VI. GPS + UWB estimating the UWB systematic errors using UWB measurements when the vehicle is within 25 m from the first UWB radio ("GPS + UWB (baseline ≤25 m)");
VII. GPS + UWB estimating the UWB systematic errors when the vehicle was within 50 m from the first UWB radio ("GPS + UWB (baseline ≤50 m)");
VIII. GPS + UWB estimating the UWB systematic errors when the vehicle was within 100 m from the first UWB radio ("GPS + UWB (baseline ≤100 m)");
IX. GPS + UWB estimating the UWB systematic errors when the vehicle was within 200 m from the first UWB radio ("GPS + UWB (baseline ≤200 m)");
X. GPS + UWB estimating the UWB systematic errors when the vehicle was within 300 m from the first UWB radio ("GPS + UWB (baseline ≤300 m)");

APPENDIX C

This appendix includes additional results for Scenario C, which was analyzed in Section 5.3.

Table C.1 Improvement in RMS and mean error (in metres, positive values means improvement, negative means degradation) of GPS + UWB compared to GPS-only solution at intersection for all runs

strategies	RMS				Median			
	Horizontal	North	East	Vertical	Horizontal	North	East	Vertical
I (m)	0.245	0.214	0.13	0.42	0.238	-0.082	0.001	-0.045
II (m)	0.25	0.219	0.156	0.413	0.271	-0.012	-0.087	-0.161
III (m)	0.306	0.316	0.129	0.612	0.224	-0.077	-0.002	-0.198
IV (m)	0.24	0.234	0.145	0.362	0.253	-0.107	0.024	0.104
V (m)	0.211	0.203	0.126	0.424	0.17	-0.046	-0.033	-0.008
VI (%)	1.4%	5.3%	-4.5%	3.3%	5.1%	-18.2%	-543.3%	54.2%
VII (%)	3.7%	4.9%	5.2%	-60.0%	24.6%	-584.9%	-39.8%	-58.3%
VIII (%)	7.7%	15.1%	-4.3%	-0.7%	20.4%	50.6%	-98.1%	-19.3%
IX (%)	24.3%	52.3%	1.0%	4.5%	23.6%	53.7%	-58.9%	34.2%
X (%)	-3.5%	9.6%	1.1%	1.7%	-33.7%	199.6%	88.8%	-2191%

XI. GPS-only when the vehicle is within 25 m from the first UWB radio ("GPS-only (baseline ≤25 m)");
XII. GPS-only when the vehicle is within 50 m from the first UWB radio ("GPS-only (baseline ≤50 m)");
XIII. GPS-only when the vehicle is within 100 m from the first UWB radio ("GPS-only (baseline ≤100 m)");
XIV. GPS-only when the vehicle is within 200 m from the first UWB radio ("GPS-only (baseline ≤200 m)");
XV. GPS-only when the vehicle is within 300 m from the first UWB radio ("GPS-only (baseline ≤300 m)");
XVI. GPS + UWB estimating the UWB systematic errors using UWB measurements when the vehicle is within 25 m from the first UWB radio ("GPS + UWB (baseline ≤25 m)");
XVII. GPS + UWB estimating the UWB systematic errors when the vehicle was within 50 m from the first UWB radio ("GPS + UWB (baseline ≤50 m)");
XVIII. GPS + UWB estimating the UWB systematic errors when the vehicle was within 100 m from the first UWB radio ("GPS + UWB (baseline ≤100 m)");
XIX. GPS + UWB estimating the UWB systematic errors when the vehicle was within 200 m from the first UWB radio ("GPS + UWB (baseline ≤200 m)");
XX. GPS + UWB estimating the UWB systematic errors when the vehicle was within 300 m from the first UWB radio ("GPS + UWB (baseline ≤300 m)");

Table C.2 Time to First Fix by Run where UWB improves results are highlighted green and runs were UWB degrades results are highlighted in red. Red text indicates an incorrect fix.

Run #	Time to First Fix (s)									
	GPS 25m	G+U 25m	GPS 50m	G+U 50m	GPS 100m	G+U 100m	GPS 200m	G+U 200m	GPS 300m	G+U 300m
1	N/A	N/A	N/A	N/A	N/A	15.3	N/A	21.9	37.1	26.5
2	7.7	7.4	8.2	7.4	14	13.3	8.9	8.9	12.4	12.3
3	N/A	N/A	N/A	29.3	22.8w	17.6w	22	19.8	39	33.4
4	N/A	N/A	N/A	N/A	N/A	N/A	30.3	22.2	N/A	31.7
5	16.8	16.7	17(w)	16.4(w)	N/A	23.1	N/A	27.3	29.5	25.3
6	N/A	N/A	N/A	11.3	N/A	N/A	20.3	13.9	43.4	33
7	8.1	6.7	6.7	N/A	17.6	14.9	17.1	18.4	16.4w	16.4w
8	6.6	6.8	6.2	5.2	13.2	9.9	13.5	13.2	12.5	12.5
9	9.4	8.6	N/A	N/A	12.5	9.6	19.6	13.1	10.5	11.7
10	14.9	14.7	14.3	13.4	14.7	N/A	N/A	N/A	27.9	25.8

Table C.3 Distance from intersection at time of first fix (m)

Run #	Distance from Intersection at Time to First Fix (m)									
	GPS 25m	G+U 25m	GPS 50m	G+U 50m	GPS 100m	G+U 100m	GPS 200m	G+U 200m	GPS 300m	G+U 300m
1	N/A	N/A	N/A	N/A	N/A	209.6	N/A	208.38	82.98	226.9
2	199.10	203.41	222.71	233.14	193.26	203.41	335.73	335.73	378.32	379.75
3	N/A	N/A	N/A	9.68	N/A	156.78	203.48	230.31	92.77	161.95
4	N/A	N/A	N/A	N/A	N/A	N/A	14.63	132.54	N/A	71.57
5	46.48	47.71	N/A	73.15	N/A	27.39	N/A	44.04	86.31	152.8
6	N/A	N/A	N/A	150.53	N/A	N/A	165	261.7	N/A	62.77
7	156.44	180.34	205.38	N/A	69.51	114.61	176.95	154.71	N/A	284.61
8	212.18	209.42	237.34	249.87	192.5	237.34	264.15	267.59	348.85	348.85
9	168.07	180.02	N/A	N/A	212.03	251.07	213.44	294.73	417.42	400.66
10	75.03	77.69	113.69	126.87	150.96	N/A	N/A	N/A	128.34	160.16

Table C.4 Ambiguity fixing performance of GPS+UWB compared to GPS alone

Change in Solution	Baseline within 25m	Baseline within 50m	Baseline within 100m	Baseline within 200m	Baseline within 300m	Total
Incorrect to Correct	0/10	0/10	0/10	0/10	0/10	0/50
Incorrect to N/A	0/10	0/10	0/10	0/10	0/10	0/50
Correct to N/A	0/10	1/10	1/10	0/10	0/10	2/50
Correct to Incorrect	0/10	0/10	0/10	0/10	0/10	0/50
N/A to Incorrect	0/10	0/10	0/10	0/10	0/10	0/50
N/A to Correct	0/10	2/10	2/10	2/10	1/10	7/50
Slower to Faster	5/10	3/10	4/10	5/10	6/10	23/50
Faster to Slower	1/10	0/10	0/10	1/10	1/10	3/50
No Change	4/10	4/10	3/10	2/10	2/10	15/50

Table C.5 Improvement in RMS and mean error (in metres) of GPS + UWB compared to GPS-only solution at intersection for all runs

strategies	RMS				Median			
	Horizontal	North	East	Vertical	Horizontal	North	East	Vertical
I (m)	0.34	0.258	0.205	0.444	0.203	0.032	0.071	0.175
II (m)	0.336	0.266	0.191	0.472	0.207	0.003	0.083	0.094
III (m)	0.307	0.23	0.19	0.499	0.185	-0.03	0.106	0.113
IV (m)	0.238	0.185	0.145	0.46	0.174	0.009	0.074	0.233
V (m)	0.214	0.156	0.149	0.399	0.209	0.024	0.076	0.014
VI (%)	-2.7%	-0.3%	-12.5%	20.6%	-4.7%	242.9%	-46%	42.6%
VII (%)	5.7%	7.3%	-0.1%	19%	-29.2%	1087.9%	-4.3%	14.8%
VIII (%)	2.4%	3.4%	-2.1%	13.1%	-34.9%	156.2%	9.6%	66.1%
IX (%)	-40.8%	-61.9%	-1.7%	0.4%	-46.1%	-68.4%	4.6%	43.6%
X (%)	-22.1%	-62.2%	-31.3%	-14.4%	-34.5%	-969.1%	-83.5%	-432.1%

I. GPS-only when the vehicle is within 25 m from the first UWB radio ("GPS-only (baseline ≤25 m)");
II. GPS-only when the vehicle is within 50 m from the first UWB radio ("GPS-only (baseline ≤50 m)");
III. GPS-only when the vehicle is within 100 m from the first UWB radio ("GPS-only (baseline ≤100 m)");
IV. GPS-only when the vehicle is within 200 m from the first UWB radio ("GPS-only (baseline ≤200 m)");
V. GPS-only when the vehicle is within 300 m from the first UWB radio ("GPS-only (baseline ≤300 m)");
VI. GPS + UWB estimating the UWB systematic errors using UWB measurements when the vehicle is within 25 m from the first UWB radio ("GPS + UWB (baseline ≤25 m)");
VII. GPS + UWB estimating the UWB systematic errors when the vehicle was within 50 m from the first UWB radio ("GPS + UWB (baseline ≤50 m)");
VIII. GPS + UWB estimating the UWB systematic errors when the vehicle was within 100 m from the first UWB radio ("GPS + UWB (baseline ≤100 m)");
IX. GPS + UWB estimating the UWB systematic errors when the vehicle was within 200 m from the first UWB radio ("GPS + UWB (baseline ≤200 m)");
X. GPS + UWB estimating the UWB systematic errors when the vehicle was within 300 m from the first UWB radio ("GPS + UWB (baseline ≤300 m)");

APPENDIX D

This appendix includes additional results for Scenario D, which was analyzed in Section 5.4.

Table D.1 Improvement in RMS and mean error (in metres) of Geodetic-Grade GPS + UWB compared to GPS-only solution at intersection for all runs (Scenario D)

strategies	RMS				Median			
	Horizontal	North	East	Vertical	Horizontal	North	East	Vertical
I (m)	0.209	0.136	0.188	0.432	0.185	0.052	-0.084	-0.206
II (m)	0.189	0.146	0.171	0.472	0.230	0.002	-0.119	-0.126
III (m)	0.190	0.151	0.132	0.339	0.158	-0.015	-0.071	-0.021
IV (m)	0.171	0.135	0.145	0.307	0.181	-0.062	-0.100	-0.174
V (m)	0.155	0.129	0.138	0.317	0.167	-0.066	-0.086	-0.185
VI (%)	2.4%	3.3%	6.7%	16.5%	14.5%	42.1%	41.6%	60.0%
VII (%)	22.2%	32.6%	12.7%	16.6%	10.9%	1237.4%	-3.1%	65.7%
VIII (%)	13.6%	35.6%	-2.3%	-27.3%	15.3%	334.1%	58.3%	482.0%
IX (%)	15.4%	28.7%	6.7%	4.1%	9.6%	200.1%	14.1%	-4.8%
X (%)	13.6%	28.9%	3.2%	-3.7%	22.2%	150.3%	27.7%	32.6%

I. GPS-only when the vehicle is within 25 m from the first UWB radio ("GPS-only (baseline ≤25 m)");
II. GPS-only when the vehicle is within 50 m from the first UWB radio ("GPS-only (baseline ≤50 m)");
III. GPS-only when the vehicle is within 100 m from the first UWB radio ("GPS-only (baseline ≤100 m)");
IV. GPS-only when the vehicle is within 200 m from the first UWB radio ("GPS-only (baseline ≤200 m)");
V. GPS-only when the vehicle is within 300 m from the first UWB radio ("GPS-only (baseline ≤300 m)");
VI. GPS + UWB estimating the UWB systematic errors using UWB measurements when the vehicle is within 25 m from the first UWB radio ("GPS + UWB (baseline ≤25 m)");
VII. GPS + UWB estimating the UWB systematic errors when the vehicle was within 50 m from the first UWB radio ("GPS + UWB (baseline ≤50 m)");
VIII. GPS + UWB estimating the UWB systematic errors when the vehicle was within 100 m from the first UWB radio ("GPS + UWB (baseline ≤100 m)");
IX. GPS + UWB estimating the UWB systematic errors when the vehicle was within 200 m from the first UWB radio ("GPS + UWB (baseline ≤200 m)");
X. GPS + UWB estimating the UWB systematic errors when the vehicle was within 300 m from the first UWB radio ("GPS + UWB (baseline ≤300 m)");

Table D.2 Time to First Fix by Run where UWB improves results are highlighted green and runs were UWB degrades results are highlighted in red. Red text indicates an incorrect fix.

Run #	Time to First Fix (s)									
	GPS 25m	G+U 25m	GPS 50m	G+U 50m	GPS 100m	G+U 100m	GPS 200m	G+U 200m	GPS 300m	G+U 300m
1	3.1	2.8	2.3	2.3	1.5	1.5	2.2	2.2	1.7	6
2	15.8	15.5	N/A	8.9	9.5	8.8	9	9	9.1	9.1
3	8.9	8.9	1.6	1.6	2.2	10.4	1.8	1.8	4.8	4.8
4	13.2	12.8	6.2	2.9	5.9	5.1	4.3	4.3	3.1	3
5	2.5	2.5	1.8	1.8	2.1	2.1	1.5	1.5	4.4	4.5
6	3	3	2.2	2.2	1.7	1.7	1.7	1.7	6	6.3
7	8	4.4	7.6	7.6	2.2	2.2	2.3	2.3	1.8	1.8
8	5	4.9	2.4	2.4	3.1	3.1	8.3	8.3	3.3	3.3
9	11.4	11.3	6.3	6.2	4.4	9.2	22.3	16.9	7.1	7
10	11.1	10.9	6.6	6.1	7.3	7.3	5.9	5.9	7.3	7.3

Table D.3 Distance from intersection at time of first fix (m)

Run #	Distance from Intersection at Time to First Fix (m)									
	GPS 25m	G+U 25m	GPS 50m	G+U 50m	GPS 100m	G+U 100m	GPS 200m	G+U 200m	GPS 300m	G+U 300m
1	249.30	253.55	283.02	283.02	344.9	344.9	439.4	439.4	540.72	481.72
2	53.35	57.46	N/A	182.18	227.18	237.53	320.93	320.93	419.90	419.90
3	142.55	142.55	288.81	288.81	326.48	191.30	435.27	435.27	490.64	490.64
4	105.14	110.83	226.04	272.95	282.54	293.40	394.89	394.89	518.60	520.30
5	256.60	256.60	287.50	287.50	335.83	335.83	440.97	440.97	500.60	499.00
6	259.11	259.11	292.88	292.88	343.97	343.97	439.29	439.29	463.14	457.56
7	172.95	224.66	210.22	210.22	336	336	430.14	430.14	537.70	537.70
8	224.49	225.92	283.34	283.34	322.61	322.61	342.09	342.09	522.80	522.80
9	122.87	124.49	229.91	231.36	298.07	229.91	130.92	213.80	456.8	458.4
10	112.43	115.33	220.89	228.89	265.80	265.80	385.61	385.61	450.78	450.78

Table D.4 Ambiguity fixing performance of GPS+UWB compared to GPS alone

Change in Solution	Baseline within 25m	Baseline within 50m	Baseline within 100m	Baseline within 200m	Baseline within 300m	Total
Incorrect to Correct	0/10	0/10	0/10	0/10	0/10	0/50
Incorrect to N/A	0/10	0/10	0/10	0/10	0/10	0/50
Correct to N/A	0/10	0/10	0/10	0/10	0/10	0/50
Correct to Incorrect	0/10	0/10	0/10	0/10	0/10	0/50
N/A to Incorrect	0/10	0/10	0/10	0/10	0/10	0/50
N/A to Correct	0/10	1/10	0/10	0/10	0/10	1/50
Slower to Faster	7/10	3/10	2/10	1/10	1/10	14/50
Faster to Slower	0/10	0/10	2/10	0/10	3/10	5/50
No Change	3/10	6/10	6/10	9/10	6/10	30/50

Table D.5 Improvement in RMS and mean error (in metres) of GPS + UWB compared to GPS-only solution at intersection for all runs

strategies	RMS				Median			
	Horizontal	North	East	Vertical	Horizontal	North	East	Vertical
I (m)	0.222	0.123	0.181	0.356	0.194	0.007	0.044	-0.013
II (m)	0.221	0.124	0.179	0.338	0.201	-0.025	0.022	0.064
III (m)	0.208	0.125	0.160	0.380	0.187	-0.034	-0.040	0.067
IV (m)	0.222	0.146	0.159	0.331	0.192	0.004	-0.032	-0.069
V (m)	0.192	0.127	0.136	0.312	0.179	0.001	-0.018	-0.059
VI (%)	-8.2%	-15.1%	-5.3%	-5.9%	-19.2%	1065.6%	-38.2%	377.3%
VII (%)	-10.3%	-43.9%	1.8%	1.5%	-23.1%	-289.9%	-16.5%	111.5%
VIII (%)	3.3%	12.9%	-2.4%	-4.6%	13.6%	55.4%	84.4%	-97.9%
IX (%)	-9.1%	-26.5%	-6%	-9.7%	5.0%	-2214.8%	155.8%	-13.4%
X (%)	-37.1%	-82.1%	-22%	-82.8%	-12.6%	-13100.9%	87.3%	-89.3%

I. GPS-only when the vehicle is within 25 m from the first UWB radio ("GPS-only (baseline ≤25 m)");
II. GPS-only when the vehicle is within 50 m from the first UWB radio ("GPS-only (baseline ≤50 m)");
III. GPS-only when the vehicle is within 100 m from the first UWB radio ("GPS-only (baseline ≤100 m)");
IV. GPS-only when the vehicle is within 200 m from the first UWB radio ("GPS-only (baseline ≤200 m)");
V. GPS-only when the vehicle is within 300 m from the first UWB radio ("GPS-only (baseline ≤300 m)");
VI. GPS + UWB estimating the UWB systematic errors using UWB measurements when the vehicle is within 25 m from the first UWB radio ("GPS + UWB (baseline ≤25 m)");
VII. GPS + UWB estimating the UWB systematic errors when the vehicle was within 50 m from the first UWB radio ("GPS + UWB (baseline ≤50 m)");
VIII. GPS + UWB estimating the UWB systematic errors when the vehicle was within 100 m from the first UWB radio ("GPS + UWB (baseline ≤100 m)");
IX. GPS + UWB estimating the UWB systematic errors when the vehicle was within 200 m from the first UWB radio ("GPS + UWB (baseline ≤200 m)");
X. GPS + UWB estimating the UWB systematic errors when the vehicle was within 300 m from the first UWB radio ("GPS + UWB (baseline ≤300 m)");

Table D.6 Time to First Fix by Run where UWB improves results are highlighted green and runs were UWB degrades results are highlighted in red. Red text indicates an incorrect fix.

Run #	Time to First Fix (s)									
	GPS 25m	G+U 25m	GPS 50m	G+U 50m	GPS 100m	G+U 100m	GPS 200m	G+U 200m	GPS 300m	G+U 300m
1	N/A	N/A	N/A	N/A	N/A	N/A	N/A	26.0	N/A	29.0
2	N/A	N/A	N/A	N/A	N/A	N/A	N/A	N/A	N/A	N/A
3	N/A	N/A	N/A	N/A	N/A	N/A	32.0	24.0	32.0	28.0
4	N/A	N/A	N/A	N/A	N/A	N/A	N/A	29.0	34.0	30.0
5	N/A	N/A	N/A	N/A	N/A	N/A	N/A	30.0	37.0	28.0
6	N/A	N/A	N/A	N/A	31.0	30.0	32.0	29.0	32.0	27.0
7	N/A	N/A	N/A	N/A	N/A	24.0	30.0	25.0	30.0	25.0
8	N/A	N/A	N/A	N/A	N/A	N/A	N/A	32.0	N/A	34.0
9	N/A	N/A	N/A	N/A	N/A	N/A	N/A	N/A	N/A	N/A
10	N/A	N/A	N/A	N/A	N/A	N/A	N/A	N/A	N/A	N/A

Table D.7 Distance from intersection at time of first fix (m)

Run #	Distance from Intersection at Time to First Fix (m)									
	GPS 25m	G+U 25m	GPS 50m	G+U 50m	GPS 100m	G+U 100m	GPS 200m	G+U 200m	GPS 300m	G+U 300m
1	N/A	N/A	N/A	N/A	N/A	N/A	N/A	97.92	N/A	152.73
2	N/A	N/A	N/A	N/A	N/A	N/A	N/A	N/A	N/A	N/A
3	N/A	N/A	N/A	N/A	N/A	N/A	9.06	63.14	37.50	94.44
4	N/A	N/A	N/A	N/A	N/A	N/A	N/A	29.21	41.13	93.98
5	N/A	N/A	N/A	N/A	N/A	N/A	N/A	4.39	4.39	131.61
6	N/A	N/A	N/A	N/A	2.22	9.43	49.31	85.03	123.98	188.78
7	N/A	N/A	N/A	N/A	N/A	25.16	36.41	103.51	117.49	188.71
8	N/A	N/A	N/A	N/A	N/A	N/A	N/A	6.12	N/A	66.20
9	N/A	N/A	N/A	N/A	N/A	N/A	N/A	N/A	N/A	N/A
10	N/A	N/A	N/A	N/A	N/A	N/A	N/A	N/A	N/A	N/A

Table D.8 Ambiguity fixing performance of GPS+UWB compared to GPS alone

Change in Solution	Baseline within 25m	Baseline within 50m	Baseline within 100m	Baseline within 200m	Baseline within 300m	Total
Incorrect to Correct	0/10	0/10	0/10	0/10	0/10	0/50
Incorrect to N/A	0/10	0/10	0/10	0/10	0/10	0/50
Correct to N/A	0/10	0/10	0/10	0/10	0/10	0/50
Correct to Incorrect	0/10	0/10	0/10	0/10	0/10	0/50
N/A to Incorrect	0/10	0/10	0/10	0/10	0/10	0/50
N/A to Correct	0/10	0/10	1/10	4/10	2/10	7/50
Slower to Faster	0/10	0/10	1/10	3/10	5/10	9/50
Faster to Slower	0/10	0/10	0/10	0/10	0/10	0/50
No Change	10/10	10/10	8/10	3/10	3/10	34/50